CHARACTERIZATION OF SMALL MOLECULES USING TANDEM MASS SPECTROMETRY AND COMPUTATIONAL CHEMISTRY IN THE CONTEXT OF ASTROCHEMISTRY

CHARACTERIZATION OF SMALL MOLECULES USING TANDEM MASS SPECTROMETRY AND COMPUTATIONAL CHEMISTRY IN THE CONTEXT OF ASTROCHEMISTRY

By
M. Ruzni Hanifa, B. Sc. (Hons.)

A Thesis
Submitted to the School of Graduate Studies
In Partial Fulfillment of the Requirements
For the Degree
Master of Science

McMaster University

MASTER OF SCIENCE (2009)
(Chemistry)

McMaster University
Hamilton, Ontario

TITLE:	Characterization of Small Molecules Using Tandem Mass Spectrometry and Computational Chemistry in the Context of Astrochemistry
AUTHOR:	M. Ruzni Hanifa, B.Sc. (Hons.) - York University
SUPERVISOR:	Dr Johan K. Terlouw
NUMBER OF PAGES:	xiv, 147

ABSTRACT

Ionized and neutral forms of small organic molecules containing nitrogen and/or oxygen have always intrigued experimental and theoretical chemists the world over. The reason is that such molecules could play a vital role in interstellar chemistry, potentially giving rise to larger homologues of groups such as sugars and other organic classes such as amino acids. Therefore, the chemistries of the ionic and neutral counterparts of these species are of considerable interest in the context of astrochemistry and prebiotic synthesis.

The ions studied in this thesis were generated in the rarefied gas phase of the mass spectrometer by electron ionization of carefully selected precursor molecules. The reactivity and structural characterization of these species were probed using a variety of tandem mass spectrometry based techniques. These include the acquisition of metastable ion (MI) mass spectra to study the dissociation chemistry of low energy ions and (multiple) collision experiments to establish the atom connectivity of such species. The structure and stability of the neutral counterparts of these ions was probed by using the technique of neutralization-reionization mass spectrometry (NRMS). Theoretical findings derived from CBS-QB3 and CBS-APNO model chemistries formed an essential component in the interpretation of experimental observations.

The above approach was used to study proton transport catalysis by water in the isomerization of ionized glycolaldehyde, $HOCH_2CHO^{\bullet+}$, into its enol ion $HOCH{=}CHOH^{\bullet+}$. A mechanistic analysis using the CBS-QB3 model chemistry reveals that an alternative pathway involves ionized glycolaldehyde rearranging into a hydrogen-bridged radical cation consisting of a ketene ion $CH_2{=}C{=}O^{\bullet+}$ interacting with two water molecules. The water component of this ion then catalyzes the interconversion of $HOCH_2CHO^{\bullet+}$ into $CH_2{=}C(OH)_2^{\bullet+}$, the enol of acetic acid. Tandem mass spectrometry based studies reveal that a mixture of $C_2H_4O_2^{\bullet+}$ ions are generated out of which $CH_2{=}C(OH)_2^{\bullet+}$ is the major component.

Next, the ionic and neutral $C_2H_2N_2$ potential energy surfaces were studied using CBS-QB3/APNO model chemistries. In other words, we probed the stability and reactivity of various ionic and neutral $C_2H_2N_2$ isomers, particularly the HNC dimer HN=C=C=NH (ethenediimine) and H_2N-C-C=N (aminocyanocarbene). They were generated from stable precursor molecules i.e. HN=C=C=NH from xanthine and H_2N-C-C=N from aminomalononitrile. NRMS experiments reveal that the neutral counterparts of these species are stable in the rarefied gas phase. Another precursor molecule, diaminomaleonitrile, is shown to generate $HN=C=C=NH^{\bullet+}$ after HCN loss from the hydrogen-bridged radical cation $[HNC\bullet\bullet\bullet H_2N\text{-}C\text{-}C=N]^{\bullet+}$ via a remarkable *quid-pro-quo* catalysis.

In a similar manner, the stability of the ionic and neutral forms of the HCN dimer, HC=N-N=CH, was probed. The pertinent ion was generated from ionized *s*-tetrazine via elimination of N_2. Using CBS-QB3/APNO model chemistries, the mechanism for its generation was probed and confirmed. However, $HC=N\text{-}N=CH^{\bullet+}$ is found to be generated with sufficient internal energy to facilitate its rearrangement into the more stable $HC=N\text{-}C(=N)H^{\bullet+}$ ion. This nitrene ion was separately generated from *s*-triazine. Collision experiments were used to characterize the ionic species. Despite the stability of the ionic species, NRMS experiments showed their neutral counterparts not to be stable in the gas phase.

The final component of this work deals with the generation and characterization of various isomers of ionized *N*-methylethenediimine $CH_3N=C=C=NH^{\bullet+}$ and *N,N*-dimethylethenediimine $CH_3N=C=C=NCH_3^{\bullet+}$. Ionized theophylline and paraxanthine were proposed to generate *m/z* 68 $CH_3N=C=C=NH^{\bullet+}$ ions.

Theory and experimental observations reveal that theophylline co-generates $CH_3N=C=C=NH^{\bullet+}$ with its 1,4-H shift isomer, $CH_2N=C=C(H)=NH^{\bullet+}$, where the neutral counterpart of the latter is found to be kinetically more stable than that of the former. Paraxanthine is found to generate isomerically pure $CH_3N=C=C=NH^{\bullet+}$ ions. Ionized *s*-methyltetrazine was proposed to generate another *m/z* 68 isomer presumed to be

$CH_3C{=}N{-}N{=}CH^{\bullet+}$. Experimental and theoretical results reveal that these ions are generated with sufficient internal energy to transform into various other isomers generating a mixture of *m/z* 68 ions, out of which, a majority do not have stable neutral counterparts in the gas phase. *N,N*-dimethylethenediimine $CH_3N{=}C{=}C{=}NCH_3^{\bullet+}$ ions were generated from ionized caffeine. Analogous to the *m/z* 68 ions from theophylline, these ions were found to be generated in admixture with its 1,4-H shift isomer, $CH_2N{=}C{=}C(H){=}NCH_3^{\bullet+}$. Theory shows that these species do not readily interconvert as ions. However, as neutral species, they readily isomerize resulting in a mixture of stable neutral isomers as seen from relevant NRMS experiments.

ACKNOWLEDGEMENTS

Working on this thesis within the Chemistry department at McMaster University has brought a lot of insight, challenges and milestones along with it, and during my time here, I have had the pleasure of working with some wonderful people.

First and foremost, I would like to thank Professor Terlouw for taking me under his wing. His passion and expertise in the subject matter has allowed me to gain a broad understanding of the theory behind my work and has given me the ability to focus on my research. Professor Terlouw has been the inspiration behind my research and thesis. I would like to extend my gratitude to Professor Paul Ayers for being such an amazing committee member. He has always been approachable and able to break down complex computational problems. I would also like to thank Karl Jobst for his patience; guiding me through the process, mentoring and supporting me.

I would like to thank all my friends in the department. Dr Kirk Green for being so quick to assist and lighten up the spirits of any room. Yemi Sofowote and Sujan Fernando for always cheering me up with great company and humour. Sumaya Bakbak for putting up with me and always listening to me complain. A big thank you to many more including, Leah Allan, Steve Kornic, Tomoko Aharen and everyone in the Mass Spec Group.

I want to sincerely thank my closest friends Kumaran Thillainadarajah and Linda Major. Linda, thank you for listening to me, supporting and keeping me motivated. I also want to thank a little furball, Cookie, who has made many long trips time and time again to cheer me up.

Last but not least, I want extend my appreciation to my family who have been an endless source of support through it all. To my ever-loving mother; her encouragement has brought me to where I stand today and my father, who has always believed in me.

TABLE OF CONTENTS

CHAPTER 1

Introduction

CHAPTER 2

CHAPTER 3

CHAPTER 4

CHAPTER 5

LIST OF FIGURES

Page

List of Abbreviations

AE = appearance energy
B = magnetic sector
B3LYP = hybrid Hartree-Fock/density functional theory
BMK = Boese-Martin for Kinetics (density functional theory exchange-correlation functional)
CCSD(T) = coupled cluster singles doubles and triples
CI = chemical ionization
CID = collision-induced dissociation
CBS-QB3 = complete basis set model chemistry
CBS-APNO = complete basis set model chemistry
DFT = density functional theory
EI = electron ionization
ESA (E) = electrostatic analyzer
eV = electron Volt (1 eV=23.061 kcal/mol or 96.487 kJ/mol)
ffr = field-free region
G3 = Gaussian-3 theoretical method
$\Delta_f H$ = enthalpy of formation
HBRC (HB) = hydrogen-bridged radical cation
HF = Hartree-Fock
IE = ionization energy
KER = kinetic energy release
MI = metastable ion
MP = Möller-Plesset (perturbation theory)
MS = mass spectrometry
NDMA = *N,N*-dimethylaniline
m/z = mass to charge ratio
NR(MS) = neutralization-reionization (mass spectrometry)
PA = proton affinity
PES = potential energy surface
PTC = proton transport catalysis
q = charge
QPQ = quid-pro-quo catalysis
r,R = radius
T = kinetic energy release (value)
TS = transition state
ZAB-R = BEE three-sector mass spectrometer
ZPVE/ZPE = zero-point vibrational energy

Chapter 1

1.1 Introduction, scope of this thesis

The gas phase ion chemistry described in this thesis focuses on the study of gaseous ions derived from small organic molecules. These ionic species are generated within a mass spectrometer. The structure and reactivity of these species are probed using techniques involving tandem mass spectrometry and computational chemistry. A majority of the ions studied are radical cations. In selected cases, the ions of interest may be generated within the source of the mass spectrometer by direct electron ionization (EI) of their gaseous neutral counterparts. In other cases, dissociative electron ionization of an appropriate precursor molecule may be used to generate the pertinent ions. It is crucial that the pressure in the ion source is maintained very low during such experiments. The reason is that, this way, the ions do not interact with (sample) molecules via ion-molecule reactions. This implies that the chemistry and reactivity of the ion studied is observed in a "solvent-free" environment.

Most of the radical cations studied have stable isomers of conventional or unconventional structure. The ions of unconventional structure include : (i) distonic ions, where the charge and radical sites are located on separate (adjacent or non adjacent) atoms within the ion, (ii) ion-dipole complexes, species that are stabilized by the interaction between the charge of the ionic component and the dipole of the neutral component, and (iii) hydrogen bridged radical cations (HBRCs), species consisting of ionic and neutral components stabilized through a hydrogen bond. In the case of the methanol radical cation, $CH_3OH^{\bullet+}$, it has only one stable distonic isomer, $CH_2OH_2^{\bullet+}$ [1]. On the other hand, the formic acid radical cation, $H\text{-}C(=O)OH^{\bullet+}$, has four stable isomers: the ion-dipole complex, $[H_2O{\bullet\bullet\bullet}CO]^{\bullet+}$, the hydrogen-bridged radical cations $[OC{\bullet\bullet\bullet}H{\bullet\bullet\bullet}OH]^{\bullet+}$ and $[CO{\bullet\bullet\bullet}H{\bullet\bullet\bullet}OH]^{\bullet+}$, and the ionized carbene, $HO\text{-}C\text{-}OH^{\bullet+}$ [2].

Radical cations generated in the low pressure experiments described above do not necessarily retain their atom connectivity. The internal energy content of these ions may be high enough to result in their isomerization into one or more stable isomers, often via H-shift. Conversely, there are other systems where the barrier for such H-shift associated with the unimolecular isomerization is significantly high prohibiting rearrangement. However, recent research by our group and other laboratories have revealed that, such high isomerization barriers can be lowered when the ion of interest is in an encounter complex with a carefully selected neutral molecule. In our instrument, this phenomenon is observed by executing the reaction under chemical ionization (CI) conditions. This experiment is carried out when the pressure in the source is much greater (by a factor of c. 10 000) compared to a standard EI experiment. This mechanism involving a single (solvent) molecule catalyzing the isomerization of a given radical cation into a more stable isomer has been coined "proton-transport catalysis" and is further discussed in Section 1.3.

Chapter 2 deals with the above scenario. It focuses on the isomerization of $HOCH_2CHO^{\bullet+}$, the glycolaldehyde radical cation, into its 1,3-H shift isomer, $HOCH{=}CHOH^{\bullet+}$, the 1,2-dihydroxyethene ion. Theoretical calculations predict that the 1,2-dihydroxyethene ion is the more stable isomer. This elusive ion was generated and characterized by tandem mass spectrometry and, in agreement with the calculations, it does not communicate with $HOCH_2CHO^{\bullet+}$ prior to dissociation by loss of H_2O. However, under conditions of chemical ionization and using H_2O as the catalyst, the glycolaldehyde radical cation can be promoted to isomerize into $HOCH{=}CHOH^{\bullet+}$, via a mechanism characteristic of proton-transport catalysis. However, theoretical calculations show an alternative pathway involving an intermediate hydrogen-bridged radical cation consisting of a ketene ion $CH_2{=}C{=}O^{\bullet+}$ in complex with two H_2O molecules. It is one of these H_2O molecules that catalyzes the transformation of the glycolaldehyde ion into another isomer, $CH_2C(OH)_2^{\bullet+}$, the enol of acetic acid. One incentive to study this system is that glycolaldehyde is one of the C, H and O containing molecules that has been identified as an important biomarker in interstellar chemistry as it is the simplest monosaccharide sugar.

The theoretical study of the $C_2H_2N_2$ ionic and neutral potential energy surface, particularly the isomers, the HNC dimer; ethenediimine ($HN{=}C{=}C{=}NH$), and aminocyanocarbene ($H_2N\text{-}C\text{-}C{=}N$), is discussed in Chapter 3. Experiments involving collision-induced dissociation (CID) and neutralization-reionization (NR) mass spectrometry are used to probe the structure, stability and reactivity of these ions in the gas phase.

Chapter 4 describes the generation and characterization of a *m/z* 54 ion derived from ionized *s*-tetrazine presumably corresponding to the HCN dimer, $HC=N-N=CH^{\bullet+}$. Computational chemistry and tandem mass spectrometry (including CID and NR techniques) indicate that this ion is generated but possesses enough internal energy to isomerize into another isomer, $HC=N-C(=N)H^{\bullet+}$. This ion is separately characterized after dissociation from ionized *s*-triazine.

Finally, Chapter 5 deals with the generation and characterization of various isomers of *N*-methylethenediimine $CH_3N=C=C=NH^{\bullet+}$ and *N,N*-dimethylethenediimine $CH_3N=C=C=NCH_3^{\bullet+}$. A variety of precursor molecules including theophylline, paraxanthine, *s*-methyltetrazine and caffeine is used to generate the isomers studied. The reactivity and the stability of the ionic and neutral species were probed using MI, CID and NR mass spectrometry in conjunction with computational chemistry.

The next two sections of this chapter offer the non-expert reader with background information on the various mass spectrometry based techniques and the computational chemistry methods used in the studies reported in this thesis.

Section 1.2 provides a brief introduction to the instrumentation used in various experiments ; a state-of-the-art tandem magnetic sector mass spectrometer. This section also describes a variety of techniques used to generate and characterize the ions, in addition to the computational methods used to assist in the interpretation of the experimental results.

Section 1.3 presents a brief overview of the methods used to carry out ion-molecule reactions under chemical ionization (CI) conditions with an emphasis on the parameters that influence molecule-assisted isomerization reactions of radical cations.

The results described in Chapters 3 and 4 of this thesis have been reported in the literature. Some of the computational chemistry in Chapter 4 was performed in collaboration with Prof. P.J.A. Ruttink (University of Utrecht, The Netherlands) whose expertise is greatly appreciated. The results of Chapter 2 are being interpreted in collaboration with Dr P. Gerbaux (University of Mons, Belgium). The experiments discussed in the chapter are currently being conducted by Dr P. Gerbaux on the Mons AutoSpec 6F mass spectrometer. His knowledge and efforts are greatly valued.

1.2. The generation and characterization of ions by tandem mass spectrometry

The VG Analytical ZAB-R Mass Spectrometer

Mass spectrometry is used for structural elucidation of ions and neutrals generated in the mass spectrometer. The instrument used for our experiments is the VG ZAB-R mass spectrometer. A schematic diagram indicating the various components of the mass spectrometer is shown in Fig. 1.1. As it can be seen, it is a multiple sector instrument consisting of three mass analyzers separated by three field free regions (ffr). The first mass analyzer is a magnet (B) followed by two electrostatic analyzers (E) giving the instrument its BEE geometry. The field free regions separating these respective mass analyzers consist of collision cells within which intricate experiments such as collision induced dissociation (CID) and neutralization-reionization (NR) mass spectrometry can be conducted.

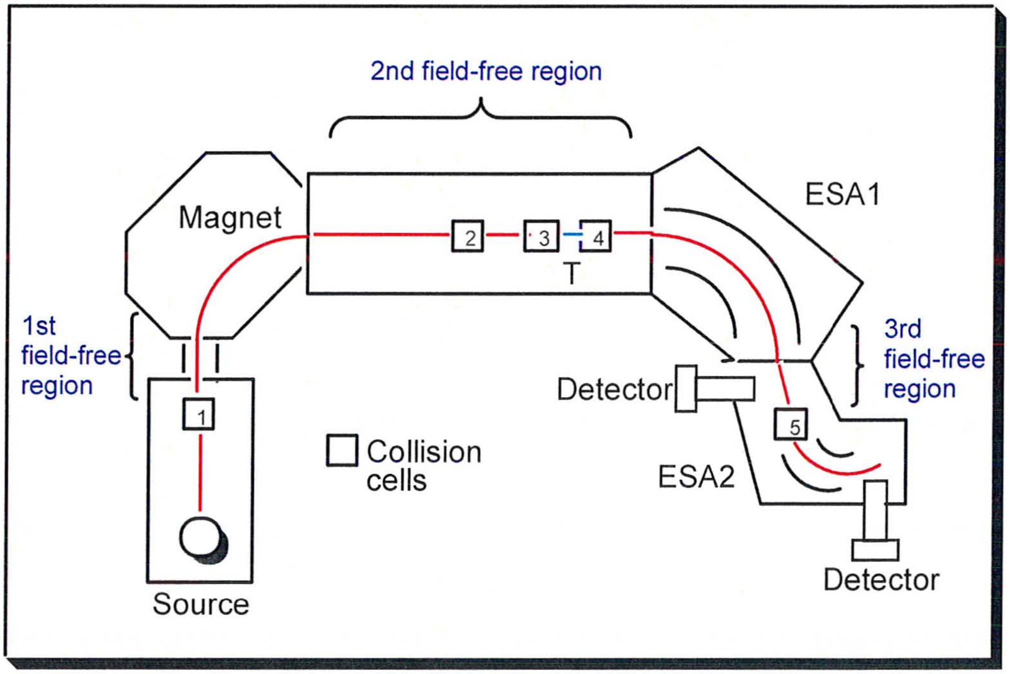

Figure 1.1 Schematic diagram portraying the different components of the VG ZAB-R Mass Spectrometer.

The sample of interest is introduced into the mass spectrometer via a leak valve into the ion source. Within the source, fast moving electrons produced by a tungsten filament collide with the neutral sample molecules resulting in their ionization. These high energy electrons are accelerated by establishing a potential between the filament and the ion source (approximately 70 eV) [3]. It is this bombardment of the electron with the neutral molecule that results in the removal of another electron from the molecule leading to the generation of a positively charged ion. An equation illustrating this ionization is shown below :

$$M + e^{-} \rightarrow M^{\bullet +} + 2e^{-}$$

In the above equation, M denotes the neutral molecule, e^{-} is the electron and $M^{\bullet +}$ indicates that the positive ion generated is a radical cation. This is due to the fact that a majority of the organic molecules contain an even number of electrons, which when ionized, generate odd electron ions. The equation shown above and its accompanying explanation ideally describes electron impact ionization (EI).

The time taken for this type of ionization is approximately 10^{-16} seconds, which, when compared to the time span for the motion of the nuclei in any molecule (i.e. the fastest possible molecular vibration takes around 10^{-14} seconds), is at least a hundred times faster [3]. Given this difference in time frames of the two processes, it would be fair to assume that the nuclei within a molecule remain motionless during the ionization process meaning that this ionization could be regarded to be a vertical ionization process governed by the Frank-Condon principle. Therefore, during the ionization, if the electron colliding with the molecule imparts energy in excess of the ionization energy (IE) of the molecule, the surplus energy is contained within the molecule as internal energy. The presence of this additional internal energy causes the molecule to undergo excitations into higher energy vibrational, rotational and electronic states. Despite this fact, the amount of internal energy imparted by each ionizing electron on a molecular ion is different in each case leading to the eventual dissociation of certain ions while others remain intact. Given that an ion undergoes dissociation, this could happen in two different ways; the ion could simply undergo direct bond cleavage or the ion could undergo a bond cleavage after a rearrangement.

Most of the dissociations that occur within the mass spectrometer take place in the ion source yielding source-generated ions. Given that the amount of time it takes for such an ion to reach the detector is approximately 10 microseconds, the period of time spent in the ion source before entering the 1ffr is about 1 microsecond. Therefore, the minimum rate constant for the dissociation of the incipient molecular ions within the ion source works out to be 10^6 per second. As mentioned before, there are two types of dissociations that can take place within the ion source. The determining factor for the type of dissociation a molecular ion will undergo is its internal energy content. The typical maximum rate for the direct bond cleavage reactions is 10^{14} per second whereas the maximum rate for rearrangement reactions is 10^{10} per second. Hence, the rate constant for the dissociation of any incipient ions in the source should be greater than 10^6 per second but less than 10^{14} per second. Due to this reason and the fact that these ions are generated within 1 microsecond of entering the source, these source generated ions are referred to as **unstable** ions. In contrast, any molecular ion that reaches the detector without undergoing any dissociation is referred to as a **stable** ion. The reason why stable ions do not dissociate is that they do not possess sufficient internal energy to facilitate the process. Hence, they are low internal energy ions. Typically, the rate constant for the dissociation of a stable ion should lie below 10^4 per second. Any ions with an intermediate amount of energy are referred to as **metastable** ions. In other words, these are ions that do not possess sufficient energy to dissociate within the source of the mass spectrometer but do possess enough internal energy to dissociate before reaching the detector. Therefore, the rate constant for these low energy or metastable dissociations should be greater than 10^4 per second but less than 10^6 per second. Hence, the ions resulting from these metastable dissociations are studied separately using any of the collision cells in one of the field-free regions of the mass spectrometer.

The rate constant 'k' discussed above is related to the internal energy of an ion and this relationship has been best explained using two different statistical theories : the Quasi-Equilibrium Theory (QET) and the Rice, Rampsberger, Kassel and Markus (RRKM) Theory. In the simplest adaptation of the QET, the dissociation reaction of an ion is described using the rate constant in the following equation : $k = v\ [\varepsilon_i\text{-}\varepsilon_o/\varepsilon_i]^{s-1}$, where v is the frequency factor, ε_i is the internal energy of a fragmenting ion, ε_o is the activation energy for the process and s is the number of effective oscillators in the ion [3].

Metastable Ion spectra

A metastable ion (MI) spectrum is generally acquired to comprehend the low energy dissociation behaviour of a given ion.

Similar to all tandem mass spectrometric experiments, metastable ion spectra of specific ions are obtained by mass selecting the ion of interest into the 2ffr of the instrument using the magnet. As the source generated ions are accelerated towards the magnet, the ions enter a magnetic field which is in a direction normal to the ion beam. As a result, the ions follow a circular path which is described by the equation : $r = mv/Be$, where r is the radius of the circular path, m is the mass of the ion, v is the velocity of the ion, B is the strength of the magnetic field and e is the ionic charge [3]. From the equation, it is apparent that the radius of the ion beam in the magnetic field is proportional to its momentum (mv). Hence, the magnet is capable of separating the ions based on their momentum. The mathematical representation of the separation of ions by the magnet is as follows : $m/z = B^2r^2/2v$ [3]. Once the precursor ions, $m_1^{\bullet+}$, have been mass selected into 2ffr, a minute fraction of these ions undergo spontaneous dissociation into product ions, $m_2^{\bullet+}$ and m_3. In this process, the kinetic energy of the precursor ion, $m_1^{\bullet+}$, is redistributed among the fragmentation products, $m_2^{\bullet+}$ and m_3, based on their relative mass. The mass-weighted relationship illustrating this distribution is given by the equation $(m_2/m_1)V_{acc}$, where V_{acc} is the acceleration voltage. Therefore, using this relationship, the first electrostatic analyzer (ESA1) can be used to mass analyze the respective product ions based on their individual translational energies. Fig. 1.2 shows the metastable dissociation events in the 2ffr. Overall, the main beam of incipient ions consists of ions generated from both, stable and metastable dissociations. However, only about 1% of the main beam contributes to the total intensity of the peaks seen in the MI spectrum.

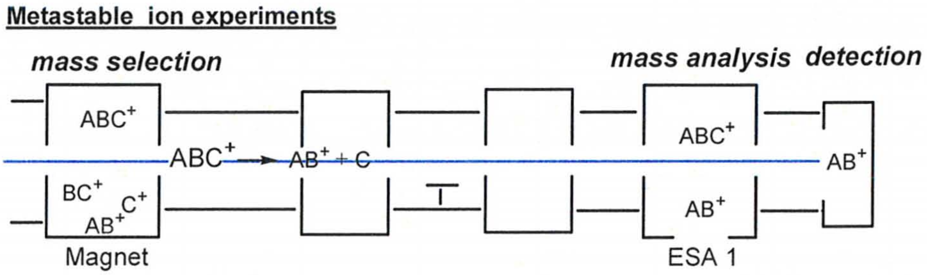

Figure 1.2. A schematic diagram depicting the events in a metastable ion experiment.

In general, peaks in MI spectra result from ions with a narrow range of internal energies. However, in comparison to the width of the non-dissociating main beam ion peak, the width of the MI peaks is consistently larger [4]. The reason for this stems from the conversion of the internal energy of the precursor ion, $m_1^{\bullet+}$, into the translational energy of the dissociating products, $m_2^{\bullet+}$ and m_3. One other important contributor to the kinetic energy of the products is the reverse activation energy of the associated fragmentation.

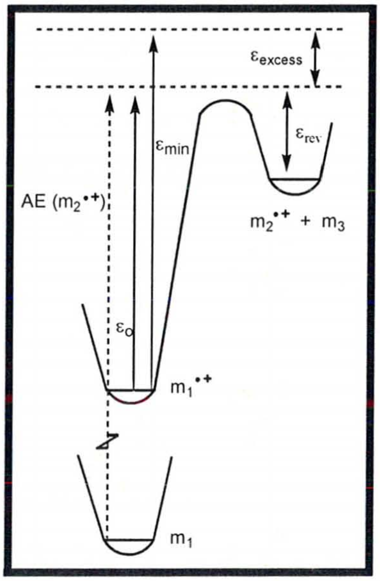

Figure 1.3. A potential energy diagram illustrating an endothermic reaction in the gas phase.

Fig. 1.3 displays an energy diagram that illustrates an endothermic dissociation reaction with a sizeable reverse activation barrier. The minimum amount of internal energy necessary to observe the dissociation, $m_1^{\bullet+} \rightarrow m_2^{\bullet+} + m_3$, in the metastable timeframe is ε_{min} [3] which simultaneously has to be greater than the forward activation energy, ε_o, to meet the energy requirements. The difference between ε_{min} and ε_o is denoted by ε_{excess} to represent the excess energy. The reverse activation energy is denoted by ε_{rev} which is obtained from the difference in the enthalpy of formation of the products and that of the transition state for the process. It is the sum of this reverse activation energy and the excess energy that converts into the translational energy of the dissociation products.

During the dissociation of a metastable ion, the above mentioned energy conversion may also result in a kinetic energy release (KER) T [3]. The KER may originate from the excess energy of the activated complex and the reverse activation energy of the dissociation. A rearrangement reaction, where the products include a stable ion and a neutral molecule, is a good example of a reaction with considerable reverse activation energy [3]. Direct bond cleavage reactions are generally associated with little or no reverse activation barriers. In MI spectra, the KER can be observed as a widening of the metastably generated ion peak relative to the peak corresponding to the main ion beam, $m_1^{\bullet+}$. Therefore, dissociation reactions such as direct bond cleavage reactions that are associated with small KER values generate MI peaks with a Gaussian shape. However, reactions having larger KER values are characterized by metastable peaks that are either flat-topped or dish-shaped [3]. Hence, the shape of the peaks generated give insight into the physical kinetic aspects of the dissociating ions. In the same vein, the shapes of the MI peaks help comprehend the connectivity of the dissociating ions and understand the distribution of the internal energy of the precursor ion into the kinetic energy of the fragmentation products [4]. The KER (T) can be acquired from the width of a MI peak at a certain height 'h' and mathematically represented as follows : $T_h = (m_1^2/16m_2m_3)(V_{acc})[(\Delta E_h)^2/E^2]$, where V_{acc} is the accelerating voltage, ΔE_h is the metastable peak width at a height h and E is the electric sector voltage of the ions transmitted. Generally, KER values are reported as the metastable peak widths at half-height ($T_{0.5}$).

Collision-Induced Dissociation spectra

A collision-induced dissociation (CID) spectrum provides information with regards to the connectivity of a particular ion through the analysis of fragment ions generated. Such a spectrum is acquired as follows; the source generated ions are accelerated towards the magnet, typically using an accelerating potential of 8 kV, and the ion of choice is mass selected into the 2ffr. Here, the beam of ions passes through multiple collision cells, one of which is pressurized with an appropriate collision/target gas, typically oxygen (O_2) or Helium (He). As a result, a fraction of these traversing ions is bombarded with a target gas molecule causing the consequent conversion of a portion of the ion's kinetic energy into internal energy. Hence, collisionally activated ions have a moderately broad distribution of internal energies facilitating a wide variety of possible dissociation reactions. Simple direct bond cleavage reactions take precedence over rearrangement processes as a rule. Therefore, CID spectra are characterized by a multitude of direct bond cleavage reactions and/or rearrangement reactions in comparison to the one or two peaks representing low energy rearrangement processes seen in MI spectra. It is these high energy direct bond cleavage reactions that assist in the evaluation and characterization of the ion structure. Fig. 1.4 illustrates the collision events that take place during a typical CID experiment.

In a given CID spectrum, the number of peaks detected and their relative intensities are dependent on several factors including the type of collision gas used, its pressure and the translational energy of the ion beam. Helium, oxygen, argon and nitrogen are typical collision gases used by various research groups. Out of these, helium is the most popular due to its high target efficiency.

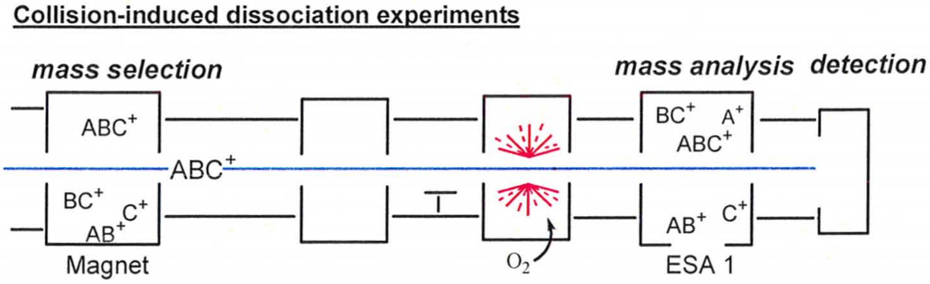

Figure 1.4. A schematic diagram portraying the events in a collision-induced dissociation experiment.

In this thesis, all reported CID experiments use oxygen as the collision gas and compared to the CID spectra obtained using helium, as the target gas, in select cases. Most of the time, CID spectra acquired using oxygen are very similar to those generated using helium as the collision gas. However, it has been noted in a number of experiments that oxygen is capable of inducing distinct high energy fragmentations resulting in weak peaks in the spectra not observed in CID spectra obtained using other collision gases [5].

The pressure of the target gas used in a collision cell is another important factor affecting the appearance of a CID spectrum. The reason is that the pressure is proportional to the number of collisions the target ion undergoes in the cell (single or multiple collision events). For the purposes of our experiments, the pressure of the gas used is maintained sufficiently low to allow only single collision events. To ensure the pressure is always kept low and consistent, the pressure of the gas is observed through the use of a remote ionization gauge placed outside the collision cell. Collision gas pressure is approximated using the observed effects on the main beam intensity as the pressure is altered. Ideally, main beam reduction should be approximately 30 – 40 %. Further lowering of the main beam intensity through increase in collision cell pressure will lead to multiple collision events and high energy dissociations resulting in a drastic reduction in structure-specific information obtained [6].

The translational energy content of the collisionally activated ions is also known to affect the CID experiment and therefore, the respective spectrum generated. As mentioned earlier, a fraction of the translational energy of the incipient ions is converted into internal energy upon collision with the target gas molecules. Therefore, as the translational energy is increased, the range of the internal energy content of the collisionally derived ions is increased resulting in more collision induced dissociations [6]. During a collision, the approximate amount of energy transferred, E_{max}, is given by the following relationship : $E_{max} = h/a(2eV/m)^{1/2}$, where h is Planck's constant ($h = 6.626 \times 10^{-34}$ Js), a denotes the interaction distance, eV is the translational energy of the ion and m is the mass of the ion [6]. The mass of the collision gas molecule or atom is a factor recognized to affect the amount of translational energy transferred to an ion. As a rule, heavier collision gases are more efficient at energy deposition that lighter gases due to a larger center-of-mass kinetic energy (E_{cm}) [7]. The mathematical definition of E_{cm}, or the highest amount of translational energy accessible to be converted into internal energy, is as follows : $E_{cm} = E_{lab}m_t / (m_t + m_i)$, where E_{lab} denotes the translational energy of the ion (in eV), m_t is the mass of the target gas and m_i is the mass of the ion [7].

Neutralization-Reionization spectra

A neutralization-reionization (NR) mass spectrum of a certain ion is normally acquired to study the stability of elusive and/or highly reactive neutral counterparts in the gas phase. This method has developed into a highly important research technique. The reason for this stems from the fact that NR mass spectrometry facilitates the study of neutral species that are generally complicated to generate by other means due to their affinity toward unimolecular dissociation or bimolecular rearrangement [6a]. Fig. 1.5 demonstrates the main events that take place in a NR experiment after the ions of interest have been generated from a suitable precursor molecule in the source, and then mass selected into the 2ffr using the magnet.

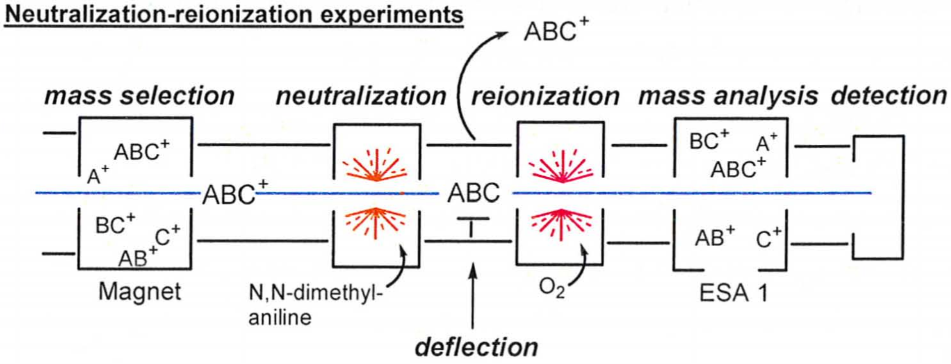

Figure 1.5. A schematic diagram illustrating the events in a neutralization-reionization experiment.

Fig. 1.5 shows that these fast moving ions are then subjected to two successive collisions in collision cells that are pressurized with the appropriate target gases. The purpose of the first collision event is to neutralize a majority of the ions which is done by pressurizing the first collision cell along the flight path with *N,N*-dimethylaniline. The neutralization process takes place via a single charge transfer upon collision. The population of non-neutralized ions are then deflected away by a positively charged deflector electrode that is situated between the two collision cells. Hence, only the neutral species (and some uncharged dissociation products) continue along the flight path past the deflector into the second collision cell which is pressurized with oxygen gas. Here, the fast moving neutrals undergo a second collision to be reionized. A fraction of these reionized species undergo dissociation prior to leaving the collision cell. Thereafter, the resulting ions are mass analyzed using the first electrostatic analyzer (ESA1), detected by the first photomultiplier and the NR mass spectrum generated. In this NR spectrum, if a peak is seen at the *m/z* corresponding to that of the original ion of interest, this indicates that the neutral counterpart of the ion survived the neutralization process. Therefore, the peak is referred to as a 'survivor' signal and is indicative of a stable neutral species in the microsecond timescale of the experiment.

Xenon is another gas that could be used to efficiently neutralize ions in NR experiments regardless of its high ionization energy (12.2 eV) which implies that the neutralization process, $AB^+ + N \rightarrow AB + N^+$, is endothermic. However, this does not impede nor prohibit the charge transfer from occurring due to the fact that the discrepancy, in terms of energy, is counterbalanced by the large translational energy of the ion (8 keV) [6b].

Normally, for the reionization process, $AB + R_1 \rightarrow AB + R_1^+ + e^-$, a 'hard' target gas such as helium may be used. However, the use of such a target gas induces extensive fragmentation upon reionization prohibiting the generation of a potential 'survivor' ion despite the high yield of structurally relevant fragment ions. Therefore, in our experiments, oxygen is used for reionization as it is a softer target gas generating a high yield of 'survivor' ions. The reaction for the reionization process using oxygen is as follows : $AB + O_2 \rightarrow AB^+ + O_2^-$.

In order to verify that the incipient neutral species retained its original connectivity and did not rearrange into a more stable isomer prior to reionization, a NR/CID spectrum is acquired. Fig. 1.6 shows the principal events in a NR/CID experiment.

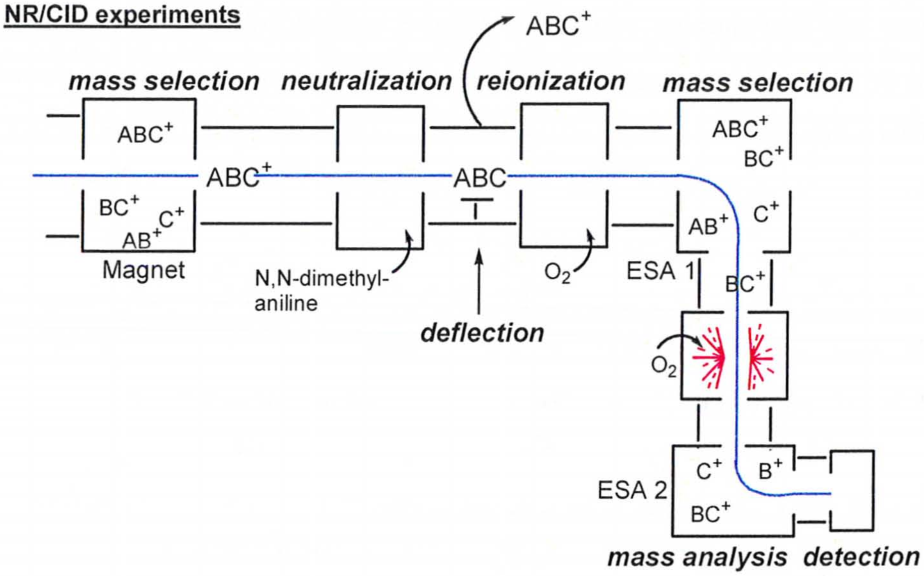

Figure 1.6. A schematic diagram showing the events in a neutralization-reionization/collision-induced dissociation experiment.

In order to carry out such an experiment, the reionized potential 'survivor' species has to be mass analyzed and transmitted into the 3ffr using ESA1. Next, the mass selected ion beam passes through yet another collision cell that is pressurized with oxygen gas. Therefore, the ions are subjected to collisions with neutral oxygen molecules inducing high energy dissociations. Finally, the fragmenting ions are mass analyzed using ESA2 and then detected using the second photomultiplier detector to generate the NR/CID spectrum.

To confirm whether the neutral species did retain its structural integrity, the acquired NR/CID spectrum is compared to the 3ffr CID spectrum of the source generated ions. The close resemblance of the two spectra in the number of peaks and their relative intensities is indicative of the neutrals having retained their structure prior to reionization. More importantly, the similarity provides strong evidence for the stability of the neutral counterpart in the gas phase. Conversely, if it appears that the two spectra are dissimilar, it maybe an indication that the neutral species isomerized into a more stable structure. This can be verified by comparing the acquired spectrum to a reference CID spectrum of the more stable isomer. In the same vein, it should be duly noted that the NR/CID spectrum will vary from the CID spectrum if the mass-selected source generated ions comprises of a mixture of isomeric and/or isobaric impurities [9].

Additionally, computational/theoretical chemistry also assists in the interpretation of NR spectra. The size of the dissociation and/or isomerization barriers of the incipient ion and its neutral counterpart helps explain the probability of either the neutral or the ion undergoing isomerization.

Collision-Induced Dissociative Ionization spectra

A collision-induced dissociative ionization (CIDI) spectrum is obtained to study the connectivity and relative stability of a neutral species that is spontaneously lost in a fragmentation. Fig. 1.7 illustrates the key features in CIDI experiment. As with all other experiments in this thesis, the precursor ion of interest is initially mass selected into the 2ffr using the magnet. A minute fraction of these ions spontaneously undergo unimolecular dissociation prior to entering the collision cell. The resulting fragmenting ions, $m_2^{\bullet+}$, and their respective parent ions, $m_1^{\bullet+}$, are then deflected away using the positive deflector electrode allowing only the fast moving neutral species from the fragmentations to enter the collision chamber [10]. This chamber is pressurized with oxygen gas that reionizes the neutrals upon impact. Thereafter, the reionized species and their respective dissociation products are mass analyzed using ESA1 before reaching the photomultiplier to generate the CIDI spectrum.

Similar to the NR/CID experiment, the structural integrity of the reionized neutrals can be probed by mass selecting the species into the 3ffr using ESA1 and inducing high energy dissociation via collision with oxygen gas. The dissociating ions are then mass analyzed using ESA2 before detection and generation of the respective CID spectrum.

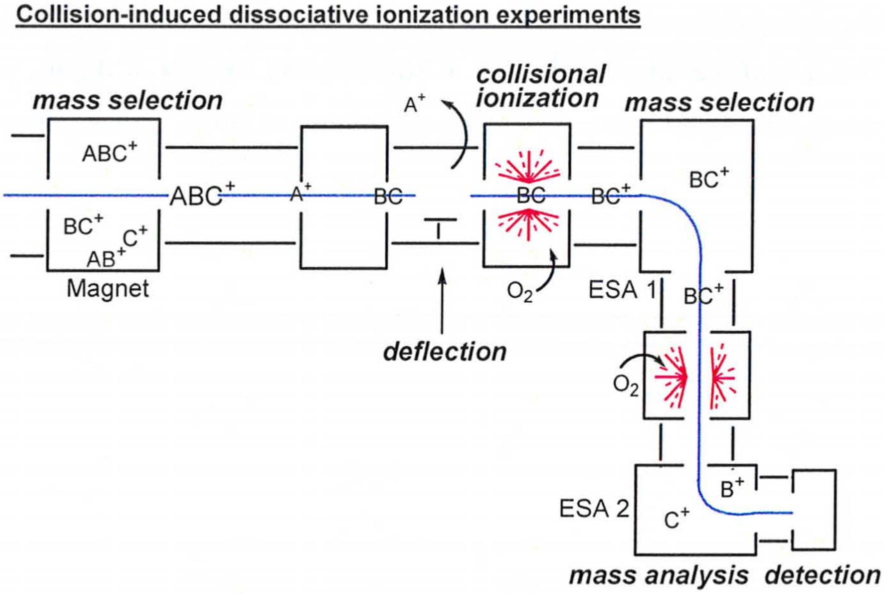

Figure 1.7. A schematic diagram illustrating the events in a collision-induced dissociative ionization experiment.

Computational Chemistry

In our studies, computational chemistry has been considerably used as a complementary aid to theoretically derive information regarding the connectivity of the desired species and the mechanism of its subsequent formation [11]. Combining these theoretical findings with our experimental results, we have been able to comprehend and explain the behaviour and generation of various elusive species.

For the purposes of this thesis, the preferred model chemistry for all our computations (yielding the reported enthalpies of formation of minima and transition states) is the CBS-QB3 model chemistry [12]. It is a Complete Basis Set Quadratic (CBS-Q) configuration interaction model chemistry which utilizes a hybrid empirical correction/pair correlation energy extrapolation scheme. The scheme encompasses the B3LYP (B3) density functional method in conjunction with the 6-311G(2d,d,p) basis set for geometry optimization of minima and transition states and their respective absolute enthalpies of formation. The CBS-QB3 model chemistry calculation comprises of four computations at different levels of theory in combination with varying basis sets to generate the absolute enthalpy of formation for the species of interest.

The primary step of this calculation entails the optimization of the input geometry (initial guess) of the ionic or neutral structure submitted. This is done using the density functional method (B3LYP) to converge to an appropriate stationary point on the potential energy surface (PES). The structure submitted is deemed optimum once all the forces converge to zero [13]. However, the optimized structure may be consistent with either a local minimum or a transition state (also known as a first order saddle point). A frequency analysis is performed on the structure to verify if the stationary point is a minimum (no imaginary frequencies) or a transition state (one imaginary frequency). Additionally, it is very important to acknowledge the presence of multiple minima and transition states on the PES requiring the careful selection of the input geometry. These minima correspond to energy wells on the PES indicating stable isomers or conformers of the initial structure. The transition states correspond primarily to isomerization reactions.

During the steps of the CBS-QB3 calculation, the energy computed at the B3LYP level of theory is not used. Instead, only the optimized structure is used in the following steps to eventually generate the respective total absolute enthalpies of formation (in Hartrees) at 0 and 298 K. Simultaneously, the corresponding vibrational frequencies are also calculated in this step. For a given polyatomic ion or molecule, there are 3N-6 vibrational frequencies, where N is the number of atoms. However, for transition states, one of these vibrational frequencies is a negative value corresponding to the single imaginary frequency identifying the transition state. The zero-point vibrational energy (ZPVE or ZPE) for the neutral or ionic minima or transition state is computed in the frequency calculation [14].

In the steps that follow in the CBS-QB3 calculation, the energy of the primary optimized structure is determined using electron correlation methods. The corresponding Hartree-Fock (HF) energy of the structure is ascertained via a Møller-Plesset (MP) calculation at the MP2 level of theory. Next, a coupled-cluster singles, doubles and triples (CCSD(T)) calculation and a MP4 calculation are performed at higher levels of theory. The coupled-cluster approach is the highest order electron correlation utilized by the CBS-QB3 model chemistry taking into account the single, double and triple excitations. With regards to MP calculations, as listed above, there are various types of calculations incorporating different orders of electron correlation [15]. The purpose of performing these computations at these two levels of theory is to assess the overall effect of the higher order electron correlation on the enthalpies calculated and improve the accuracy of the model [16].

Finally, using the energy determined at the MP2 level of theory and correcting it with the energies calculated using the CCSD(T) and MP4 theories, the total energy corresponding to the structure studied is presented in the computational output as E(CBS-QB3). This total energy reported corresponds to a temperature at 0 K. In order to derive the enthalpy of formation for the associated structure at 298 K, $\Delta_fH^0_{298}$, the following mathematical equation is used :

$$\Delta_fH^0_{298} = \Delta_fH^0_0(\text{exp}) - E_{AT} + E(\text{CBS-QB3}) + E_{\text{thermal}} - \text{ZPE} - \Delta_fH^0_{298}(\text{exp})$$

where $\Delta_fH^0_0(\text{exp})$ denotes the sum of the experimentally derived $\Delta_fH^0_0$ values corresponding to the atoms in the species studied, E_{AT} is the sum of the atomization energies corresponding to each atom in the species, E_{thermal} represents the thermal energy correction from the frequency calculations, ZPE is the zero point vibrational energy (scaled to a factor of 0.99) and $\Delta_fH^0_{298}(\text{exp})$ denotes the sum of the experimental $\Delta_fH^0_{298}(\text{exp})$ values for each atom in the species. A list of all the $\Delta_fH^0_0$ and $\Delta_fH^0_{298}$ values corresponding to the first and second row elements in the periodic table is presented in the publication by Nicolaides et al. [17].

In regards to the accuracy of the enthalpies of formation generated from our computations, it has been reported that there is an estimated error of 1-2 kcal/mol for enthalpies of minima and 2-5 kcal/mol for those corresponding to connecting transition states [12,18]. Another factor known to affect the accuracy of the values generated is the spin contamination. This is the contamination that derives from a mixture of spin states in the species yielding high spin polarization [14b]. In general, the influence of the spin contamination in the calculation of the total energy reasonably yields a much higher value due to the consideration of a higher energy state. In a more severe contamination, there will be changes seen in the actual geometry and the spin density [14b]. Normally, the total spin value is reported in the computational output as $<S^2>$. If there is no spin contamination, the value corresponding to $<S^2>$ must be equal to s(s+1) where s represents the number of unpaired electrons multiplied by ½. As we deal with radical cations a majority of the time, the presence of a single unpaired electron implies a value of 0.75 corresponding to $<S^2>$. However, it is deemed acceptable if the computed total spin value is within 10% of the value corresponding to s(s+1) [14b].

All computations were performed using the Gaussian suite of programs installed on desktop personal computers and on the SHARCNET cluster of computers at McMaster University.

1.3. Ion-molecule reactions and proton-transport catalysis

The bimolecular reactivity of gas phase ions and molecules has been of considerable interest to researchers, fuelling substantial research [19]. The interactions of such ions and molecules can be investigated through experiments using chemical ionization (CI) conditions. CI is a softer ionization method relative to electron impact (EI) ionization. During a CI experiment, the pressure maintained in the source is relatively high, 10^{-4}-10^{-5} Torr. This is to ensure multiple collisions of the originally introduced sample molecule before exiting the source [20]. The pressure is increased in the source by pressurizing the source with a suitable reagent gas, R. Once the experiment is under way, it is the reagent gas that is primarily ionized by the fast moving electrons from the tungsten filament. Thereafter, the ionized reagent gas particle react with either other reagent gas molecules or the relatively less numerous substrate molecules 'M' to generate several reactive ionic species [20]. All possible routes of reaction and generation of possible encounter complexes are shown below :

$R + e^- \rightarrow R^{\bullet+} + 2e^-$

$R^{\bullet+} + M \rightarrow [R{\bullet}{\bullet}{\bullet}M]^{\bullet+}$ (ion-dipole complex)

$R^{\bullet+} + R \rightarrow [R{\bullet}{\bullet}{\bullet}R]^{\bullet+}$ (dimer radical cation)

$R^{\bullet+} + R \rightarrow RH^+ + [R\text{-}H]^{\bullet}$

$RH^+ + M \rightarrow [R{\bullet}{\bullet}H{\bullet}{\bullet}M]^+$ (proton bound mixed dimer)

$RH^+ + R \rightarrow [R{\bullet}{\bullet}H{\bullet}{\bullet}R]^+$ (proton bound dimer)

$R^{\bullet+} + M \rightarrow [R{\bullet}{\bullet}H{\bullet}{\bullet}(M\text{-}H)]^{\bullet+}$ (hydrogen-bridged radical cation)

Based on the properties of the reagent gas used and the substrate molecule, many different ion-molecule reactions can take place to generate different types of encounter complexes. The type of complex produced depends on the kind of interaction between the participating species. The different kinds of interactions include electrostatic, hydrogen-bonding and van der Waals forces. An ion-dipole complex is an encounter complex formed as a result of the stabilizing electrostatic interaction between an ion and the dipole of a neutral molecule. A hydrogen-bridged radical cation (HBRC) is a complex resulted from the stabilizing interaction between the reagent ion and the hydrogen atom of neutral molecule. Such complexes are represented as follows : $[R{\bullet\bullet}H{\bullet\bullet}(M\text{-}H)]^{\bullet+}$, where the two interacting species are linked by a hydrogen bridge. If the interaction generating a complex is between the protonated reagent RH^+ ion and the neutral molecule, the complex is referred to as a proton-bound dimer (PBD). These complexes are illustrated as either $[R{\bullet\bullet}H{\bullet\bullet}M]^+$ or $[R{\bullet\bullet}H{\bullet\bullet}R]^+$ in the list above. Finally, another possible complex is a dimer radical cation that is comprised of reagent radical cation interacting with a neutral counterpart. The type of interaction in such an ion is similar to either an ion-dipole complex or a HBRC.

Stabilization Energy

In the past, prior to embracing the mathematical problem-solving abilities of computational chemistry to determine enthalpies, the enthalpy of formation of a proton-bound dimer (PBD) was experimentally ascertained utilizing the empirical connection between the bond dissociation energies of the bonds within the PBD and the proton affinities (PA) of the individual species in the dimer.

As mentioned before, a PBD is an even electron ion complex that is comprised of two uncharged species bound together by a proton. If the interacting species are identical to each other, the PBD generated is symmetrical such as the water PBD, $[H_2O{\bullet\bullet}H{\bullet\bullet}OH_2]^+$. In contrast, if the two species involved in the PBD are different, an asymmetrical PBD is generated. An example of such a mixed PBD is that involving water and methanol, $[H_2O{\bullet\bullet}H{\bullet\bullet}O(H)CH_3]^+$.

Larson and McMahon [21], and Meot-Ner [22] developed an empirical relationship to experimentally derive the enthalpy of formation of the PBD, $O{\bullet\bullet}H{\bullet\bullet}O$.

Multiple PBDs were generated at high pressures using complex CI type mass spectrometric methods and their exchange equilibria (with selected bases) studied. Using these results, important information was obtained such as the thermochemistry of the process (PBD solvent-exchange equilibria), Gibbs' free energy and the bond dissociation energies within the respective PBD. The relationship between the difference in hydrogen bond energies of the two species within the PBD to the difference in their respective PA yields an empirical connection that can be similarly used to study other O••H••O PBD dimer not considered before.

However, comparing the relationships determined by the two research groups, they are not completely identical. The reason is that the PBD species studied by the two groups are different. The empirical relationship determined by Meot-Ner [22] revealed the stabilization energy (SE) for the O••H••O PBDs in kcal/mol to be; SE = 30.4 – 0.30 [ΔPA], while Larson and McMahon [21] reported; SE = 30.8 – 0.46 [ΔPA]. These determined relationships were based on a set of approximately 35-45 PBDs. In the equations shown, the first term denotes the average bond dissociation energy of the set of PBDs studied. The second term represents the slope of the correlation plot; bond dissociation energy vs. ΔPA.

The method for determining the SE of a PBD depends on whether the PBD studied is symmetric or not. For a symmetric PBD such as $[H_2O{\bullet\bullet}H{\bullet\bullet}OH_2]^+$, there is only one possible set of dissociation products; $H_3O^+ + H_2O$. Therefore, as the enthalpy of formation for this set of products is well established, the SE of the symmetric PBD is calculated using the following equation : $SE = \Delta_fH(\text{product}_1) + \Delta_fH(\text{product}_2) - \Delta_fH(\text{PBD}^+)$. Additionally, given the symmetry in the PBD, the ΔPA is zero as the two participating species are identical having the same PA. Thus, the SE for the PBD, $[H_2O{\bullet\bullet}H{\bullet\bullet}OH_2]^+$, works out to be 30.0 kcal/mol. Using this value, the enthalpy of formation of the PBD $[\Delta_fH(\text{PBD}^+)]$ can be calculated from the equation for SE.

If the PBD studied is asymmetric, for example $[H_2O{\bullet\bullet}H{\bullet\bullet}O(H)CH_3]^+$, there are two possible sets of fragmentation products; $H_3O^+ + CH_3OH$ and/or $H_2O + CH_3OH_2^+$. In such a scenario, the set of products corresponding to the lowest enthalpy of formation is used to determine the enthalpy of formation of the associated PBD. Scheme 1.8 below illustrates this point. The difference in the well established PA of the two species involved, H_2O and CH_3OH, yields ΔPA.

It should also be noted that the studies of Meot-Ner [22] expanded to include the effects of the ionic hydrogen bond and ion salvation measurements within PBDs such as $[N\bullet\bullet H\bullet\bullet O]^+$ and $[N\bullet\bullet H\bullet\bullet N]^+$. The expressions corresponding to the SE (in kcal/mol) of these PBDs are 30.0 – 0.26 [ΔPA] and 23.2 – 0.25 [ΔPA] respectively. Deviations from these relationships that result in errors in the determination of the SE, and the reasons for such deviations have also been reported [22].

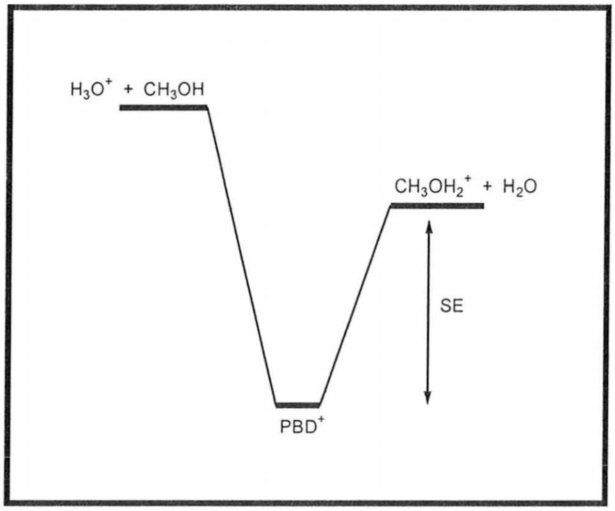

Scheme 1.8. An estimated energy diagram illustrating the relative enthalpies of the sets of dissociation products in comparison to the proton-bound dimer (PBD).

In our studies, we have taken these empirical relationships and applied them to odd-electron hydrogen-bridged radical cations (HBRCs). One such HBRC is $[CH_3O\bullet\bullet H\bullet\bullet OH_2]^+$, where the hydrogen from methanol provides as the bridge within the cation. Using the same equation for the stabilization energy, SE = 30.0 – 0.30 [ΔPA], an approximate value for the enthalpy of formation of the HBRC can be calculated. Similar to asymmetric PBDs, HBRCs can potentially generate two different combinations of dissociation products. Therefore, like before, the set of products corresponding to the lowest enthalpy of formation is chosen to derive the enthalpy of formation of the HBRC. In this case, the ΔPA term refers to the difference in the PA of the methoxy radical ($CH_3O^\bullet$) and the water molecule (H_2O) respectively.

Catalyzed Isomerization Reactions

There have been several studies that have reported the catalyzed isomerization of various radical cations by appropriate neutral molecules [19]. A majority of the time, such catalyzed interconversions are observed to involve distonic radical ions. According to Radom et al. [23], the group that coined the term, a distonic ion is a radical cation in which the radical and the charge are apart, thus, they are located on different atoms. Compared to their conventional counterparts, distonic ions are much more stable and are separated from these isomers by a large energy barrier residing in deep potential wells. Therefore, interconversion is unlikely allowing the two types of isomers to be observed separately. A good example of such a case is the isomerization of methanol, $CH_3OH^{\bullet+}$, into the more stable methylene oxonium ion, $^{\bullet}CH_2OH_2^{+}$, studied by Radom et al. [23] and Holmes et al. [24]. These ions do not interconvert due to a prohibitively high activation barrier associated with the particular 1,2-H shift. However, in the presence of a water molecule, the isomerization readily takes place. This is because water behaves as a catalyst lowering the activation barrier enabling the transformation. Such reactions are termed proton-transport catalyses.

Proton-transport catalysis (PTC) [17d] is a reaction where a gaseous radical cation, $[H\text{-}X\text{-}Y]^{\bullet+}$, rearranges into a more stable isomer, $[X\text{-}Y\text{-}H]^{\bullet+}$, through interaction with an appropriate solvent molecule in a three step process. This solvent molecule primarily behaves as a base, B. The three step process is illustrated below :

$$[H\text{-}X\text{-}Y]^{\bullet+} + B \rightarrow B{\bullet\bullet}H^{+}{\bullet\bullet}[X\text{-}Y]^{\bullet}$$

$$B{\bullet\bullet}H^{+}{\bullet\bullet}[X\text{-}Y]^{\bullet} \rightarrow B{\bullet\bullet}H^{+}{\bullet\bullet}[Y\text{-}X]^{\bullet}$$

$$B{\bullet\bullet}H^{+}{\bullet\bullet}[Y\text{-}X]^{\bullet} \rightarrow B + [H\text{-}Y\text{-}X]^{\bullet+}$$

As demonstrated, the neutral molecule, B, functions as a 'base' abstracting the proton from the high energy site on $[H\text{-}X\text{-}Y]^{\bullet+}$ and 'transporting' it to the low energy site on the species thereby functioning as a catalyst. For the above reaction to proceed as explained, the PA of the base must be ideally greater than the PA of the X site on the $XY^{\bullet}$ radical but lower than the PA of the Y site. This way, the base can feasibly abstract the proton from the X site and 'transport' it to the Y site. The intermediate complex, B••H$^+$••[X-Y]$^•$, generated in between is weakly-bound allowing rotation of the XY species within the complex to facilitate the isomerization. If the PA of B is considerably lower than the PA of the XY$^•$ radical at the X site, the intermediate encounter complex, B••H$^+$••[X-Y]$^•$, will not be generated. Alternatively, if the PA of B is much greater than the PA of the XY$^•$ radical at the Y site, the encounter complex, B••H$^+$••[X-Y]$^•$, will fragment undesirably into the XY$^•$ radical and BH$^+$ ion. A thorough analysis of the conditions for efficient proton-transport catalysis (PTC) by Gauld and Radom [17b] has revealed that the PA of the base, B, should be intermediate between the PA of the sites of proton abstraction (X site) and donation (Y site) respectively. This required condition for PTC is termed the Radom criterion.

References

[1] a) L. Radom, W.J. Bouma, R.H. Nobes, B.F. Yates. Pure Appl. Chem. 56 (1984) 1831; b) W.J. Bouma, J.K. MacLeod, L. Radom. J. Am. Chem. Soc. 104 (1982) 2930; c) J.L. Holmes, F.P. Lossing, J.K. Terlouw, P.C.Burgers. J. Am. Chem. Soc. 104 (1982) 2931; d) B.F. Yates, W.J. Bouma, L. Radom. J. Am. Chem. Soc. 109 (1987) 2250; e) J.W. Gauld, L. Radom. J. Phys. Chem. 98 (1994) 777.

[2] E. Uggerud, W. Koch, H. Schwarz. Int. J. Mass Spectrom. Ion Proc. 73 (1986) 187.

[3] R.G. Cooks, J.H. Beynon, R.M. Caprioli, G.R. Lester. *Metastable Ions*. Elsevier. Amsterdam. 1973.

[4] J.L. Holmes , J.K. Terlouw. Org. Mass Spectrom. 15 (1980) 383.

[5] a) R. Flammang, V. Henrotte, P. Gerbaux, M.T. Nguyen. Eur. J. Mass Spectrom. 6 (2000) 3; b) G.A. McGibbon, P.C. Burgers, J. K. Terlouw. Int. J. Mass Spectrom. Ion Process. 136 (1994) 191.

[6] J.L. Holmes. Organic Mass Spectrometry. 20 (1985) 169.

[7] a) K.M. Stirk, P. Lin, T.D. Ranatunga, L.C. Zeller, J.T. Farrell Jr., H.I. Kenttamaa. Int. J. Mass Spectrom. Ion Process. 130 (1994) 187; b) K.L. Schey, H.I. Kenttamaa, V.H. Wysocki, R.G. Cooks. Int. J. Mass Spectrom. Ion Process. 90 (1989) 71.

[8] a) C.A. Schalley, G. Hornung, D. Schröder, H. Schwarz. Chem. Soc. Rev. 27 (1998) 91; b) F. Cacace. Chem. Eur. J. 8 (2002) 3838.

[9] L.N. Heydorn, C.Y. Wong, R. Srinivas, J.K. Terlouw. Int. J. Mass. Spectrom. 225 (2003) 11.

[10] J.K. Terlouw, H. Schwarz. Angew. Chem. Int. Ed. Engl. 26 (1987) 805.

[11] P.C. Burgers, J.K. Terlouw. *The Encyclopedia of Mass Spectrometry – Volume 4*. Elsevier. Amsterdam. 2005.

[12] a) J.A. Montgomery, Jr., M.J. Frisch, J.W. Ochterski, G.A. Petersson. J. Chem. Phys. 112 (2000) 6532; b) J.A. Montgomery, Jr., M.J. Frisch, J.W. Ochterski, G.A. Petersson. J. Chem. Phys. 110 (1999) 2822.

[13] J.B.Foresman, A.Frisch. *Exploring Chemistry with Electronic Structure Methods*. Second Edition. Gaussian, Inc. Pennsylvania. 1996.

[14] a) A.D.Becke. J. Chem. Phys. 98 (1993) 5648; b) A.D.Becke. J. Chem. Phys. 98 (1993) 1372.

[15] W.J. Hehre, L. Radom, R.v.R. Schleyer, J.A. Pople. *Ab Initio Molecular Orbital Theory*. Wiley. New York. 1986.

[16] a) F. Jensen. *Introduction to Computational Chemistry*. John Wiley and Sons. New York. 1999; b) D.Young. *Computational Chemistry; A Practical Guide for Applying Techniques to Real World Problems*. John Wiley and Sons. New York. 2001.

[17] A. Nicolaides, A. Rauk, M.N. Glukhovstev, L. Radom. J. Phys. Chem. 100 (1996) 17640.

[18] L.N. Heydorn, Y. Ling, G. de Oliveira, J.M.L. Martin, C. Lifshitz, J.K. Terlouw. Zeitschrift für Physikalische Chemie. 215 (2001) 141.

[19] a) D.K. Bohme. Int. J. Mass Spectrom Ion Processes. 115 (1992) 95; b) J.W. Gauld, L. Radom. J. Am. Chem. Soc. 119 (1997) 9831; c) M.A. Trikoupis, J.K. Terlouw, P.C. Burgers. J. Am. Chem. Soc. 120 (1998) 12131; d) M.A. Trikoupis, P.C. Burgers, P.J.A. Ruttink, J.K. Terlouw. Int. J. Mass Spectrom. 217 (2002) 97 and references cited therein.

[20] F.W. McLafferty, F. Turecek. *Interpretation of Mass Spectra*. Fourth Edition. University Science Books. California. 1993.

[21] J.W. Larson, T.B. McMahon. J. Am. Chem. Soc. 104 (1982) 6255.

[22] M. Meot-Ner. J. Am. Chem. Soc. 106 (1984) 1257.

[23] L. Radom, W.J. Bouma, R.H. Nobes, B.F. Yates. Pure & Appl. Chem. 56 (1984) 1831.

[24] J.L. Holmes, F.P. Lossing, J.K. Terlouw, P.C.Burgers. J. Am. Chem. Soc. 104 (1982) 2931.

Chapter 2

Does a water molecule catalyze the isomerization of ionized glycolaldehyde ? Answers from model chemistry calculations.

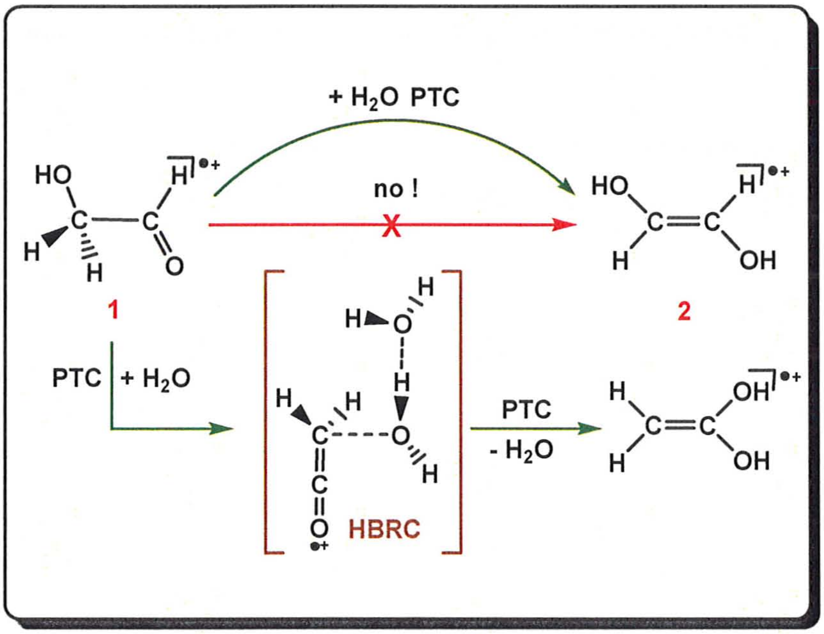

Model chemistry calculations (CBS-QB3 and CBS-APNO) indicate that the reaction of ionized glycolaldehyde, $HOCH_2CHO^{\bullet+}$, and water, an ion-molecule reaction of potential interest in astrochemistry, could lead to the formation of its enol ion $HOCH{=}CHOH^{\bullet+}$ by proton transport catalysis (PTC). An alternative pathway of lower energy involves formation of the above hydrogen-bridged radical cation (HBRC) comprised of the ketene ion $CH_2{=}C{=}O^{\bullet+}$ interacting with two H_2O molecules. Theory predicts that the H_2O component of this HBRC catalyzes the otherwise prohibitive transformation of the glycolaldehyde ion into $CH_2{=}C(OH)_2^{\bullet+}$, the enol ion of acetic acid. Exploratory tandem mass spectrometry based experiments indicate that a mixture of $C_2H_4O_2^{\bullet+}$ ions is generated and that the predominant reaction product is $CH_2{=}C(OH)_2^{\bullet+}$.

1. Introduction

The glycolaldehyde molecule, $HOCH_2CHO$, is an important biomarker, as it is the simplest monosaccharide sugar and its hydroxyaldehyde group is a constituent of many important biochemicals. Its generation as a secondary atmospheric photo-oxidation product [1] and particularly its recent detection in the interstellar medium [2] has sparked considerable interest in the gas-phase chemistry of this small molecule and its radical cation [3]. In the interstellar medium, one important source of glycolaldehyde and its earlier identified $C_2H_4O_2$ isomers methyl formate [4,5,6] and acetic acid [7] is the hot core known as the Large Molecule Heimat located in Sagittarius B2(N) [Sgr B2(N)–LMH] [8].

The enol isomer of glycolaldehyde, 1,2-dihydroxyethene (HOCH=CHOH), is yet to be detected in the interstellar medium. In this context, the intriguing question arises whether ionized glycolaldehyde (**1**) can isomerize into the more stable 1,2-dihydroxyethene ion (**2**). Previous theoretical work shows that the barrier for the unimolecular isomerization is too high (~32 kcal/mol relative to **1**). However, in a recent study of the chemistry of 2-aminoxyethanol ions by our group [9], it was proposed that ionized glycolaldehyde generated in complex with NH_3 isomerizes into the 1,2-dihydroxyethene ion via proton-transport catalysis (PTC) [10].

Water is also a confirmed interstellar species [11], which raises the question whether the same isomerization would take place in a complex with H_2O. The goal of this study is therefore to use model chemistry calculations and tandem mass spectrometry based experiments to investigate the ion-molecule reaction of the glycolaldehyde radical cation with H_2O.

It will be shown that the aforementioned transformation of **1** into **2** is energetically feasible. However, it may not compete with the more favourable water catalyzed transformation of **1** into the ketene-water ion $H_2O/CH_2{=}C{=}O^{\bullet+}$. In line with the findings of an earlier study by Bohme and co-workers [12], the resulting complex is expected to rearrange into the ionized enol of acetic acid, the 1,1-dihydroxyethene ion $CH_2{=}C(OH)_2^{\bullet+}$.

2. Experimental and Theoretical Methods

The calculations were performed using the Gaussian 03 Revision C.02 (and D.01) suite of programs [13] on SHARCNET. The optimized geometries (Appendix Figures 2.8 and 2.9) and 298 K enthalpies (Tables 1-4) of the various ions and neutrals were derived from the CBS-QB3 and CBS-APNO model chemistries [14]. The identity of local minima and connecting transition states (TS) was confirmed by frequency analysis.

The experiments performed at McMaster University involved the VG Analytical ZAB-R mass spectrometer [15]. The instrument is of BE_1E_2 geometry (B = magnet, E = electric sector) and for the study of the ion-molecule reaction it was equipped with a standard chemical ionization (CI) source. The repeller voltage was held close to 0 V and the primary electron ionization (EI) was accomplished using 70 eV electrons. Gaseous glycolaldehyde, H_2O and CO_2 were introduced into the ion source via separate inlet systems. Hydrated copper (II) sulphate was used as a source to leak H_2O vapour into the source. The total pressure within the source was monitored using a remote ionization gauge and maintained at around 7-10 x 10^{-5} Torr.

A sample of the commercially available (Aldrich) glycolaldehyde dimer 2,5-dihydroxy-1,4-dioxane [16a] was used to introduce the monomer into the instrument, by gently heating the solid sample in a quartz probe with an oil bath. We note in this context that in the molten state glycolaldehyde exists as a mixture of different monomeric and dimeric forms [16b]. In the vapour phase under equilibrium conditions only the monomer exists in *cis* orientation exhibiting a single carbonyl absorption band at 1753 cm^{-1} [16c]. However, when the dimer sample is introduced into the mass spectrometer with the direct solids insertion probe the degree of dedimerization may be negligible and an EI mass spectrum characteristic of the dimer, which does not display a peak at *m/z* 60, is obtained [16d]. In solution, the dimer undergoes rearrangement and dissociation into various monomeric forms [16e].

To obtain reference metastable ion (MI) and collision induced dissociation (CID) mass spectra [17] of the 1,2-dihydroxyethene ion, solid samples of DL-glyceraldehyde (Sigma, research grade), 1,4-dioxane-2,3-diol and D-erythronic γ-lactone (Aldrich) were introduced via the direct solids insertion probe. This set of experiments was carried out under electron ionization (EI) conditions (70 eV) at an accelerating voltage of 8 kV in the second field-free region (2ffr) of the instrument. The CID mass spectra were acquired using O_2 as the collision gas.

The ion-molecule reaction of *mass selected* glycolaldehyde ions with neutral water is currently being studied in the context of a joint project with Dr P. Gerbaux on the Mons AutoSpec 6F mass spectrometer. This is a six-sector magnetic deflector instrument of EBEEBE geometry, equipped with three collision cells (C_{1-3}) to study high-energy collision-induced dissociation reactions and an rf-only hexapole (HEX) reaction chamber to study the ion-molecule reaction. The current configuration is as follows : $C_1E_1B_1C_2E_2$-HEX-$E_3B_2C_3E_4$ [18].

To briefly explain the experiment, the first three sectors of the instrument are used to mass select the *m/z* 60 glycolaldehyde ions (8 keV) towards the hexapole. These ions are decelerated to ~5 eV prior to entering the hexapole cell to optimize the yield of the ion-molecule reaction. The water vapour introduced into the cell is at a pressure of $\sim 5 \times 10^{-4}$ mbar measured with a Pirani gauge located within the cell. Thereafter, the ions leaving the cell are reaccelerated to 8 keV before being mass analyzed by the field of B_2. Finally, any resulting *m/z* 60 ions can be mass selected and subjected to CID with O_2 in chamber C_3. The CID spectra generated are obtained by scanning sector E_4.

3. Results and Discussion

3.1. The dissociation chemistry of the glycolaldehyde cation (1)

3.1.1. The structure and stability of the neutral and ionic conformers

An early theoretical study at the HFSDCI/6-31G**//RHF/4-31G level of theory by Postma et al. [19] on the glycolaldehyde radical cation (**1**) and its dissociation chemistry, proposes that ion **1** has two stable conformers, denoted as **1**(Ct) and **1**(Tt), which are closely similar in energy and have a low interconversion barrier. The notation refers to the dihedral angles for rotation around the CC bond ϕ_1 (C or T) and the CO(H) bond ϕ_2 (c or t) respectively. For **1**(Ct) $\phi_1 = 0°$ and $\phi_2 = 180°$ and for **1**(Tt) $\phi_1 = 180°$ and $\phi_2 = 180°$.

This result is consistent with the CBS-QB3 and CBS-APNO calculations of this study. Fig. 2.1 (top part) shows the CBS-QB3 derived optimized geometries and 298 K enthalpies of the two stable ionic conformers, **1a** and **1b**. They are closely similar in energy and could be classified as **1**(C) and **1**(T), but the notation c/t loses its meaning because the optimized geometries of the model chemistries have ϕ_2 = ~90°. However, this is not the case with the neutral conformers **1N**. Here, see Fig. 2.1 (bottom part), four stable conformers were identified, **1N**(Cc), **1N**(Ct), **1N**(Tc) and **1N**(Tt), of which the **1N**(Cc) conformer is considerably more stable because of internal hydrogen bridging. It is this hydrogen bridged conformer that has been identified as the prevailing species in the IR and microwave studies of gaseous glycolaldehyde [16b,c].

The calculations of Ref. 19 could not provide a value for the heat of formation of ion **1** and therefore a value was adopted from experimental obeservations that served as the anchor point in their mechanistic study of the decarbonylation of the ion, which will be addressed below. The value adopted was ΔH_f **1** = 162.5 kcal/mol, from IE **1N** = 10.26 ± 0.03 eV [19b] and ΔH_f **1N** = −74 kcal/mol. The latter value is an estimate based upon Benson's Group Additivity approach [20], using C-$(H)_2(O)(CO)$ = −7.0 kcal/mol [20a]. In this context, we note that a recent (re)evaluation of the thermochemical properties of the ions [17] proposes a lower value, ΔH_f **1** = 157.5 kcal/mol from IE **1N** = 10.20 ± 0.10 eV [3a] and ΔH_f **1N** = −77.5 kcal/mol, a number derived from a G2 calculation because the Benson approach does not acount for internal hydrogen bridging. However, see Table 1 Appendix, this revised ΔH_f **1** = 157.5 kcal/mol value is still a little higher (~3 kcal/mol) than the CBS-QB3 and APNO values derived for the two conformers. For conformer **1N**(Cc), the CBS-QB3 method predicts an adiabatic ionization energy (IEa) of 10.06 eV, a little below the IE values of 10.26 and 10.20 eV. These IE values are deemed to be satisfactory IEa values, provided that the IEv – IEa difference is less than ~0.3 eV, because in general the cross section for electron ionization falls quite rapidly away from the Franck-Condon (vertical) region [17]. A computational estimate (from the B3LYP energies) of IEv for **1N**(Cc) yields ~10.6 eV and this suggests that the experimental IE's may not be true adiabatic values.

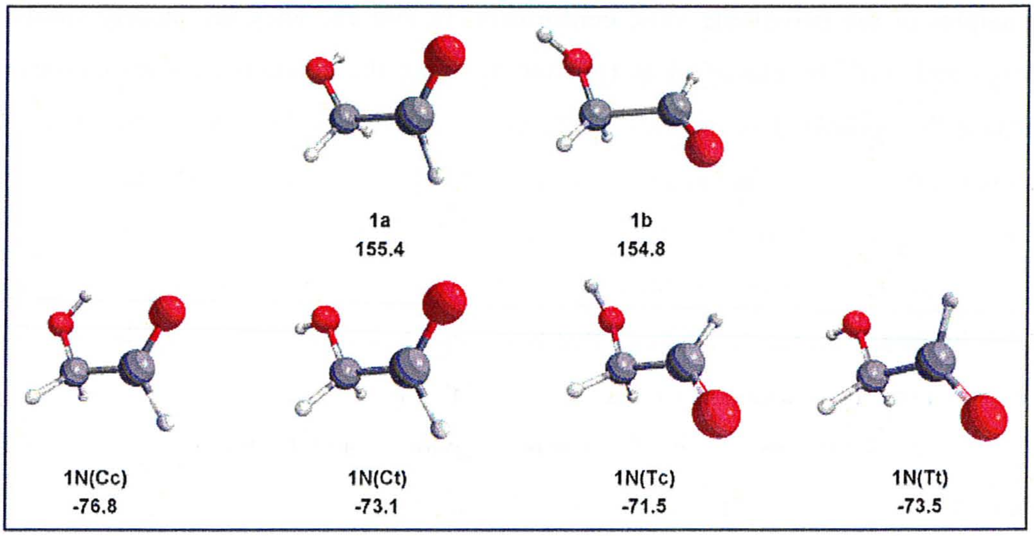

Figure 2.1. Stable conformers of ionized and neutral glycolaldehyde and their 298 K enthalpies of formation derived from CBS-QB3 calculations.

3.1.2. The dissociation chemistry of low energy glycolaldehyde ions.

Decarbonylation is the only dissociation observed for low-energy (metastable) glycolaldehyde radical cations **1**. The metastable peak for this reaction is associated with a very small kinetic energy release ($T_{0.5}$ = 1.5 meV), indicating that the reaction takes place at the thermochemical threshold [17].

Experiment and theory [21] agree that the resulting *m/z* 32 product ion is the distonic ion $CH_2OH_2^{\bullet+}$ rather than ionized methanol, $CH_3OH^{\bullet+}$. Experiments show that isomerization of ion **1** into $CH_3OCHO^{\bullet+}$, the enol ions $HOCH{=}CHOH^{\bullet+}$ and $CH_2{=}C(OH)_2^{\bullet+}$,or the ketene-water ion-dipole complex $H_2O/CH_2{=}C{=}O^{\bullet+}$ clearly does not occur : the CID mass spectra of the respective species [19,22] are characteristically different. Moreover, $CH_3OCHO^{\bullet+}$ decarbonylates into $CH_3OH^{\bullet+}$ [22c], which is easily differentiated from $CH_2OH_2^{\bullet+}$ on the basis of their CID mass spectra [17,21a]. In the same vein, the metastable ions of both 1,1- and 1,2-dihydroxyethene and the ketene-water ion-dipole complex abundantly lose water (and not CO) [22].

The computational study of Postma et al. [19] considered two mechanistic proposals for the loss of CO from ion **1**. The proposed mechanism is shown below in Scheme 2.2, where all relative energies are presented in kcal/mol.

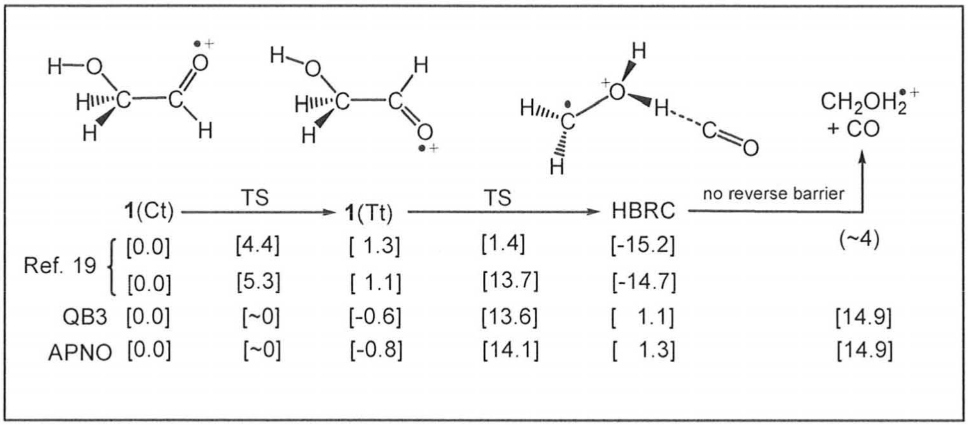

Scheme 2.2. Proposed mechanism for the decarbonylation of ionized glycolaldehyde (**1**). The CBS-QB3 and APNO relative energies were taken from the $\Delta_fH^0_{298}$ values in Tables 1 and 4; **1**(Ct) = **1a**; **1**(Tt) = **1b**.

The mechanism basically involves a 1,3-H shift in **1**(T) which leads to an HBRC, a hydrogen bridged radical cation [23] with a C-H-O bridge from which CO may be lost in a continuously endothermic reaction. The overall energy requirement for this process proposed in Ref. 19 is based upon the Pople-corrected SDCI/6-31G** numbers of the top row of Scheme 2.2 (the second row represents the RHF/6-31G** energies for comparison) which would agree with the difference between the measured values of IE **1** and the AE [$CH_2OH_2^{\bullet+}$] derived therefrom [21a], 3.5 ± 1 kcal/mol. However, this agreement may be entirely fortuitous, considering the discussion of the previous section and the CBS-QB3/APNO results of Scheme 2.2, which leave little doubt that the barrier to the 1,3-H shift is substantial and that **1** and its C-H-O bridged HBRC are comparable in energy.

One point deserves further comment. The reported AE [$CH_2OH_2^{\bullet+}$] from $HOCH_2CHO$ (**1N**) is 10.42 ± 0.05 eV [19,22a] and considering that :

$$AE\,[CH_2OH_2^{\bullet+}] = \Delta_fH^0\,[CH_2OH_2^{\bullet+}] + \Delta_fH^0\,[CO] - \Delta_fH^0\,[HOCH_2CHO]$$

one obtains, using Δ_fH^0 values for CO and **1N** of –26.4 and –76.8 kcal/mol respectively, Δ_fH^0 [$CH_2OH_2^{\bullet+}$] = 190 kcal/mol. A more recent measurement [3a] yields AE [$CH_2OH_2^{\bullet+}$] = 10.51 ± 0.19 eV, which translates into Δ_fH^0 [$CH_2OH_2^{\bullet+}$] = 192 kcal/mol. These values are lower than the recommended (experimentally derived) value of Ref. 17, 195 kcal/mol, and also our CBS-QB3 and APNO values of 196.9 and 195.6 kcal/mol respectively.

It is conceivable that the discrepancy between the derived $\Delta_f H^0_{298}$ values arises from differences in the thermochemical treatment of the appearance energies [24,17] : applying the Traeger-McLoughlin correction term, $\Delta H_{corr} = \Delta H_{298}$ ($CH_2OH_2^{\bullet+}$ + H_2O) – 1.48 kcal/mol, raises the AE derived $\Delta_f H^0_{298}$ values by 3.5 kcal/mol (using the ΔH_{298} values available from the CBS-QB3 calculations). This correction holds rigorously if all the available internal energy of the precursor ion is used for dissociation, which is, the products are formed at 0 K. The actual thermal content of the products is not known and hence, the correction term only provides an upper limit to the derived enthalpy.

3.2 The dissociation chemistry of the 1,2-dihydroxyethene cation (2)

The stable conformers of $HOCH{=}CHOH^{\bullet+}$ (**2a-f**) are shown in Fig. 2.3.

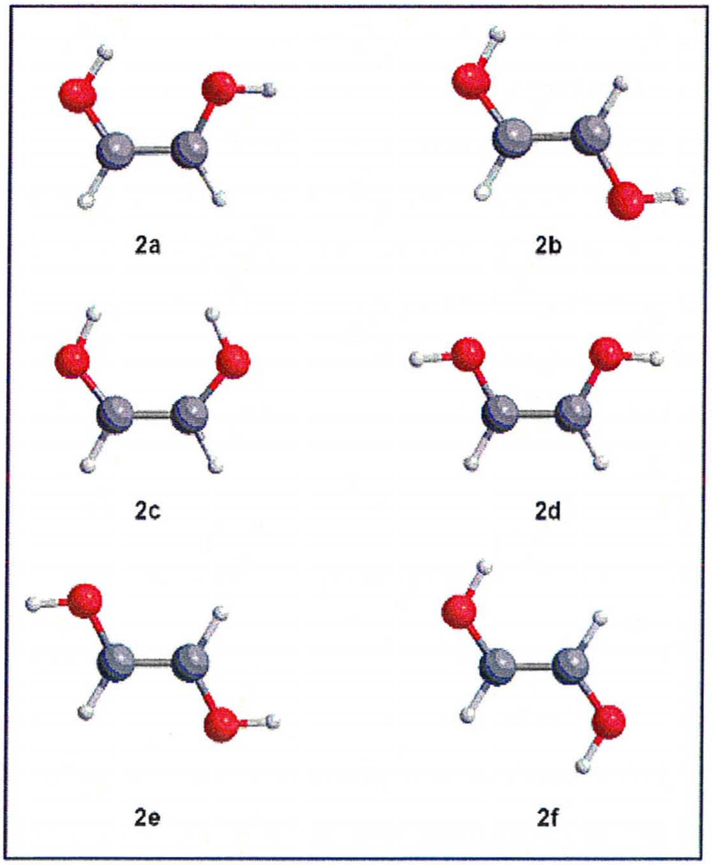

Figure 2.3. CBS-QB3 structures for conformers of $HOCH{=}CHOH^{\bullet+}$

Of these, the two *cis* conformers **2a** and **2d** have the same low enthalpy of formation as the *trans* conformer **2e**, 124.5 kcal/mol (APNO Table 1). The enthalpy lies only ~2 kcal/mol above that of the $CH_2{=}C(OH)_2^{\bullet+}$ isomer, which represents the global minimum on the $C_2H_4O_2^{\bullet+}$ potential energy surface.

Not surprisingly, a substantial barrier (~35 kcal/mol) is found for the *cis-trans* interconversion but exploratory calculations indicate that 1,2-, 1,3- or 1,4-H-shifts require much more energy (~60 kcal/mol). This makes it unlikely that the MI or CID characteristics of the *cis*- and *trans*-type ions **2** will be different.

A pioneering study by Terlouw et al. [22] reports that metastable ions **2** lose H_2O. The resulting broad *m/z* 42 peak in the MI mass spectrum is a composite consisting of a broad and a narrow component in a 5:1 ratio with estimated $T_{0.5}$ values for the two components of 20 and 390 meV respectively. A mechanistic proposal for the loss of H_2O from ion **2** has not been reported. Pathways for the loss of H_2O from ion **2a** were therefore explored using computational chemistry. Scheme 2.4 shows our proposed mechanism for the loss of water from ion **2a**.

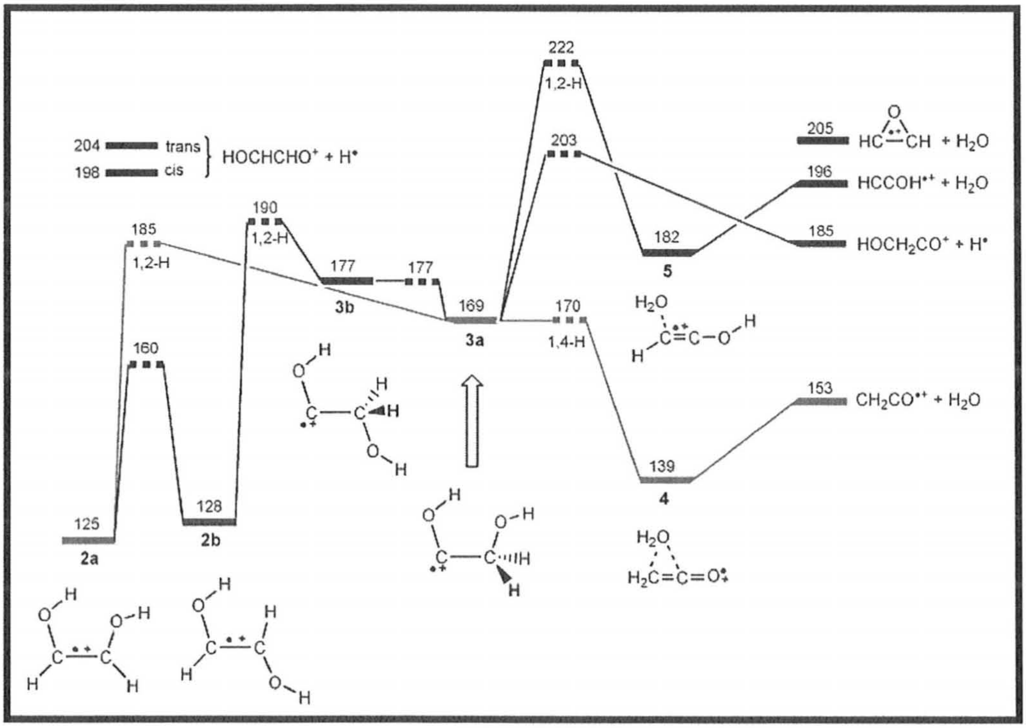

Scheme 2.4. CBS-QB3 derived energy level diagram describing the possible dissociation reactions of ionized 1,2-dihydroxyethene (**2**). All values refer to $\Delta_fH^0_{298}$ values in kcal/mol.

The reaction involves a 1,2-H shift to yield ion **3a**, followed by the loss of water to generate ionized ketene, which represents by far the most stable isomer on the $C_2H_2O_2$ potential energy surface. As seen in Scheme 2.4, the ketene-water ion-dipole complex **4** is generated via the carbene ion **3** as a stable intermediate in this pathway prior to water loss. However, the composite peak observed by Terlouw and co-workers [22] shows that there is more than one mechanism for the water loss from **2**. The alternate reaction that would best explain the composite nature of this peak is, at this point, unclear.

We therefore repeated the experiment reported in Ref. 22a : ion **2** was generated by dissociative ionization of glyceraldehyde. As reported, a composite peak is observed at *m/z* 42. One may envisage that the broad and narrow components of this peak correspond to the generation of different ionic $C_2H_2O_2$ isomers. To probe this question, we selectively investigated the two components of the peak by acquiring their respective CID mass spectra. The CID spectra obtained from the center of the peak (narrow component) and the shoulders (broad component) of the composite peak are shown in Figs. 2.5a and 2.5b.

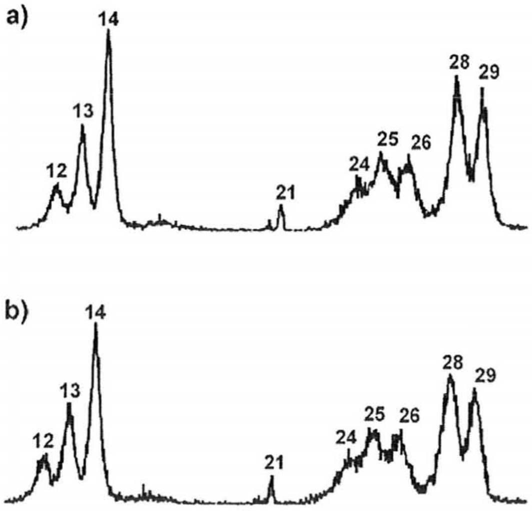

Figure 2.5. 3ffr CID mass spectra of (a) the center (narrow component) and (b) the shoulders (broad component) of the *m/z* 42 CID peak generated from ion **2**. The figure shows the structure diagnostic *m/z* 12-29 region of the spectra.

It is seen that the spectra are virtually identical and, not surprisingly, they are very close to a reference spectrum of the ketene ion rather than its hydroxyacetylene or oxirene isomers [17]. This observation leaves little doubt that the composite peak is indicative of two reaction pathways generating the same product ion, ionized ketene (*m/z* 42). We have explored several pathways for water loss other than the one proposed in Scheme 2.4, but have not (yet) been able to find a satisfactory alternative.

In this context we note that all three precursor molecules used to generate ion **2** (see Experimental) yield the same composite peak at *m/z* 42 in their *m/z* 60 MI spectra. Further, the CID mass spectra of the *m/z* 60 ions generated from glyceraldehyde and the γ-lactone are closely similar ; that derived from the 1,4-dioxane-2,3-diol precursor contains an additional peak at *m/z* 32 which points to the co-generation of the distonic isomer $CH_2O\text{-}C(H)OH^{\bullet+}$.

3.3. The reaction of the glycolaldehyde radical cation (1) with H_2O

The energy diagram of Scheme 2.6 provides a summary of the CBS-QB3 calculations on the ion-molecule reaction of ionized glycolaldehyde (**1**) with H_2O.

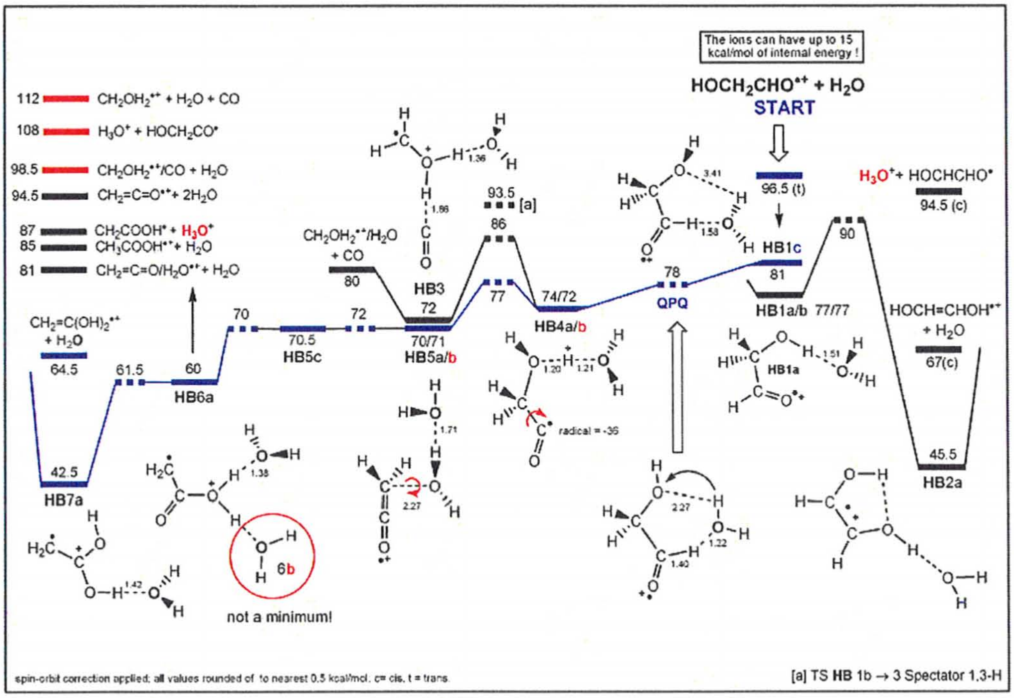

Scheme 2.6. CBS-QB3 derived energy level diagram describing the reaction of the glycolaldehyde radical cation **1** with H_2O. All values refer to $\Delta_fH^0_{298}$ values in kcal/mol.

The calculations indicate that **1** interacts with a single H_2O molecule to generate the very stable hydrogen-bridged radical cation **HB**1.

The resulting species is stabilized by ~20 kcal/mol with respect to the combined enthalpies of **1** + H_2O.

The calculations of Section 3.1 indicate that the energy requirement for the decarbonylation of solitary ions **1** is lower than that for the back-dissociation reaction, **HB**1 → **1** + H_2O. Indeed, the calculations of Scheme 2.6 show that the 1,3-H shift reaction, **HB**1 → 3, lies about 3 kcal/mol below the combined enthalpies of **1** + H_2O. Thus, the decarbonylation of **HB**1 is energetically feasible. A further question to consider is whether H_2O plays a role in the decarbonylation reaction. The H_2O molecule may act as a base (B) and accept the aldehyde proton of the $HOCH_2CHO^{\bullet+}$ substrate, and then donate it back to the hydroxyl oxygen as illustrated in Eq. 1.

$HOCH_2CHO^{\bullet+} + H_2O \rightarrow [HOCH_2C(O)\bullet\bullet\bullet H\bullet\bullet\bullet OH_2]^{\bullet+} \rightarrow H_2OCH_2C{=}O^{\bullet+} + H_2O$ (Eq. 1)

This type of reaction has been coined proton-transport catalysis (PTC) [10].

Criteria for successful PTC have been developed by Radom and co-workers [24], the most important of which states that a smooth isomerization for the reaction of Eq. 1 occurs if the proton affinity (PA) of B lies between the PA of the carbonyl carbon (donor) and that of the hydroxyl oxygen (acceptor) of the $HOCH_2C{=}O^{\bullet}$ radical. CBS-QB3 calculations show the PA of the respective donor and acceptor sites to be 175 and 169 kcal/mol.

While H_2O appears not to be an ideal catalyst (PA = 164 kcal/mol), our calculations, see Scheme 2.6, reveal that **HB**1 ions can communicate with the more stable **HB**4 ions, via a TS at only 78 kcal/mol. This reaction involves the abstraction of a proton from the CHO moiety of the glycolaldehyde ion by the H_2O molecule followed by a back-donation of another proton from the protonated base, a so called *quid-pro-quo* (QPQ) reaction. The resulting **HB**4 ions then undergo decarbonylation. The TS for this water assisted decarbonylation of ion **1** lies at 86 kcal/mol, c. 10 kcal/mol below the combined enthalpies of **1** + H_2O.

However, the theoretical findings of Scheme 2.6 indicate that the **HB**4 ions can also isomerize into **HB**5 ions, via an activated complex at 77 kcal/mol. Ion **HB**5 represents a ketene-water complex ion stabilized by a second H_2O molecule. A combined experimental and theoretical study by Bohme and co-workers [12] has shown that the second H_2O molecule in this complex serves as a catalyst for the transformation of ionized ketene-water into $CH_2=C(OH)_2^{\bullet+}$, the ionized enol of acetic acid. In line with this, Scheme 2.6 shows that ions **HB**5 ions may indeed undergo an association reaction to generate **HB**6 ions without a significant barrier. Thereafter, a rotation about the C-OH_2 bond via a small barrier of 1.5 kcal/mol yields a favorable geometry for the H_2O molecule to catalyze the tranformation of $CH_2C(=O)OH_2^{\bullet+}$ into $CH_2=C(OH)_2^{\bullet+}$. The overall rearrangement of the H_2O stabilized ketene-water complex ion (**HB**5) into the enol ion of acetic acid (**HB**7) proceeds downhill energetically. Loss of H_2O by a simple O-H-O bond elongation in **HB**7 yields the lowest energy threshold for the dissociation reaction, $CH_2=C(OH)_2^{\bullet+} + H_2O$.

Finally, the catalyzed 1,3-H shift converting **HB**1 into an HBRC involving ionized 1,2-dihydroxyethene (**HB**2) was found to be associated with a transition state that lies c. 6 kcal/mol below the combined enthalpies of **1** + H_2O. Despite lowering the unassisted barrier from c. 32 kcal/mol to a mere 13 kcal/mol, the associated transition state lies well above the barrier leading to **HB**7. Therefore, the generation of ionized 1,2-dihydroxyethene from ionized glycolaldehyde in the presence of water, while energetically feasible, is not likely to compete with $CH_2=C(OH)_2^{\bullet+}$ formation.

The studies of Bohme and co-workers [12] also considered that **HB**7 may rearrange into a $CH_3COOH^{\bullet+}/H_2O$ complex (**HB**8). Our theoretical findings on this reaction are shown in Scheme 2.7. The CBS-QB3 model chemistry shows two different PTC mechanisms corresponding to the interconversion, **HB**7 → 8. The transition state at 83 kcal/mol refers to a H_2O catalyzed 1,3-H shift, whereby the proton that is abstracted is the same that is donated back. In contrast, the activated complex at 78 kcal/mol refers to a mechanism involving the abstraction of a proton by H_2O from the hydroxyl O followed by the back-donation of another proton by the protonated base to the methylene C. This type of mechanism is also known as the *quid-pro-quo* (QPQ) mechanism. However, both routes are associated with energy barriers significantly higher than the dissociation threshold, **HB**7 → $CH_2=C(OH)_2^{\bullet+} + H_2O$.

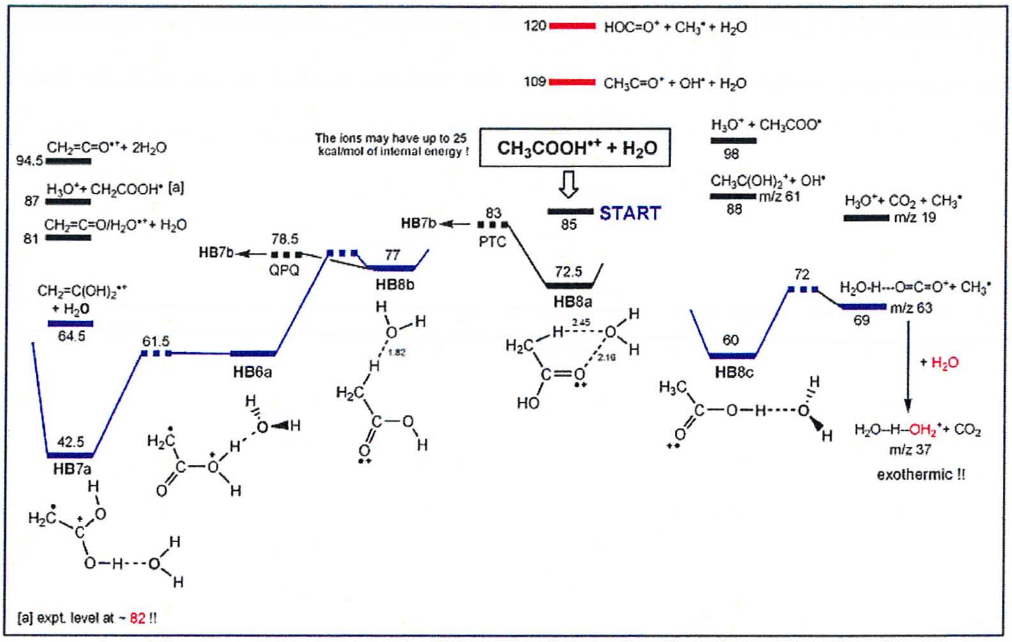

Scheme 2.7. CBS-QB3 derived energy level diagram describing the generation of acetic acid in the presence of a water molecule. All values refer to $\Delta_fH^0_{298}$ values in kcal/mol.

We have also explored the possibility that **HB6** is tranformed into **HB8**. Computational results revealed this transformation to be yet another example of a QPQ mechanism. Scheme 2.7 shows the pertinent transition state to lie at 78 kcal/mol. This is comparatively higher in energy than the barrier associated with the **HB6** → 7 rearrangement and its subsequent dissociation. Thus, theory predicts that we are likely to experimentally observe the ionized enol of acetic acid in complex with water (**HB7**) as a product of the ion-molecule reaction of the glycolaldehyde cation with water.

Finally we note that Scheme 2.7 predicts that in the ion-molecule reaction of ionized acetic acid with water, the formation of the HBRC $H_2O\text{-}H{\bullet\bullet\bullet}O{=}C{=}O^{\bullet+}$ (*m/z* 63 ions) is energetically quite attractive.

3.4. Experimental approach to observe the ion-molecule reaction of ion 1.

As described in the Experimental section, we have attempted to perform the ion-molecule reaction of ionized glycolaldehyde with water under chemical ionization (CI) conditions, using CO_2 as the bath gas for collisional stabilization. Although this approach has been successful in many other PTC studies using a variety of catalysts [10], the desired HBRC of glycolaldehyde and water could not be generated in a sufficiently large yield to permit further experiments in the field free regions of the instrument. Instead, we observed a very intense signal at *m/z* 61, corresponding to the protonated glycolaldehyde, in the conventional CI mass spectrum. The reason for this observation is best explained by considering the ionization energies (IE) of the H_2O catalyst and the CO_2 bath gas. The IE of H_2O is lower than that of CO_2 (12.6 vs. 13.8 eV), so that upon electron ionization of CO_2 in the source, $H_2O^{\bullet+}$ ions are easily generated by charge-exchange. As the pressure of H_2O is relatively higher than that of gaseous glycolaldehyde, the reaction $H_2O^{\bullet+} + H_2O \rightarrow H_3O^+ + OH^\bullet$ ($\Delta H_{298} = -23$ kcal/mol), readily takes place. The PA of H_2O is much lower than that of glycolaldehyde (164 vs. 181 kcal/mol), so that, given the supreme acidic strength of H_3O^+, neutral glycolaldehyde is swiftly protonated yielding the peak at *m/z* 61. As the glycolaldehyde radical cation is hardly generated, the desired ion-molecule reaction with H_2O is not observed. To circumvent this problem, the ion-molecule reaction of *mass selected* glycolaldehyde ions with neutral water is currently being studied using the Mons AutoSpec 6F mass spectrometer. This approach was quite successful in a recent study of the H_2O catalyzed isomerization of the cyanamide ion [25].

Conclusions

Our CBS-QB3/APNO based computational analysis of the ion-molecule reactions of $HOCH_2CHO^{\bullet+}$ and $CH_3COOH^{\bullet+}$ with H_2O indicates that :

(i) enolization of $HOCH_2CHO^{\bullet+}$ into $HOCH{=}CHOH^{\bullet+}$ by PTC is energetically possible but less favourable than (ii); (ii) a tandem PTC mechanism involving the ketene-water ion-dipole complex $H_2O/CH_2{=}C{=}O^{\bullet+}$ as a key intermediate, leads to a smooth transformation of $HOCH_2CHO^{\bullet+}$ into the $CH_2{=}C(OH)_2^{\bullet+}$ ion, which represents the global minimum on the $C_2H_4O_2^{\bullet+}$ potential energy surface. The co-generation of $CH_3COOH^{\bullet+}$ is very unlikely since all PTC transition states explored lie well above the dissociation threshold of $CH_2{=}C(OH)_2^{\bullet+} + H_2O$; (iii) the ion-molecule reaction $CH_3COOH^{\bullet+} + H_2O$ may lead to enolization of the acetic acid ion, but the formation of the HBRC H_2O-$H{\bullet\bullet\bullet}O{=}C{=}O^{\bullet+}$ (*m/z* 63 ions) is energetically more attractive.

References

[1] Y.N. Lee, X. Zhou, K. Hallock. J. Geophys. Res. 100 (1995) 25933.

[2] (a) J.M. Hollis, F.J. Lovas, P.R. Jewell. Astrophys. J. 540 (2000) L107; (b) R.A.H. Butler, F.C. De Lucia, D.T. Petkie, H. Møllendal, A. Horn, E. Herbst. Astrophys. J. Suppl. Series 134 (2001) 319.

[3] (a) C.J. Bennett, R.I. Kaiser. Astrophys. J. 661 (2007) 899; (b) A.F. Jalbout, L. Abrell, L. Adamowicz, R. Polt, A.J. Apponi, L.M. Ziury. Astrobiology. 7 (2007) 433; (c) R.L. Hudson, M.H. Moore, A.M. Cook. Adv. Space Res. 36 (2005) 184; (e) S. Ptasinska, S. Denifl, P. Scheier, D.M. Tilmann. Int. J. Mass Spectrom. 243 (2005) 171; (f) G. Bouchoux, F. Penaud-Berruyer, W. Bertrand. Eur. J. Mass Spectrom. 7 (2001) 351; (g) F.J. Lovas, R.D. Suenram, D.F. Plusquellic, H. Møllendal. J. Mol. Spectrosc. 222 (2003) 263; (h) S. Ptasinska, P. Limao-Vieira, S. Denifl, P. Scheier, T.D. Märk. Chem. Phys. Lett. 401 (2005) 227.

[4] L.E. Snyder. Proc. Natl. Acad. Sci. 103 (2006) 12243.

[5] A. Horn, H. Møllendal, O. Sekiguchi, E. Uggerud, H. Roberts, E. Herbst, A.A. Viggiano, T.D. Fridgen. Astrophys. J. 611 (2004) 605.

[6] T.J. Millar, G.H. Macdonald, A.G. Gibb. Astron. Astrophys. 32 (1997) 1163.

[7] A. Nummelin, P. Bergman, Å. Hjalmarson, P. Friberg, W.M. Irvine, T.J. Millar, M. Ohishi, S. Saito. ApJS. 128 (2000) 213.

[8] D.M. Mehringer, L.E. Snyder, Y. Miao, F.J. Lovas. ApJ. 480 (1997) L71.

[9] K.J. Jobst, P.J.A. Ruttink, J.K. Terlouw. Int. J. Mass. Spectrom. 269 (2008) 165.

[10] (a) C.Y, Wong, P.J.A. Ruttink, P.C. Burgers, J.K. Terlouw. Chem. Phys. Lett. 390 (2004) 176; ibid. Chem. Phys. Lett. 387 (2004) 204; (b) R. Lee, P.J.A. Ruttink, P.C. Burgers, J.K. Terlouw. Int. J. Mass Spectrom. 255/256 (2005) 244 and references cited therein.

[11] A.C. Cheung, D.M. Rank, C.H. Townes, D.D. Thornton, W.J. Welch. Nature. 221 (1969) 626.

[12] G. Orlova, V. Blagojevic, D.K. Bohme. J. Phys. Chem. 110 (2006) 8266.

[13] M.J. Frisch et al., GAUSSIAN 03 (Rev. C.02 and D.01), Gaussian Inc., Wallingford, CT, 2004.

[14] (a) J.A. Montgomery Jr., M.J. Frisch, J.W. Ochterski, G.A. Petersson, J. Chem. Phys. 112 (2000) 6532; (b) J.W. Ochterski, G.A. Petersson, J.A. Montgomery Jr., J. Chem. Phys. 104 (1996) 2598.

[15] H.F. van Garderen, P.J.A. Ruttink, P.C. Burgers, G.A. McGibbon, J.K. Terlouw. Int. J. Mass Spectrom. Ion Processes. 121 (1992) 159.

[16] (a) Y. Kobayashi, H. Takahara, H. Takahashi, K. Higasi. J. Mol. Struct. 32 (1976) 235; (b) H. Michelsen, P. Klaboe. J. Mol. Struct. 4 (1969) 293; (c) K. Marstokk, H. Møllendal. J. Mol. Struct. 5 (1970) 205; (d) E.F.H. Brittain, W.O. George, G.C.S. Collins. J. Chem. Soc. (B) 1971 2414 ; (e) V.A. Yaylayan, S. Harty-Majors, A. Ismail. Carbohydr. Res. 309 (1998) 31.

[17] J.L. Holmes, C. Aubry, P.M. Mayer. *Assigning Structures to Ions in Mass Spectrometry*, CRC Press, Boca Raton (2007).

[18] K.J. Jobst, J. De Winter, R. Flammang, J.K. Terlouw, P. Gerbaux. Int. J. Mass Spectrom. 286 (2009) 83..

[19] (a) R. Postma, P.J.A. Ruttink, J.H. Van Lenthe, J.K. Terlouw. Chem. Phys. Lett. 156 (1989) 245; (b) IE quoted in (a) measured by the late Dr. F.P. Lossing, using energy selected electrons.

[20] (a) S.W. Benson, F.R. Cruickshank, D.M. Golden, G.R. Haugen, H.E. O'Neal, A.S. Rogers, R. Shaw, R. Walsh. Chem. Rev. 69 (1969) 279; (b) J.L. Holmes, K.J. Jobst, J.K. Terlouw. Eur. J. Mass Spectrom. 15 (2009) 261.

[21] (a) J.L. Holmes, F.P. Lossing, J.K. Terlouw, P.C. Burgers. J. Am. Chem. Soc. 104 (1982) 2931; (b) W.J. Bouma, R.H. Nobes, L. Radom. J. Am. Chem. Soc. 104 (1982) 2929.

[22] (a) J.K. Terlouw, C.G. de Koster, W. Heerma, J.L. Holmes, P.C. Burgers. Org. Mass Spectrom. 18 (1983) 222; (b) R. Postma, P.J.A Ruttink, J.K. Terlouw, J.L. Holmes. J. Chem. Soc. Chem. Commun. (1986) 683; (c) N. Heinrich, T. Drewello, P.C. Burgers, J.C. Morrow, J. Schmidt, W. Kulik, J.K. Terlouw, H. Schwarz. J. Am. Chem. Soc. 114 (1992) 3776.

[23] P.C. Burgers, J.K. Terlouw In: N.M.M. Nibbering, Editor, *Encyclopedia of Mass Spectrometry* **vol** 4, Elsevier, Amsterdam (2005), p. 173.

[24] R.Lee, P.J.A. Ruttink, P.C. Burgers, J.K. Terlouw. Can. J. Chem. 83 (2005) 1847.

[25] J.W. Gauld, L. Radom, J. Am. Chem. Soc. 119 (1997) 9831.

[26] K.J. Jobst, P. Gerbaux, G. Dimopoulos-Italiano, P.J.A. Ruttink, Chem. Phys. Lett. 478 (2009) 144

Appendix to Chapter 2

Table 1. Energetic data [a] derived from CBS-QB3 and APNO calculations for minima of stable ionic isomers of glycolaldehyde (**1**) and 1,2-dihydroxyethene (**2**), and their connecting transition states.

Ionic species	**CBS-QB3 E(total)** [0K]	**QB3 ZPE**	**QB3 $\Delta_fH^0_0$**	**QB3 $\Delta_fH^0_{298}$**	**APNO $\Delta_fH^0_{298}$**
1a	-228.353126	36.5	158.2	155.4	154.6
1b	-228.353918	36.7	157.7	154.8	153.8
2a	-228.400275	39.1	128.6	125.2	124.6
2b	-228.395607	38.9	131.5	128.3	127.5
2c	-228.386508	38.7	137.2	134.1	133.3
2d	-228.400191	39.1	128.6	125.3	124.6
2e	-228.400609	38.9	128.4	125.1	124.5
2f	-228.391673	38.9	134.0	130.7	129.9
3a	-228.330960	37.0	172.1	169.1	168.8
3b	-228.318833	36.3	179.7	176.9	176.7
4	-228.380260	35.0	141.2	139.1	136.7
5	-228.312252	35.6	183.8	181.6	[b]
TS **1b** → ***m/z* 32** [c]	-228.331675	33.5	171.6	169.0	168.7
TS **2a** → **2b**	-228.344917	37.2	163.3	160.0	159.8
TS **2a** → **3a**	-228.304658	35.1	188.6	185.3	184.4
TS **2b** → **3b**	-228.297261	34.9	193.2	190.0	189.0
TS **3a** → **3b**	-228.317948	36.6	180.3	176.9	176.9
TS **3a** → **4**	-228.328253	35.5	173.8	170.3	168.2
TS **3a** → **5**	-228.246888	33.4	224.8	221.9	220.7
TS **3a** → ***m/z* 59**	-228.277184	31.3	205.8	203.3	202.8
Neutral species					
1N(Cc)	-228.722436	37.8	-73.6	-76.8	-
1N(Ct)	-228.716915	37.6	-70.1	-73.1	-
1N(Tc)	-228.714345	37.5	-68.5	-71.5	-
1N(Tt)	-228.717689	37.3	-70.6	-73.5	-

[a] $E_{(total)}$ in Hartrees, all other components, including the ZPE scaled by 0.99, are in kcal/mol.
[b] The desired geometry could not be found; [c] The TS leads to the HBRC $[CH_2O(H)\text{-}H\text{--}CO]^{\bullet+}$

Table 2. Energetic data for various dissociation products of ionized glycolaldehyde (**1**) and 1,2-dihydroxyethene (**2**) derived from CBS-QB3 and APNO calculations [a].

Species	*m/z*	**CBS-QB3** **E(total)** [0 K]	**QB3** **$\Delta_fH^0_0$**	**QB3** **$\Delta_fH^0_{298}$**	**APNO** **$\Delta_fH^0_{298}$**
$HOCHCHO^+$ (cis) + $H^\bullet$	**59**	-	**199.8**	**197.8**	**198.1**
$HOCHCHO^+$ (trans) + $H^\bullet$		-	**205.9**	**204.2**	**204.5**
$HOCH_2CO^+$ + $H^\bullet$		-	**186.2**	**184.5**	**184.3**
$HOCHCHO^+$ (cis)		-227.787015	148.2	145.7	146.0
$HOCHCHO^+$ (trans)		-227.777293	154.3	152.1	152.4
$HOCH_2CO^+$		-227.808662	134.6	132.4	132.2
$H^\bullet$		-0.499818	51.6	52.1	52.1
$CH_2CO^{\bullet+}$ + H_2O	**42**	-	**154.1**	**152.6**	**152.2**
$HCCOH^{\bullet+}$ + H_2O		-	**198.4**	**197.1**	**196.2**
$HCOCH^{\bullet+}$ (Δ) + H_2O		-	**208.3**	**206.7**	**206.0**
$CH_2CO^{\bullet+}$		-152.022176	211.4	210.6	209.7
$HCCOH^{\bullet+}$		-151.951494	255.7	255.1	253.7
$HCOCH^{\bullet+}$ (Δ)		-151.935819	265.6	264.7	263.5
H_2O		-76.337491	-57.3	-58.0	-57.5
$CH_2OH_2^{\bullet+}$ + CO	**32**	-	**171.9**	**170.3**	**169.5**
$CH_2OH_2^{\bullet+}$		-115.149226	199.3	196.9	195.6
CO		-113.182008	-27.4	-26.6	-26.1

[a] $E_{(total)}$ in Hartrees, all other components, including the ZPE scaled by 0.99, are in kcal/mol.

Table 3. Energetic data [a] derived from CBS-QB3/APNO calculations for minima and connecting transition states of ionic isomers of the complexes of glycolaldehyde with H_2O (**HB**).

Ionic species	CBS-QB3 E(total) [0K]	QB3 ZPE	QB3 $\Delta_fH^0_0$	QB3 $\Delta_fH^0_{298}$	APNO $\Delta_fH^0_{298}$
HB1a	-304.721663	51.6	81.4	77.3	76.5
HB1b	-304.722323	51.9	81.0	76.9	76.1
HB1c	-304.716018	51.3	84.9	80.9	
HB2a	-304.771773	54.1	50.0	45.4	44.9
HB2b	-304.762749	54.3	55.6	50.9	50.3
HB3	-304.731257	49.4	75.4	72.2	72.0
HB4a	-304.726583	51.2	78.3	74.1	74.1
HB4b	-304.729900	52.6	76.2	71.7	71.4
HB5a	-304.733652	51.2	73.9	70.3	
HB5b	-304.731950	51.2	74.9	71.3	
HB5c	-304.733716	49.3	73.8	70.6	69.3
HB6a	-304.748960	51.2	64.3	60.0	58.8
HB7a	-304.776549	52.4	47.0	42.6	41.9
HB7b	-304.778105	53.2	46.0	41.3	40.5
HB8a	-304.728925	53.4	76.8	72.4	71.0
HB8b	-304.722348	51.7	81.0	76.8	
HB8c	-304.749000	51.5	64.2	59.9	59.4
TS **HB**1a → 1b	-304.721495	51.6	81.5	77.0	74.9
TS **HB**1a → 2a	-304.701494	49.7	94.1	89.4	[b]
TS **HB**1b → 2b	-304.698317	49.6	96.1	91.4	91.6
TS **HB**1b → 3	-304.696512	48.0	97.2	93.4	92.9
TS **HB**1c → 4a	-304.718755	50.0	83.2	78.5	78.1
TS **HB**3 → 4a	-304.707745	49.6	90.1	86.2	85.2
TS **HB**3 → 4b	-304.707640	49.8	90.2	86.0	
TS **HB**4a → 4b	-304.720579	51.8	82.1	77.4	76.9
TS **HB**4a → 5a	-304.711268	51.3	87.9	83.6	82.4
TS **HB**4b → 5a	-304.721393	51.6	81.6	77.3	76.1
TS **HB**5a → 5b	-304.731628	51.1	75.1	71.0	
TS **HB**5b → 5c	-304.731117	49.7	75.5	71.9	
TS **HB**5c → 6a	-304.734535	49.7	73.3	69.8	
TS **HB**6a → 7a	-304.746122	51.0	66.1	61.5	60.4
TS **HB**6a → 8b	-304.718261	50.0	83.5	78.7	
TS **HB**7b → 8a **(PTC)**	-304.711540	49.2	87.8	83.1	
TS **HB**7b → 8b **(QPQ)**	-304.718918	51.4	83.1	78.3	
TS **HB**8c → *m/z* 45	-304.729757	49.3	76.3	72.4	71.1

[a] $E_{(total)}$ in Hartrees, all other components, including the ZPE scaled by 0.99, are in kcal/mol. [b] The desired transition states could not be found.

Table 4a. Energetic data for various dissociation products of the complex of ionized glycolaldehyde with H_2O (**HB**) derived from CBS-QB3 calculations [a].

Species	*m/z*	**CBS-QB3 E(total)** [0 K]	**QB3 $\Delta_fH^0_0$**	**QB3 $\Delta_fH^0_{298}$**	**APNO $\Delta_fH^0_{298}$**
$CO_2/H_3O^+ + CH_3^\bullet$	**63**	-	**71.9**	**69.1**	**68.7**
CO_2/H_3O^+		-264.991894	35.6	33.5	34.2
$CH_3^\bullet$		-39.744795	36.3	35.6	34.5
$CH_3C(OH)_2^+ + OH^\bullet$	**61**	-	**91.9**	**87.9**	**87.3**
$CH_3C(OH)_2^+$		-229.055166	82.9	78.9	78.0
$OH^\bullet$		-75.649720	9.0	9.0	9.3
$HOCHCHOH^{\bullet+}$ (cis) + H_2O	**60**	-	**71.3**	**67.2**	**67.1**
$HOCHCHOH^{\bullet+}$ (trans) + H_2O		-	**76.7**	**72.7**	**72.4**
$HOCH_2CHO^{\bullet+}$ (cis) + H_2O		-	**100.9**	**97.4**	**97.1**
$HOCH_2CHO^{\bullet+}$ (trans) + H_2O		-	**100.4**	**96.8**	**96.3**
$CH_2OH_2/CO^{\bullet+}$ + H_2O		-	**101.3**	**98.5**	**98.4**
$CH_2{=}C(OH)_2^{\bullet+}$ + H_2O		-	**68.4**	**64.4**	**63.9**
$CH_3COOH^{\bullet+}$ + H_2O		-	**88.9**	**85.1**	**84.8**
$CH_2CO/H_2O^{\bullet+}$ + H_2O		-	**83.9**	**81.1**	**79.2**
$HOCHCHOH^{\bullet+}$ (cis)		-228.400264	128.6	125.2	124.6
$HOCHCHOH^{\bullet+}$ (trans)		-228.391673	134.0	130.7	129.9
$HOCH_2CHO^{\bullet+}$ (cis)		-228.353137	158.2	155.4	154.6
$HOCH_2CHO^{\bullet+}$ (trans)		-228.353918	157.7	154.8	153.8
$CH_2O(H)\text{-}H{\bullet\bullet\bullet}CO^{\bullet+}$		-228.352449	158.6	156.5	155.9
$CH_2{=}C(OH)_2^{\bullet+}$		-228.404940	125.7	122.4	121.4
$CH_3COOH^{\bullet+}$		-228.372163	146.2	143.1	142.3
$CH_2CO/H_2O^{\bullet+}$		-228.380260	141.2	139.1	136.7
H_2O		-76.337491	-57.3	-58.0	-57.5
$CH_2OH_2/H_2O^{\bullet+} + CO$	**50**	-	**83.4**	**80.3**	**80.4**
$CH_2OH_2/H_2O^{\bullet+}$		-191.535599	110.8	106.9	106.5
CO		-113.182008	-27.4	-26.6	-26.1
$HOCO^+ + CH_3^\bullet + H_2O$		-	**122.0**	**119.9**	**119.6**
$HOCO^+$		-188.574627	143.0	142.3	142.6
$CH_3CO^+ + OH^\bullet + H_2O$	**43**	-	**111.8**	**109.4**	**109.1**
CH_3CO^+		-152.685915	160.1	158.4	157.3

[a] $E_{(total)}$ in Hartrees, all other components, including the ZPE scaled by 0.99, are in kcal/mol.

Table 4b. Energetic data for various dissociation products of the complex of ionized glycolaldehyde with H_2O (**HB**) derived from CBS-QB3 calculations continued [a].

Species	*m/z*	CBS-QB3 E(total) [0 K]	QB3 $\Delta_fH^0_0$	QB3 $\Delta_fH^0_{298}$	APNO $\Delta_fH^0_{298}$
$CH_2CO^{\bullet+} + 2H_2O$	**42**	-	**96.8**	**94.6**	**94.7**
$CH_2CO^{\bullet+}$		-152.022176	211.4	210.6	209.7
$CH_2OH_2^{\bullet+} + CO + H_2O$	**32**	-	**114.6**	**112.3**	**112.0**
$CH_3OH^{\bullet+} + CO + H_2O$		-	**121.2**	**118.7**	**119.5**
$CH_2OH_2^{\bullet+}$		-115.149226	199.3	196.9	195.6
$CH_3OH^{\bullet+}$		-115.138630	205.9	203.3	203.1
$HOCHCHO^{\bullet}$ (cis) $+ H_3O^+$	**19**	-	**98.8**	**94.7**	**94.1**
$HOCHCHO^{\bullet}$ (trans) $+ H_3O^+$		-	**105.2**	**101.4**	**100.8**
$HOCH_2CO^{\bullet} + H_3O^+$		-	**111.5**	**107.9**	**107.2**
$CH_2COOH^{\bullet} + H_3O^+$		-	**91.0**	**87.1**	**86.4**
$CH_3COO^{\bullet} + H_3O^+$		-	**101.4**	**97.7**	**99.9**
$HOCHCHO^{\bullet}$ (cis)		-228.097402	-46.6	-49.1	-49.0
$HOCHCHO^{\bullet}$ (trans)		-228.087164	-40.2	-42.4	-42.3
$HOCH_2CO^{\bullet}$		-228.077152	-33.9	-35.9	-35.9
$CH_2COOH^{\bullet}$		-228.109735	-54.4	-56.7	-56.7
$CH_3COO^{\bullet}$		-228.093169	-44.0	-46.1	-43.2
H_3O^+		-76.596520	145.4	143.8	143.1

[a] $E_{(total)}$ in Hartrees, all other components, including the ZPE scaled by 0.99, are in kcal/mol.

Figure 2.8. Selected optimized geometries (CBSB7 basis set) of stable intermediates and transition states involved in the isomerization and dissociation of ionic isomers of glycolaldehyde (**1**) and dihydroxyethene (**2**).

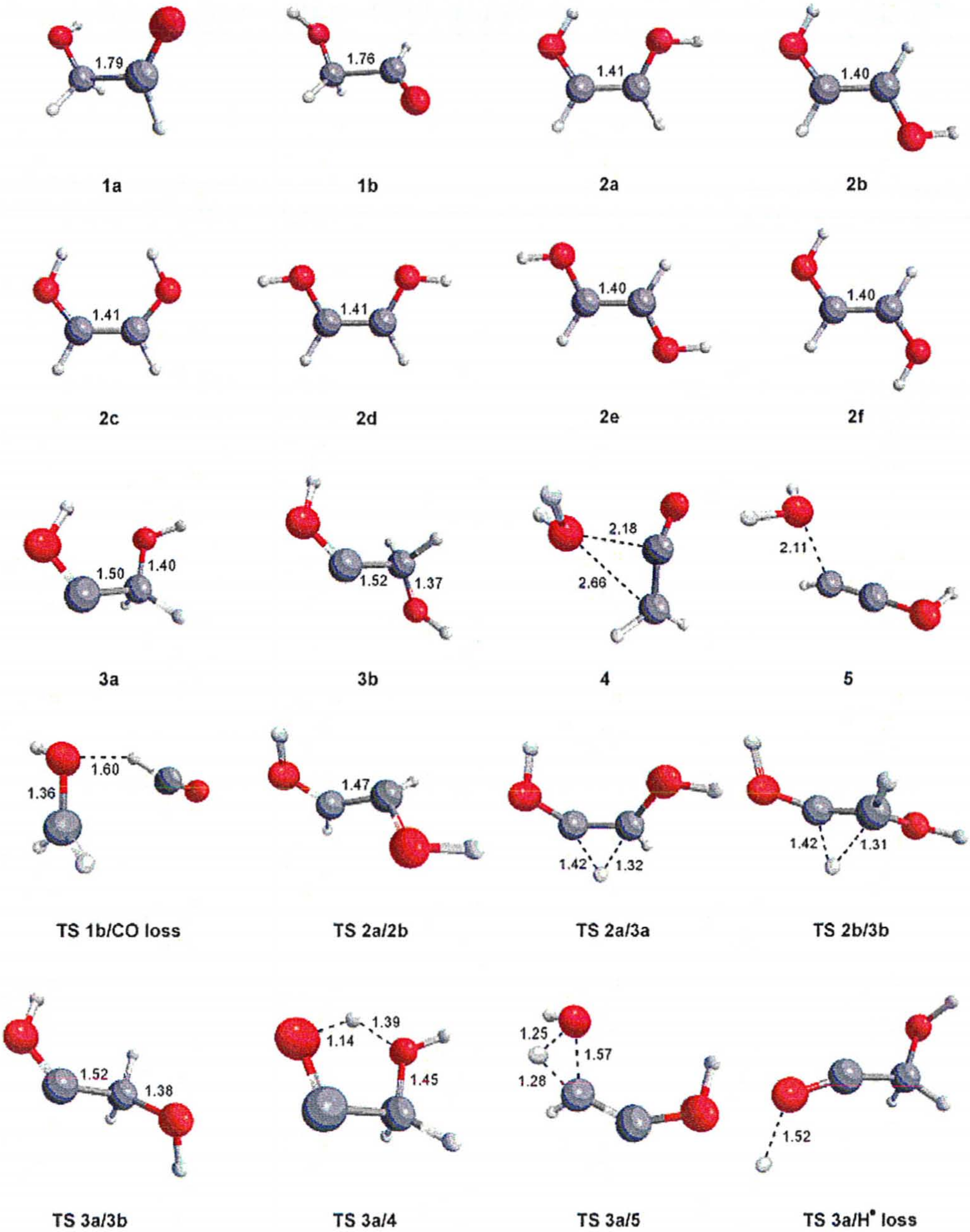

1a **1b** **2a** **2b**

2c **2d** **2e** **2f**

3a **3b** **4** **5**

TS 1b/CO loss **TS 2a/2b** **TS 2a/3a** **TS 2b/3b**

TS 3a/3b **TS 3a/4** **TS 3a/5** **TS 3a/H$^•$ loss**

Figure 2.9. Selected optimized geometries (CBSB7 basis set) of stable intermediates and transition states involved in the isomerization and dissociation of ionic isomers of the complexes of glycolaldehyde with H_2O (**HB**).

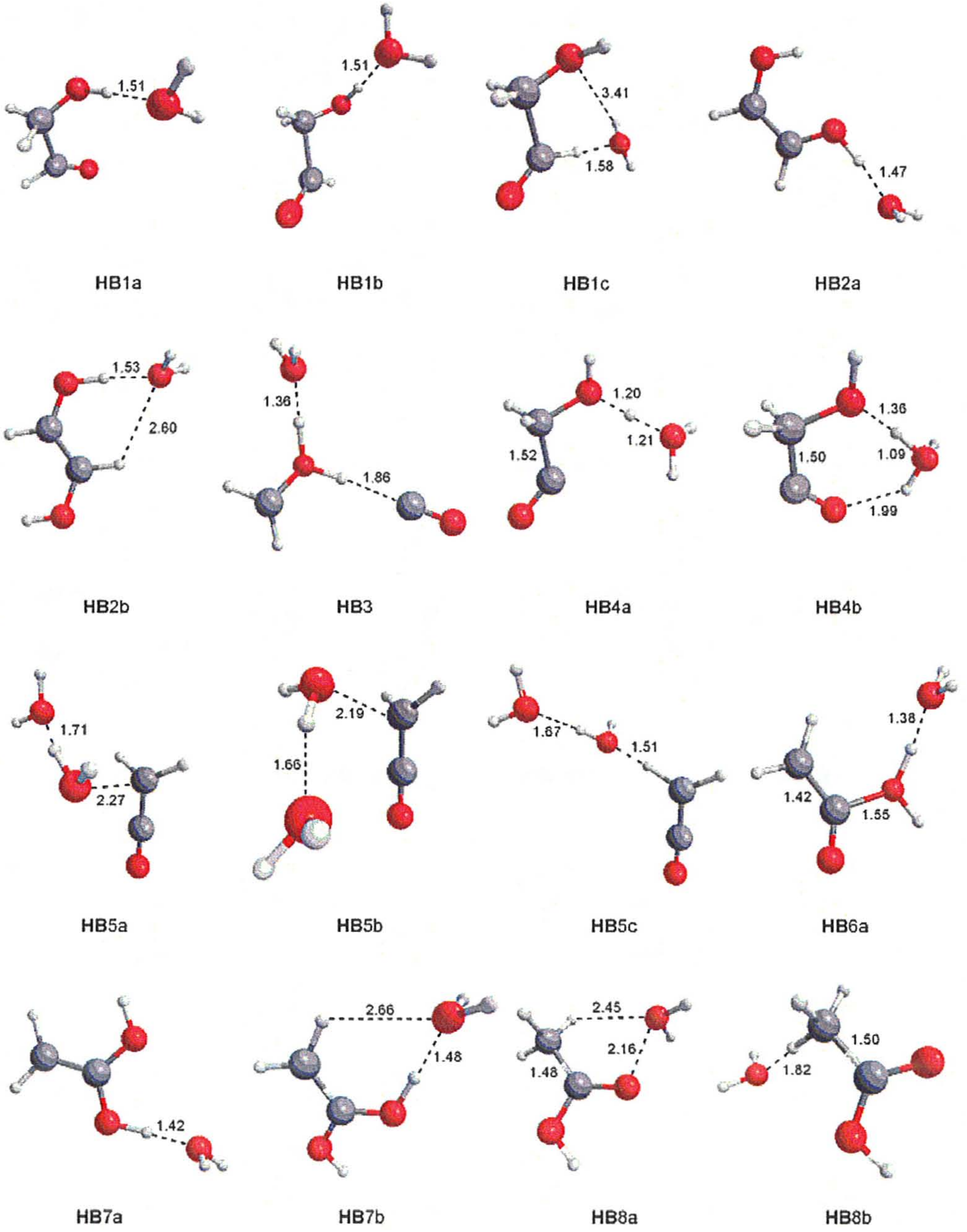
HB1a HB1b HB1c HB2a

HB2b HB3 HB4a HB4b

HB5a HB5b HB5c HB6a

HB7a HB7b HB8a HB8b

Figure 2.9 ctd.

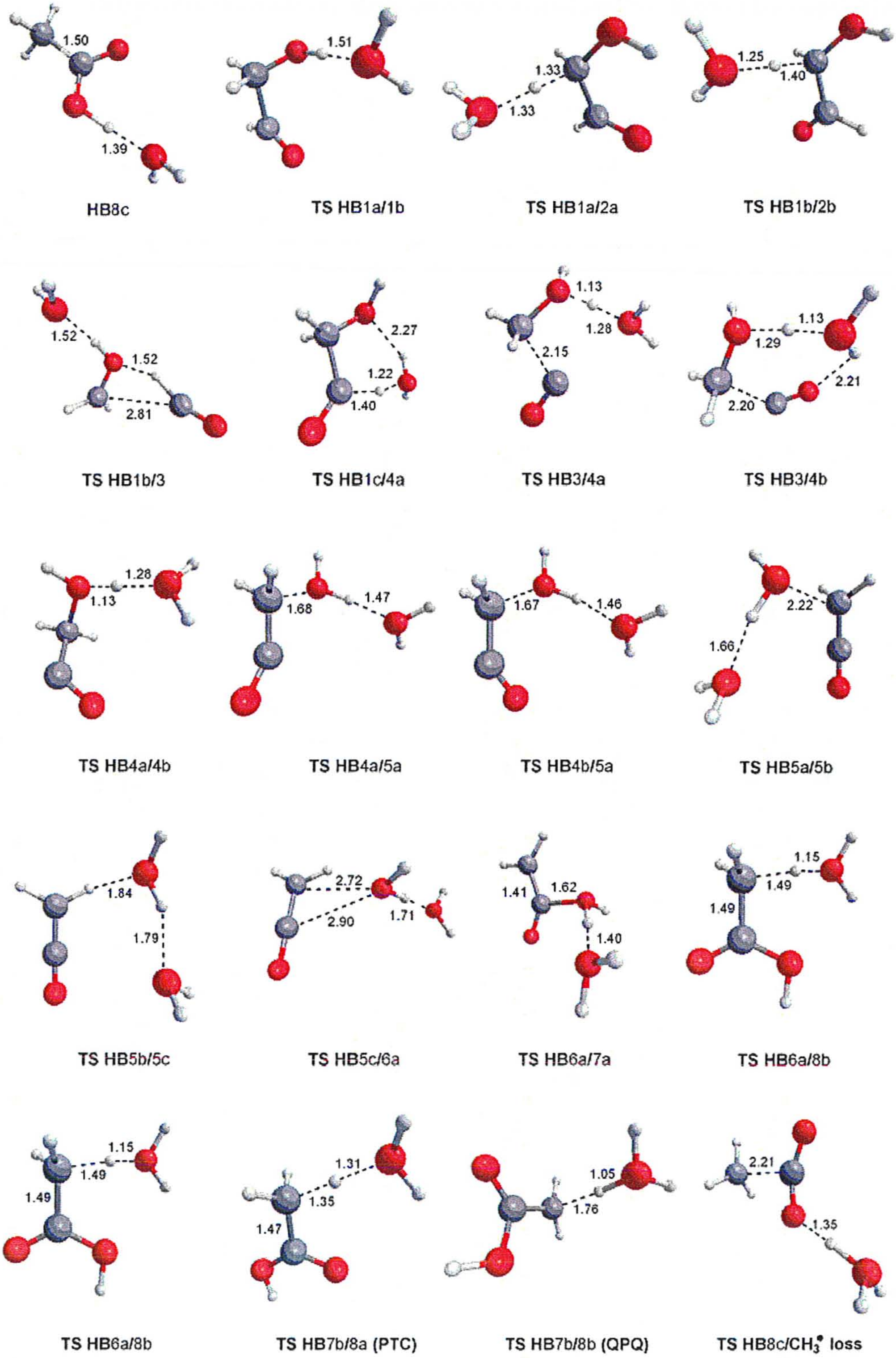

HB8c | TS HB1a/1b | TS HB1a/2a | TS HB1b/2b

TS HB1b/3 | TS HB1c/4a | TS HB3/4a | TS HB3/4b

TS HB4a/4b | TS HB4a/5a | TS HB4b/5a | TS HB5a/5b

TS HB5b/5c | TS HB5c/6a | TS HB6a/7a | TS HB6a/8b

TS HB6a/8b | TS HB7b/8a (PTC) | TS HB7b/8b (QPQ) | TS HB8c/$CH_3^{\bullet}$ loss

Chapter 3

The $C_2H_2N_2$ family of cations and their neutral counterparts : A combined theoretical and tandem mass spectrometry study

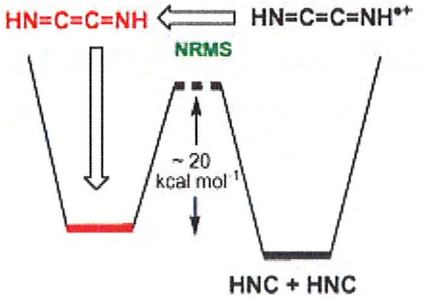

In this study, both CBS-QB3 and CBS-APNO model chemistries have been used to study the ionic and neutral $C_2H_2N_2$ potential energy surfaces. In other words, the relative stability and reactivity (isomerization and dissociation chemistry) of the isomers of $C_2H_2N_2$ have been probed.

Using the results from computational chemistry in conjunction with neutralization-reionization mass spectrometry (NRMS), we demonstrate the stability of the ionic and neutral counterparts of HN=C=C=NH (ethenediimine) and H_2N-C-C=N (aminocyanocarbene) in the rarefied gas phase.

These isomers were exclusively generated from stable precursor molecules such as HN=C=C=NH (ethenediimine) from xanthine and H_2N-C-C=N (aminocyanocarbene) from aminomalononitrile. However, another precursor molecule studied, diaminomaleonitrile (DAMN), is shown to generate the stable ethenediimine ion after the loss of HCN from the hydrogen-bridged radical cation $[HNC{\bullet\bullet\bullet}H_2N\text{-}C\text{-}C{=}N]^{\bullet+}$ via an extraordinary *quid-pro-quo* catalysis. In this catalysis, both the ion and the neutral undergo isomerization.

The work described here has been published in an article under a different title : Karl J. Jobst, M. Ruzni Hanifa, and Johan K. Terlouw. Chem. Phys. Lett. 462 (2008) 152-157.

1. Introduction

Among the several interstellar molecules that astronomers have discovered and spectroscopically characterized, HCN and HNC are of particular interest because (i) their ionic and neutral forms are known to be ubiquitous in molecular clouds and comets [1,2], and (ii) the possibility of HCN playing a crucial role in prebiotic syntheses [3,4]. This is due to the fact that purines (such as the nitrogenous bases in DNA), amino acids and pyrimidines are essentially polymers of [H,C,N] [4]. Therefore, the covalently bound dimers (both, ionic and neutral forms) of [H,C,N] are of considerable astrochemical interest [5].

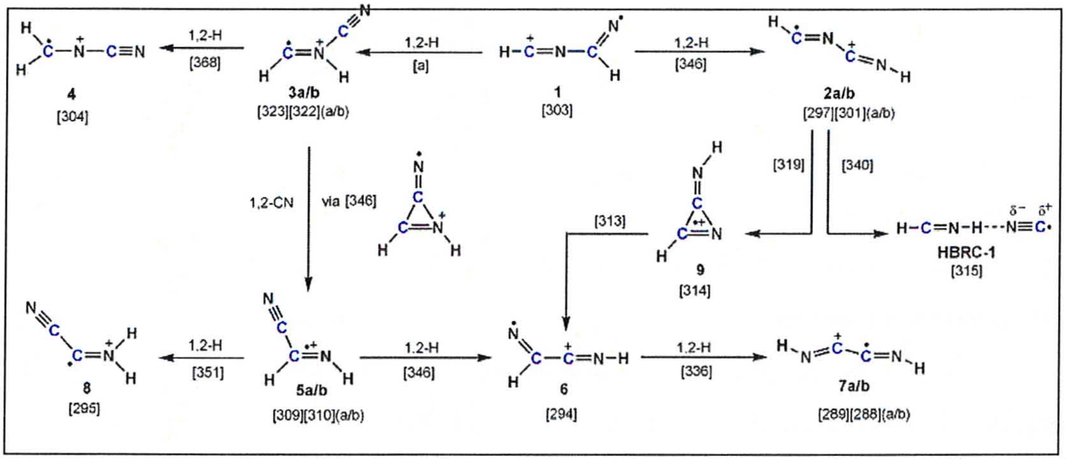

Scheme 3.1. CBS-QB3 results pertaining to key isomers and connecting transition states of the $C_2H_2N_2^{\bullet+}$ system. a/b denote different stable conformers. [a] displays a transition state that could not be found. All values are in kcal/mol derived at 298 K.

Scheme 3.1 shows a majority of the ionic isomers of $C_2H_2N_2$ studied. All enthalpies of formation (Δ_fH^0) values are in kcal/mol and have been calculated at 298 K, see Table 1a. In a previous study, two isomers of $C_2H_2N_2$ have been generated and comprehensively studied using different spectroscopic methods. These isomers are **4** CH_2=N-C≡N (*N*-cyanomethanimine) and **5** HN=C(H)-C≡N (*C*-cyanomethanimine or iminoacetonitrile). The results of the study revealed that these isomers are stable molecules in the gas-phase [5-7]. Analysis of the scheme reveals that isomeric ion **7** HN=C=C=$NH^{\bullet+}$ (ethenediimine) corresponds to the lowest enthalpy of formation (288 kcal/mol). In other words, the ethenediimine ion is the global minimum in the region of the potential energy surface studied.

In yet another previous study by Moser et al. [8], it was suggested that the thermal or photolytic decomposition of Group 1 metal salts of 1-cyanoformamide tosylhydrazone generated a third $C_2H_2N_2$ isomer (**8**); NH_2-C-C=N (aminocyanocarbene). In spite of this, the work done in references [5-7] show that this very reaction generates the iminoacetonitrile (**5**) instead. In the same vein, a separate, more recent theoretical study [9] reveals that the intramolecular isomerization of the aminocyanocarbene via a 1,2-insertion into the more stable iminoacetonitrile is associated with a significantly high energy barrier of 56 kcal/mol.

Therefore, in this study, using neutralization-reionization mass spectrometry (NRMS) [10], we probed the stability and reactivity of neutral aminocyanocarbene generated from its ionic counterpart. In a similar manner, the stability of the elusive neutral HN=C=C=NH (ethenediimine) was explored as well. The viability of the ethenediimine ion has been well established as seen in the EI mass spectra of references [11-14]. All $C_2H_2N_2$ isomers studied are generated by dissociative ionization of previously studied precursor molecules.

The neutral forms of both, the aminocyanocarbene and the ethenediimine species, are shown to be (kinetically) stable in the timeframe of the experiment.

Finally, as a side project of the computational study, all pertinent $C_2H_2N_2$ species were studied using a different density functional theory exchange-correlation functional denoted BMK (Boese-Martin for Kinetics) [15]. This was done for purposes of comparison and to better understand the reactivity of the isomers of $C_2H_2N_2$. The well established accuracy of BMK for transition state barriers within a range of 2 kcal/mol [15] was the main reason behind its choice.

2. Experimental and Theoretical Methods

All mass spectrometric experiments were performed on the VG Analytical ZAB-R mass spectrometer of BE_1E_2 geometry (B = magnetic sector, E = electric sector). Ions are generated under electron ionization conditions (70 eV) and accelerated at a potential of 8 kV. The details of this instrument and the acquisition of the NR mass spectra have been previously explained [16]. Research grade xanthine, 8-azahypoxanthine, uric acid, aminomalononitrile and diaminomaleonitrile (DAMN) were used as precursor molecules for the *m/z* 54 $C_2H_2N_2$ ions studied. They were introduced into the instrument via a heated probe. The metastable ion (MI) and neutralization-reionization (NR) mass spectra were recorded in the second field free region (2ffr) of the instrument. The collision-induced dissociation (CID) mass spectra were obtained in the 2ffr and 3ffr. All CID spectra were recorded using O_2 or He as the collision gas. The NR spectra were recorded using *N,N*-dimethylaniline as the reducing agent and O_2 for reionization. Kinetic energy release (KER) values reported were acquired using standard procedures [17].

The optimized geometries and the enthalpies of formation of various ions and neutrals pertinent to this study were probed using CBS-QB3 and CBS-APNO model chemistries [18,19]. For purposes of comparison and accuracy, all enthalpies were recalculated using the BMK functional theory [15] in conjunction with the 6-311G (2d,d,p) basis set. This was done by performing single point energy calculations on the optimized geometries using BMK and B3LYP functional theories and comparing the values generated to the reference CBS-QB3 minimum ion **1**. Table 1b lists the enthalpies calculated using the CBS-QB3 model chemistry along with those derived from the B3LYP and BMK functional theories. The calculations were performed using Gaussian 03 Revision C.02 and D.01 suite of programs on the SHARCNET computer network [20]. The calculated energies are presented in Tables 1-4 (see Appendix) and the energy diagrams of Schemes 3.1-3.17. Optimized geometries of selected species are displayed in the Appendix (Figures 3.18 and 3.19). The identity of local minima and connecting transition states (TS) were confirmed by frequency analysis. In comparison, the enthalpies generated using BMK and B3LYP functional theories were within ~6 kcal/mol of the values obtained using CBS-QB3/APNO model chemistries. The agreement is much better in the case of the enthalpies of formation of the transition state geometries.

The model chemistries predict that both conformers of the ethenediimine ($HN{=}C{=}C{=}NH^{\bullet+}$) ion are genuine minima whereas the BMK level of theory predicts that conformer **7a** from Schemes 3.1 and 3.3 is a first order saddle point. The saddle point is an 'artefact' resulting in only one stable conformer. However, unlike B3LYP, the BMK functional theory did prove useful in the determination of a saddle point for the $H^\bullet$ loss from ion **7** to establish an energy barrier for the process.

3. Results and Discussion

3.1. The generation of HN=C=C=NH$^{\bullet+}$ from xanthine, uric acid and 8-azahypoxanthine.

The 70 eV EI mass spectra of xanthine, uric acid [12] and 8-azahypoxanthine [13], all display a sizeable peak at *m/z* 54 corresponding to ions of elemental composition $C_2H_2N_2$. Fig. 3.2 shows the normal mass spectra corresponding to the three listed precursor molecules.

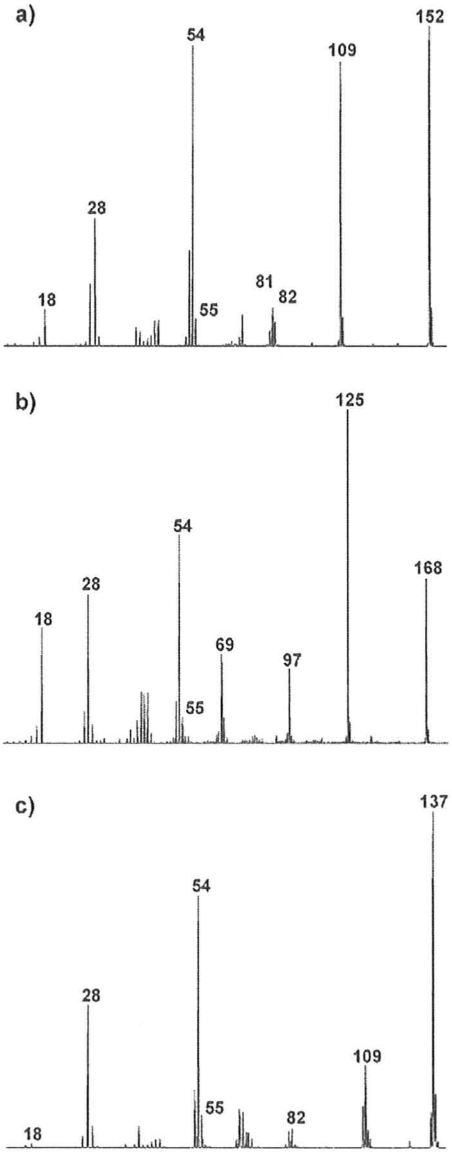

Figure 3.2. Normal mass spectra of (a) xanthine, (b) uric acid and (c) 8-azahypoxanthine.

In the case of xanthine, Scheme 3.3 shows that ion **7** : $HN=C=C=NH^{\bullet+}$ (ethenediimine) is generated following consecutive losses of HNCO, CO and HCN. It is acknowledged that we have depicted a particular tautomer to generate the ion. The reason for this is that the ethenediimine structure is the global minimum on the $C_2H_2N_2$ potential energy surface studied (Scheme 1), and only the tautomer displayed in Scheme 3.3 can generate it. Further scrutiny of other potential dissociation pathways, see Scheme 3.3, reveals that *m/z* 55 $HN=C=C=O^{\bullet+}$ (iminoethenone) may be generated which can lose $H^{\bullet}$ to yield the *m/z* 54 isobaric impurity $N=C=C=O^{+}$ ion. The species corresponding to *m/z* 55 and *m/z* 54 are confirmed stable gas-phase species in the time scale of mass spectrometry experiments [11,21].

Therefore, in this study, it is important to probe the isobaric (and isomeric) purity of the beam of mass selected ions. The NR/CID spectra from the 3ffr advantageously account for such ambiguities as discussed in Section 3.6.

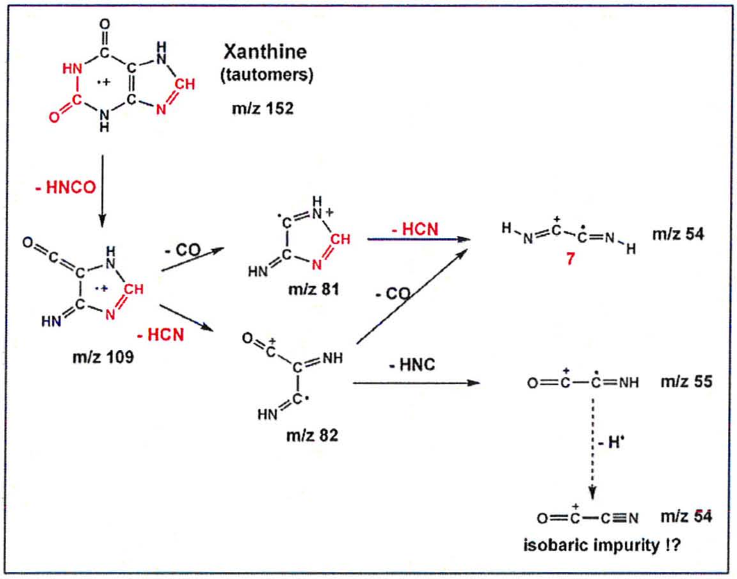

Scheme 3.3. Proposed fragmentation pathway for the generation of ion 7 from ionized xanthine.

In order to verify the proposed generation of ethenediimine ions in Scheme 3.3, the CID spectra of every prominent fragment ion that could generate the ion of interest is investigated. Fig. 3.4 displays the CID spectra of *m/z* 152, 109, 82, 81 and 55.

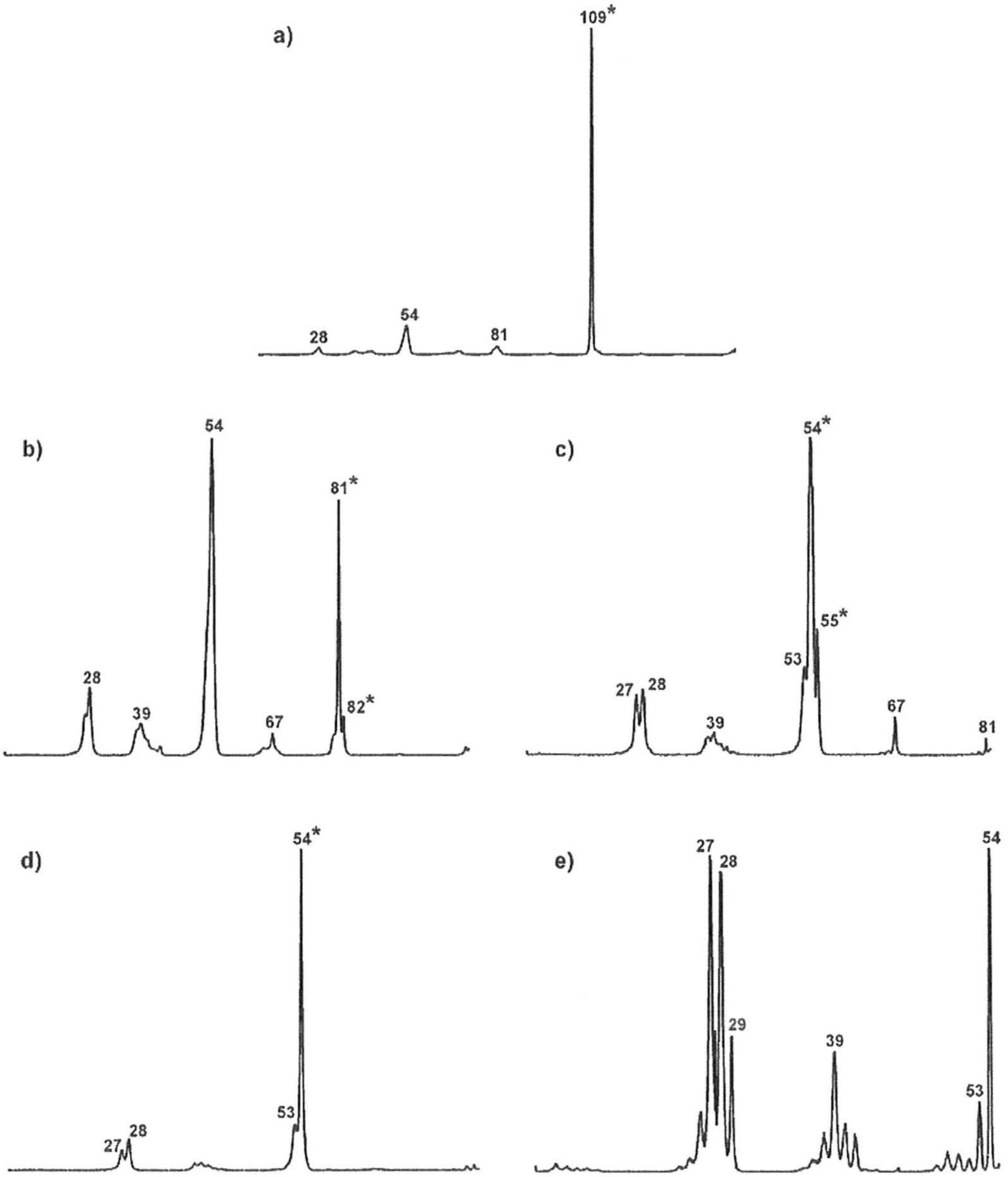

Figure 3.4. 2ffr CID mass spectra of (a) *m/z* 152 (b) *m/z* 109 (c) *m/z* 82 (d) *m/z* 81 (e) *m/z* 55 ions generated from xanthine. The asterisk (*) denotes a metastably generated peak. The *m/z* 55 MI spectrum was not intense enough to be observed.

The CID mass spectrum of *m/z* 152 (Fig. 3.4a) shows *m/z* 109 as the base peak. This is also the case for the MI spectrum (not shown). This observation is consistent with the rearrangement reaction resulting in the neutral loss of HNCO (mass 43) depicted in Scheme 3.3. The *m/z* 109 CID spectrum (Fig. 3.4b) is dominated by prominent low energy and high energy fragmentation pathways. The MI peaks corresponding to *m/z* 82 and 81 are the results of neutral losses of HCN (mass 27) and CO (mass 28) respectively.

On the other hand, a major fraction of the high energy dissociation peak at *m/z* 54 is due to the subsequent consecutive loss of HCN from the resultant *m/z* 81 fragment. A small portion of this peak could be due to the isobaric impurity ($N=C=C=O^{+}$) originating from the *m/z* 82 fragment as depicted in the scheme.

Consistent with this proposal, the predominant reactions taking place in the *m/z* 82 CID spectrum (Fig. 3.4c) correspond to the losses of CO and HNC. These processes give rise to the peaks at *m/z* 54 and 55 respectively. In contrast, unlike the *m/z* 82 fragment, see Scheme 2, the *m/z* 81 fragment loses only HCN to generate the *m/z* 54 ion $HN=C=C=NH^{\bullet+}$. The *m/z* 81 CID spectrum (Fig. 3.4d) confirms this proposal showing a solitary metastable peak at *m/z* 54. Following the generation of a *m/z* 55 fragment by the *m/z* 82 ion, one may envisage the *m/z* 55 CID spectrum (Fig. 3.4e) to consist of a mixture of peaks generated from $HN=C=C=O^{\bullet+}$ and the ^{13}C or ^{15}N isotopologues of $HN=C=C=NH^{\bullet+}$. This can be confirmed by comparing the *m/z* 55 CID spectrum to an established spectrum of the *m/z* 54 fragment and/or to the *m/z* 55 CID spectrum from a precursor ion that is not expected to generate $HN=C=C=O^{\bullet+}$.

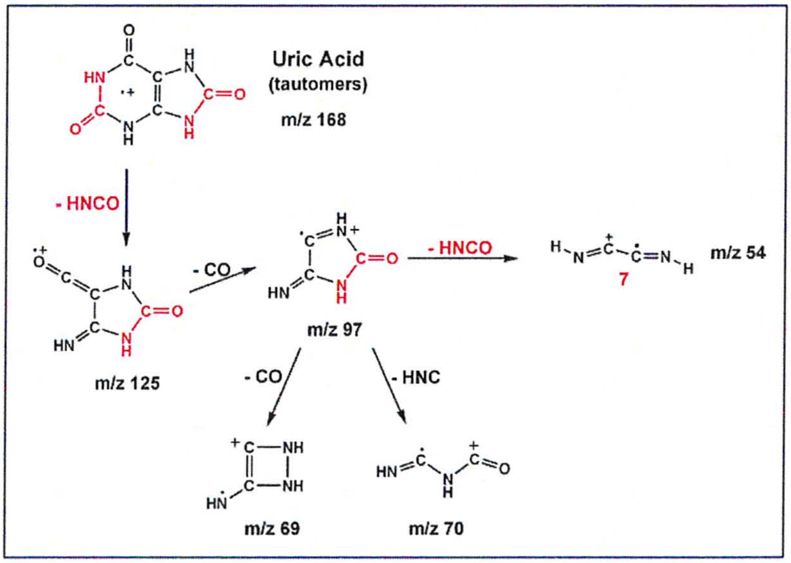

Scheme 3.5. Proposed fragmentation pathway for the generation of ion 7 from ionized uric acid.

Uric acid is another precursor molecule that is proposed to generate ion 7, see Fig 3.2b. As shown in Scheme 3.5, the ethenediimine ion can be obtained from uric acid following the consecutive losses of HNCO, CO and a second HNCO molecule. Unlike xanthine, uric acid is not expected to generate the isobaric iminoethenone ($HN=C=C=O^{\bullet+}$) ion. Its major dissociation pathways are discussed in conjunction with Fig. 3.6, which shows the CID spectra of the *m/z* 168, 125, 97, 70, 69 and 55 ions. As seen in the *m/z* 168 CID spectrum (Fig. 3.6a), the only significant reaction observed is the loss of HNCO. This process results in a peak at *m/z* 125.

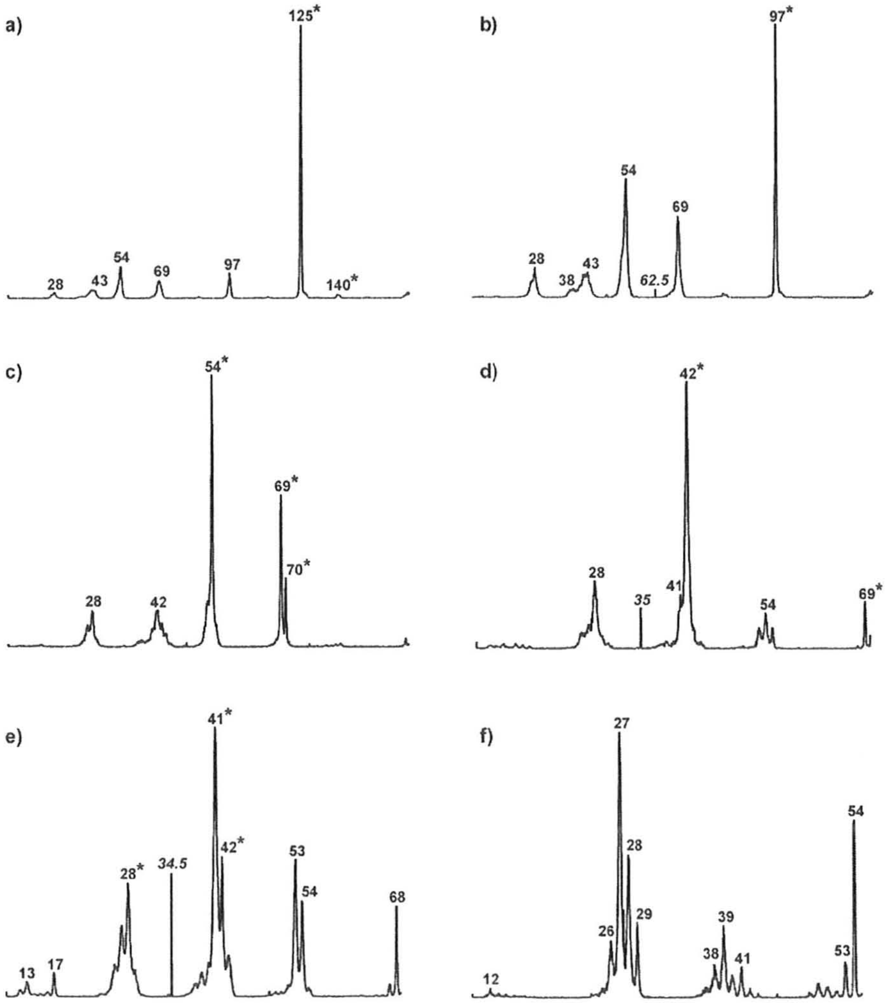

Figure 3.6. 2ffr CID mass spectra of (a) *m/z* 168 (b) *m/z* 125 (c) *m/z* 97 (d) *m/z* 70 (e) *m/z* 69 (f) *m/z* 55 ions generated from uric acid. The asterisk (*) denotes a metastably generated peak. *Italicized m/z* values correspond to doubly-charged molecular ions. The *m/z* 55 MI spectrum was not intense enough to be observed.

In a similar trend, the *m/z* 125 CID spectrum (Fig. 3.6b) displays a prominent MI peak at *m/z* 97. This peak corresponds to the loss of CO, see Scheme 3.5. However, in this spectrum, smaller CID peaks corresponding to *m/z* 69 and 54 are generated which are due to the separate consecutive losses of CO and HNCO from the *m/z* 97 fragment ion. Consistent with this observation, the *m/z* 97 CID spectrum (Fig. 3.6c) displays relatively intense peaks at *m/z* 70, 69 and 54. The peak at *m/z* 70 corresponds to the loss of neutral HNC. The dissociation pathways of Scheme 3.5 illustrate these observations.

The most significant peaks in the *m/z* 70 CID spectrum (Fig. 3.6d) correspond to *m/z* 69 and 42. They are both metastably generated peaks where the former is the result of $H^{\bullet}$ loss and the latter corresponds to CO loss. The latter reaction generates the *m/z* 42 $HN{=}C{=}NH^{\bullet+}$ ion. The *m/z* 69 CID spectrum (Fig. 3.6e) is dominated by both low and high energy dissociation reactions. The MI peaks at *m/z* 42 and 41 correspond to the losses of HNC and HNC + $H^{\bullet}$ respectively. The remaining metastable peak at *m/z* 28 corresponds to the $HCNH^{+}$ ion. On the other hand, the CID peaks in the spectrum at *m/z* 68, 54 and 53 are due to the neutral losses of $H^{\bullet}$, NH and NH + $H^{\bullet}$, respectively.

Finally, as uric acid is not expected to generate the *m/z* 55 $HN{=}C{=}C{=}O^{\bullet+}$ ion, we propose that the *m/z* 55 CID spectrum (Fig. 3.6f) primarily shows the dissociation behaviour of the ^{13}C or ^{15}N isotopologue of $HN{=}C{=}C{=}NH^{\bullet+}$. When this spectrum is compared to that from xanthine (Fig. 3.4e), it can be seen that all peaks/peak ratios reasonably agree except for the peak at *m/z* 27. This peak is relatively higher in intensity in the *m/z* 55 CID spectrum from uric acid. This observation is indicative of the exclusive generation of the $HN{=}C{=}C{=}NH^{\bullet+}$ ion from uric acid which can symmetrically dissociate into *m/z* 27 $HNC^{\bullet+}$ ions. As the discrepancy in the *m/z* 27 peak intensities from the two spectra (Figs. 3.6f and 3.4e) compared is not large, it is reasonable to assume that xanthine predominantly generates $HN{=}C{=}C{=}NH^{\bullet+}$ ions.

Ionized 8-azahypoxanthine is yet another precursor molecule that is expected to generate ion **7**, see Fig 3.2c, following successive losses of N_2, CO and HCN, see Scheme 3.7. For the same reason as that for xanthine, a particular tautomer of 8-azahypoxanthine has been depicted. In line with this, it is chemically reasonable for this precursor molecule to also generate the iminoethenone ion ($HN{=}C{=}C{=}O^{\bullet+}$), see Scheme 3.7.

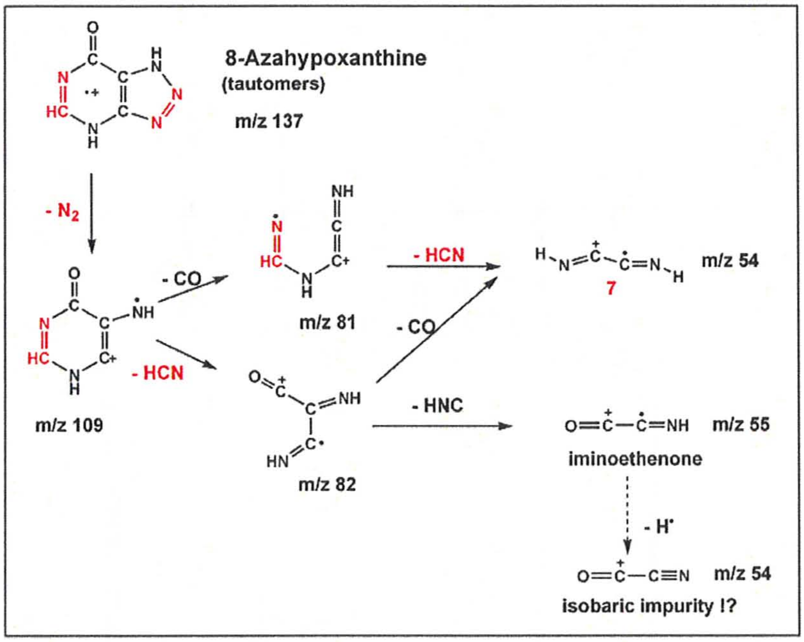

Scheme 3.7. Proposed fragmentation pathway for the generation of ion 7 from ionized 8-azahypoxanthine.

To verify this proposal and all other major dissociation pathways of 8-azahypoxanthine, the CID spectra of every prominent fragment ion is discussed. Fig. 3.8 displays the CID spectra of *m/z* 137, 109, 82, 81 and 55. In comparison to all displayed spectra in Fig. 3.8, the *m/z* 137 CID spectrum (Fig. 3.8a) shows the greatest number of dissociation processes. The metastable fragmentations of the molecular ion yielding peaks at *m/z* 136, 109 and 54 dominate the spectrum. The peaks at *m/z* 136 and 109 correspond to the losses of $H^•$ and N_2 respectively. The peak generated at *m/z* 54 corresponds to two different fragmentation pathways via *m/z* 82 and 81 fragments ions as illustrated in Scheme 3.7. Another prominent peak in the *m/z* 137 CID spectrum corresponds to *m/z* 108 resulting from the high energy dissociation reaction involving the loss of $H^• + N_2$.

The significant peak at *m/z* 28 is indicative of the generation of the $HCNH^+$ ion. The major peaks in the *m/z* 109 CID spectrum (Fig. 3.8b) of 8-azahypoxanthine are very similar to that from xanthine (Fig. 3.4b). In this case however, the peaks corresponding to *m/z* 82, 81 and 54 are the result of metastable fragmentations. The peaks at *m/z* 82 and 81 correspond to ions generated due to the loss of HCN and CO respectively. Similar to the *m/z* 137 CID spectrum (Fig. 3.8a), the *m/z* 54 peak seen in this spectrum (Fig. 3.8b) is a result of the two dissociation pathways depicted in Scheme 3.7.

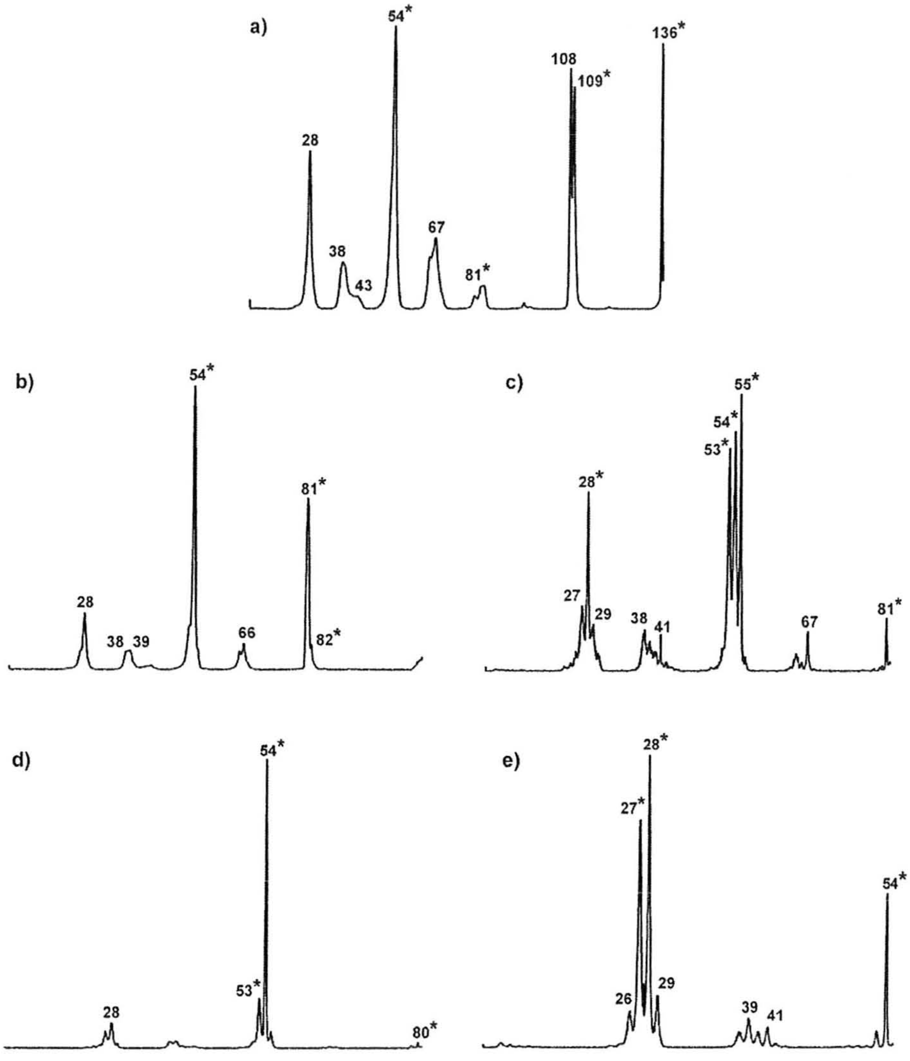

Figure 3.8. 2ffr CID mass spectra of (a) *m/z* 137 (b) *m/z* 109 (c) *m/z* 82 (d) *m/z* 81 (e) *m/z* 55 ions generated from 8-azahypoxanthine. The asterisk (*) denotes a metastably generated peak.

The *m/z* 82 CID spectrum (Fig. 3.8c) displayed is also dominated by metastable reactions yielding peaks corresponding to *m/z* 81, 55, 54, 53 and 28. The peaks at *m/z* 81 and 55 are generated due to the loss of $H^•$ and HNC respectively. When the intensity of the *m/z* 55 peak in this spectrum (Fig. 3.8c) is compared to that from the xanthine *m/z* 82 CID spectrum (Fig. 3.4c), it can be seen that the peak from the former spectrum is significantly more intense. This observation is evident of a relatively larger portion of the 8-azahypxanthine *m/z* 82 fragment ions losing HNC to generate $HN{=}C{=}C{=}O^{•+}$. As shown in Scheme 4, the *m/z* 82 fragment can lose either CO or HNC + $H^•$ to generate a peak at *m/z* 54. In line with the last observation, it is reasonable to infer that the *m/z* 54 ions generated from 8-azahypoxanthine are isobarically impure. The intense peak at *m/z* 53 corresponds to the $H^\bullet$ loss from $HN{=}C{=}C{=}NH^{\bullet+}$. The *m/z* 28 peak in the spectrum is due to the generation of $HCNH^+$.

Similar to the *m/z* 81 CID spectrum from xanthine (Fig. 3.4d), the corresponding spectrum from 8-azahypoxanthine (Fig. 3.8d) displays metastable dissociations. The base peak at *m/z* 54 corresponds to the neutral loss of HCN to yield $HN{=}C{=}C{=}NH^{\bullet+}$. The peaks at *m/z* 80 and 53 correspond to $H^\bullet$ losses from the *m/z* 81 and 54 fragment ions respectively. Finally, as 8-azahypoxanthine is a precursor molecule proposed to generate a greater fraction of $HN{=}C{=}C{=}O^{\bullet+}$ ions, the *m/z* 55 CID spectrum (Fig. 3.8e) is expected to exhibit peaks indicative of an isobaric mixture. In order to estimate the extent of isobaric contamination, this spectrum is compared to the isobarically pure counterpart spectrum from uric acid (Fig. 3.6). When compared, it can be seen that all peaks/peak ratios reasonably agree except for the peak at *m/z* 28. This peak is relatively much higher in intensity in the *m/z* 55 CID spectrum from 8-azahypoxanthine. This observation is indicative of the significant generation of the $HN{=}C{=}C{=}O^{\bullet+}$ ion which can readily dissociate to yield *m/z* 28 $CO^{\bullet+}$ ions [21]. As the difference in the *m/z* 28 peak intensities from the two precursor molecules is sizeable, it can be reasonably concluded that 8-azahypoxanthine generates an isobarically impure mixture of *m/z* 54 ions.

To further understand the extent of the contribution of the $N{=}C{=}C{=}O^+$ ion by xanthine and 8-azahypoxanthine, we compared the *m/z* 54 CID spectra from each precursor molecule. Fig. 3.9 shows the pertinent mass spectra. *Prima facie*, the three spectra are very close. However, a closer look at the relative peak ratios corresponding to *m/z* 26 (i.e. CO loss) in each spectrum reveals that the peak generated from 8-azahypoxanthine (see Fig. 3.9c) is the most intense. This further supports the claim that 8-azahypoxanthine generates a greater fraction of $N{=}C{=}C{=}O^+$ ions in admixture with $HN{=}C{=}C{=}NH^{\bullet+}$ ions [21]. The similarity of the *m/z* 54 CID spectra generated from xanthine and uric acid (Figs. 3.9a and 3.9b) suggests any isobaric impurity generated by the former to be negligible.

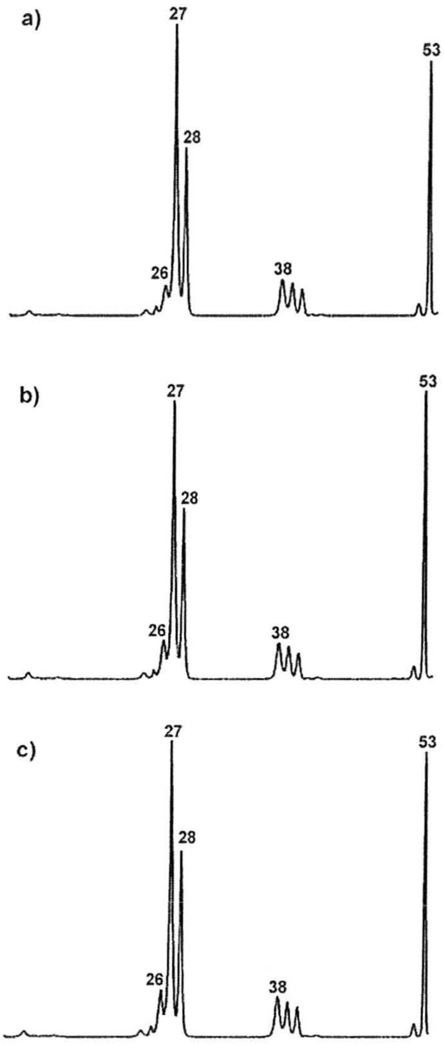

Figure 3.9. 2ffr CID mass spectra of *m/z* 54 ions generated from (a) xanthine (b) uric acid and (c) 8-azahypoxanthine.

3.2. Analysis of the CID mass spectra of $HN{=}C{=}C{=}NH^{\bullet+}$ *and* $NH_2\text{-}C\text{-}C{=}N^{\bullet+}$.

As described in Section 3.1, the 70 eV EI mass spectra of xanthine, uric acid [12] and 8-azahypoxanthine [13] display, see Fig. 3.1, a sizeable peak at *m/z* 54, corresponding with $C_2H_2N_2$ ions. Aminomalononitrile and diaminomaleonitrile also show a significant *m/z* 54 peak in their respective mass spectra corresponding to $C_2H_2N_2^{\bullet+}$.

The CID spectrum of ion 7, obtained from xanthine, is shown in Fig. 3.10a. Prominent peaks corresponding to losses of $H^{\bullet}$, $CN^{\bullet}$ and HNC give rise to peaks at *m/z* 53, 28 and 27 in the CID spectrum. As with the CID spectra of other $C_2H_2N_2$ ions studied, these particular peaks are the dominating species despite differences in relative intensities. There is also a set of peaks ranging from *m/z* 40 – 38 in Fig. 3.10a corresponding to losses of N, NH and NH + H$^•$. When the collision gas was changed from O_2 to He, the intensity of the *m/z* 40 peak dramatically lowered, consistent with the studies of reference [14]. However, the structure diagnostic peak in the spectrum is the weak *m/z* 15 peak corresponding to the =NH fragment of the ethenediimine ion (7).

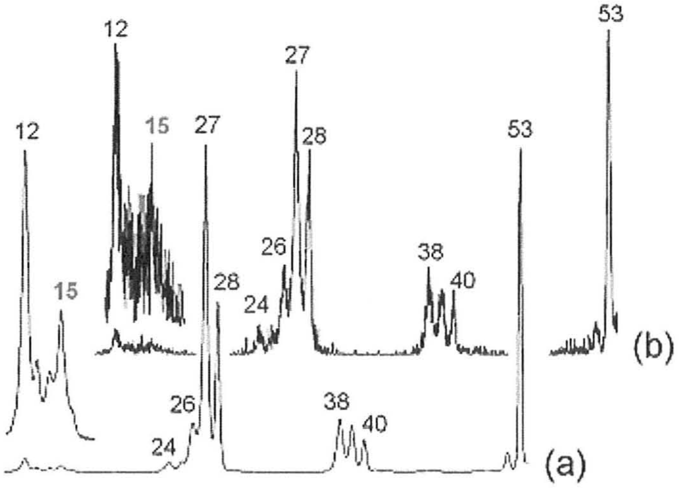

Figure 3.10. (a) 2ffr CID mass spectrum of *m/z* 54 ions generated from xanthine (b) NR-CID spectrum of reionized ethenediimine (7) ions.

Aminomalononitrile (N≡C-C(H)(NH_2)-C≡N) is also recognized to generate a sizeable peak at *m/z* 54. In this case however, the consequent ion generated is ion **8** : NH_2-C-C=N$^{•+}$ (aminocyanocarbene). Scheme 3.11 shows how aminomalononitrile yields ion **8** through the loss of HCN following a 1,2-H shift. In line with this, the calculations reveal that the TS corresponding for the 1,2-H shift in N≡C-C(**H**)(NH_2)-C≡N$^{•+}$ (320 kcal/mol) yielding N≡C(**H**)-C(NH_2)-C≡N$^{•+}$ (300 kcal/mol) lies at 342 kcal/mol. This 1,2-H shift isomer is generated with sufficient energy to overcome the barrier at 323 kcal/mol for HCN loss to yield ion **8** + HCN (327 kcal/mol). This two-step reaction, in comparison to the barrier at 344 kcal/mol for H$^•$ loss from the molecular ion, is energetically favoured.

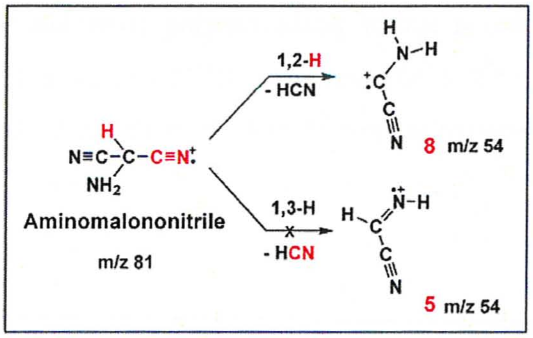

Scheme 3.11. Proposed fragmentation pathway for the generation of ion **8** from ionized aminomalononitrile.

A 1,3-H shift in the aminomalononitrile molecular ion prior to HCN loss is just as conceivable : it would yield the previously studied iminoacetonitrile ion **5**. However, the considerable dissimilarity in the *m/z* 54 CID spectra from aminomalononitrile (Fig. 3.12a) and that of **5** from the literature leaves little doubt that ion **8** is generated. Examination of the CID spectrum in Fig. 3.12a reveals a weak but structure-diagnostic signal at *m/z* 16 corresponding to the –NH_2 fragment of the aminocyanocarbene ion (**8**).

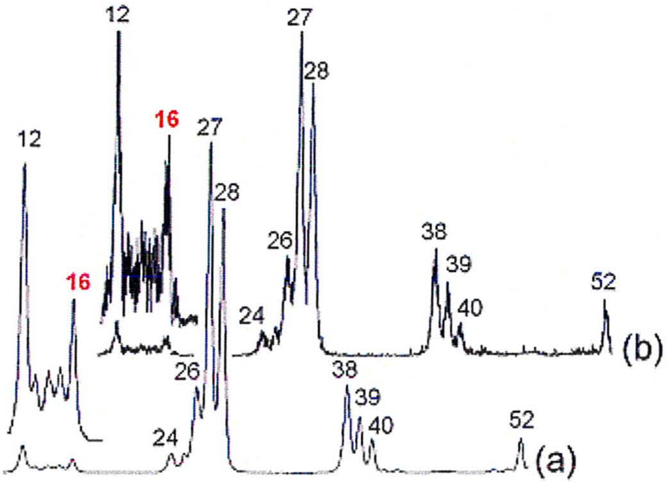

Figure 3.12. (a) 2ffr CID mass spectrum of *m/z* 54 ions generated from aminomalononitrile (b) NR-CID spectrum of reionized aminocyanocarbene (**8**) ions. The *m/z* 53 peak in either spectrum is not shown as it is four times as intense as the peak at *m/z* 27.

The mass spectrum of diaminomaleonitrile (DAMN) exhibits a significant *m/z* 54 peak in its mass spectrum. The connectivity of DAMN leads one to envisage that a direct bond cleavage of the C-C bond could generate ion **8** :

$$N{\equiv}C(NH_2)C{=}C(NH_2)C{\equiv}N^{\bullet+} \rightarrow NH_2\text{-}C\text{-}C{=}N^{\bullet+}\ (\mathbf{8}) + NH_2\text{-}C\text{-}C{=}N^{\bullet\bullet}$$

Nevertheless, a thorough inspection of the *m/z* 54 CID spectrum obtained from DAMN, see Fig. 3.13, shows both structure-diagnostics peaks at *m/z* 15 and 16, implying that ion **7** is generated in admixture with ion **8**. Additional confirmation for this inference is seen in the acquired NR mass spectra discussed in Section 3.4. A rationale for these observations is mechanistically provided in Section 3.5.

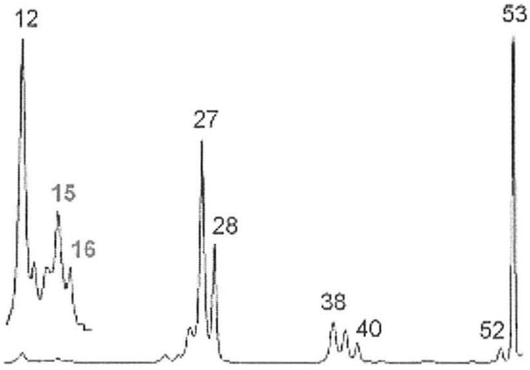

Figure 3.13. 2ffr CID mass spectrum of *m/z* 54 ions generated from diaminomaleonitrile.

*3.3. Isomerization reactions of ions **7**, **8** and their neutral counterparts **N7** and **N8**.*

The region of the ionic $C_2H_2N_2$ potential energy surface (see Scheme 3.14) connecting ions **7** and **8** reveals that the path involving consecutive 1,2-H shifts is associated with prohibitively high energy barriers. The intermediate species in this path include the nitrene isomer $HN{\equiv}C\text{-}C(H){=}N^{\bullet+}$ (**6**), and the iminoacetonitrile ion $HN{=}C(H)C{\equiv}N^{\bullet+}$ (**5**). A direct conversion of ion **7** into **8** via a 1,4-H shift is associated with an even higher TS at 365 kcal/mol. This, in comparison to the barrier corresponding to $H^{\bullet}$ loss at 338 kcal/mol proves direct isomerization prior to collision is impossible. In line with this, the *m/z* 54 CID spectra obtained from xanthine/uric acid and aminomalononitrile, see Figs. 3.10a and 3.12a, show no interconversion of ions **7** and **8**. The structure-diagnostic peak at *m/z* 16 in Fig. 3.10a is absent and the equally important peak at *m/z* 15 in Fig. 3.12a is of negligible intensity.

Moreover, the dissociation threshold for $H^{\bullet}$ loss is within ~3 kcal/mol of the barrier associated with the transformation **7** → **6** at 335 kcal/mol. Therefore, we can safely conclude that the ethenediimine structure (**7**) of a majority of the source generated *m/z* 54 ions from xanthine/uric acid is preserved. The same conclusion is true for the aminocyanocarbene ions (**8**) from aminomalononitrile.

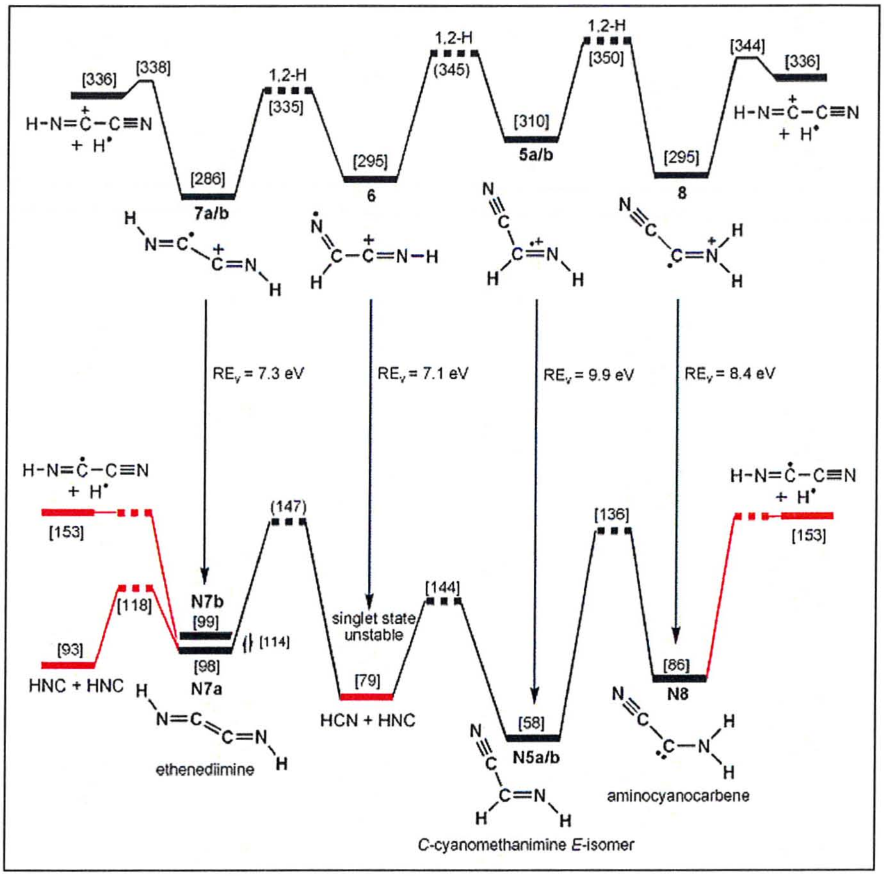

Scheme 3.14. CBS-APNO (values in square brackets) results showing the dissociation and isomerization chemistry of ions **5-8** and their neutral counterparts **N5-N8**. Vertical recombination energies (REv) shown are in eV. All values are in kcal/mol derived at 298 K.

A computational analysis of the neutral potential energy surface for the singlet-state neutral counterparts, **N7** and **N8**, yields a scenario that is analogous to that of the ions (Scheme 3.14). Triplet states were not considered [22] because the triplet-state carbene was found to be 29 kcal/mol higher than the singlet [9]. Table 2 lists the enthalpies of the neutral $C_2H_2N_2$ species discussed and their connecting transition states.

The calculations of Scheme 3.14 reveals that the energy corresponding to the ethenediimine neutral (**N7a/b**) is approximately 5 kcal/mol higher than the combined enthalpy of formation of the two HNC monomers. Given that the dedimerization of

N7a/b is associated with a sizeable barrier at 118 kcal/mol, and that any other dissociative or isomerization pathway is energetically more demanding, the dimeric conformers are therefore kinetically stable. The aminocyanocarbene neutral (**N8**) is kinetically stable as well, lying in a potential energy well at 86 kcal/mol. At elevated internal energies, the computational model predicts that **N8** would readily isomerize via a 1,2-H shift at 136 kcal/mol into the iminoacetonitrile neutral (**N5**) instead of dissociating via $H^{\bullet}$ loss at a threshold at 153 kcal/mol. **N5** could further isomerize via a 1,2-H shift at 144 kcal/mol into the neutral counterpart of the nitrene ion (**6**); which, we find, is not a stable species but rather dissociates into HCN + HNC. However, it is unlikely that most of the carbene neutrals generated in the NRMS experiments would isomerize or dissociate as their internal energy content would not be high enough to facilitate either process.

In NR mass spectrometry, the charge transfer taking place during neutralization is a vertical Frank-Condon process. Assuming resonant charge exchange takes place, an approximate internal energy content of the neutrals can be obtained from the difference between the vertical recombination energy (REv) and the adiabatic ionization energy (IEa). For a majority of the carbene neutrals (**N8**) generated, the excess internal energy (IEa-REv) computes to be ~15 kcal/mol. Therefore, they do not readily undergo isomerization. Analogously, the ethenediimine neutrals (**N7a/b**) generated possess an excess internal energy of ~20 kcal/mol which is consistent with the barrier associated with its dedimerization into the HNC monomers.

3.4. The NR mass spectra of $HN{=}C{=}C{=}NH^{\bullet +}$ *and* $NH_2\text{-}C\text{-}C{\equiv}N^{\bullet +}$.

Figs. 3.15a and 3.15b show the NR spectra of the neutral counterparts of **7** and **8**. Before scrutinizing these spectra, it is essential to be aware of the various sources for the peaks in the spectra. Peaks could result from (i) dissociation products of reionized *m/z* 54 species; (ii) collisionally-activated dissociation products of reionized *m/z* 54 neutrals; and (iii) reionization of neutral products from metastable and collision induced dissociations taking place in the 2ffr after the neutralization process but prior to deflection by the positive electrodes. Therefore, the similarity seen in the CID and the NR spectra of both **7** and **8** is reasonable and not unexpected.

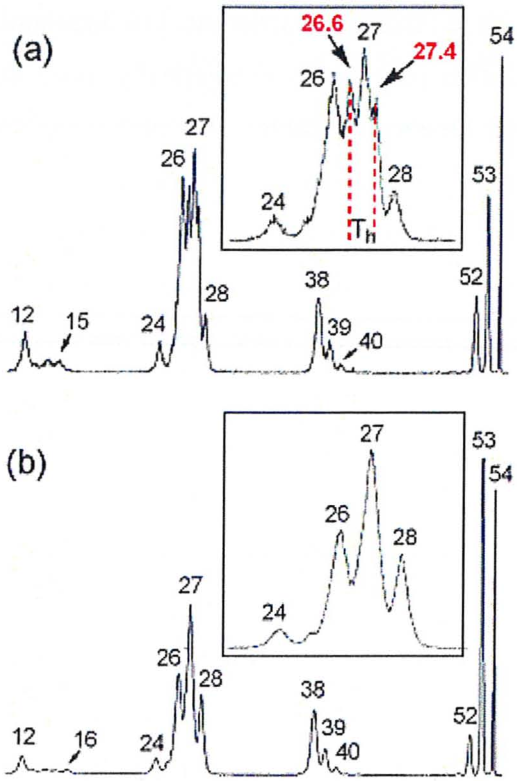

Figure 3.15. NR mass spectra of *m/z* 54 ions generated from ionized (a) xanthine and (b) aminomalononitrile. Insets display an enlarged picture of the *m/z* 23–29 region.

The NR spectra corresponding to both **7** and **8** display very prominent peaks at *m/z* 54 strongly *suggesting* that the ionic counterparts successfully underwent neutralization and survived the process. This observation only suggests and does not confirm the stability of the neutral species due to the reasonable possibility of the neutrals isomerizing prior to reionization. Hence, the isomeric purity of the reionized neutral is probed and will be discussed in Section 3.6.

Among the peaks seen in the NR spectrum of **7**, there are two peaks that correspond to non-integral values of 26.6 and 27.4. These extraordinary peaks are proposed to be ‘horns’ of a dish-shaped peak [17] centered at *m/z* 27. The reason for such a wide peak stems from a significant measured kinetic energy release ($T_h \approx 15$ kcal/mol). This value corresponds to the dissociation reaction, **N7** → 2HNC, associated with a considerable reverse barrier. To confirm the relationship of the dish-shaped peak to the above dissociation, the CID and the MI spectra were compared. The absence of such a peak in these spectra further confirmed that the dish-shaped peak described the dissociation products from neutral ethenediimine.

The model chemistry results from Scheme 3.14 predict that the two conformers of the neutral ethenediimine, **N7a** and **N7b**, lie at 98 and 99 kcal/mol respectively. These species are related by a rotational barrier of 15 kcal/mol. Computational models of the dissociation of either of the conformers into two HNC molecules predict that the reaction is associated with a barrier of approximately 20 kcal/mol. Furthermore, theory predicts that the incipient neutral species generated by vertical neutralization consist of ~20 kcal/mol of internal energy. Thus, all the listed theoretical results above are found to be remarkably consistent with the interpretation of the NR spectra.

There is sufficient kinetic stability in the neutral *m/z* 54 species generated to inhibit the dissociation of the low-energy species. However, at elevated internal energies, the incipient neutrals dissociate into two HNC molecules liberating a substantial quantity of kinetic energy.

The dish-shaped peak centered at *m/z* 27 is not seen in the NR spectrum of **8**. This observation is perfectly consistent with our model chemistry calculations that predict the dissociation reaction **N8** → 2HNC molecules (via **N5** and **N6**, respectively) to be associated with an unattainable barrier of 58 kcal/mol. This is due to the fact that the internal energy content of the neutrals generated is approximately 15 kcal/mol.

Fig. 3.16 shows the NR spectrum of *m/z* 54 ions obtained from the dissociation of DAMN. This spectrum also shows peaks at non-integral *m/z* values of 26.6 and 27.4. The presence of these peaks characterizes the dedimerization of **N7**. However, in comparison to the same peaks in the NR spectrum of **N7**, see Fig. 3.15a, the relative intensities of the peaks in the spectrum from DAMN are lower. This observation suggests that a mixture of ions **7** and **8** is generated.

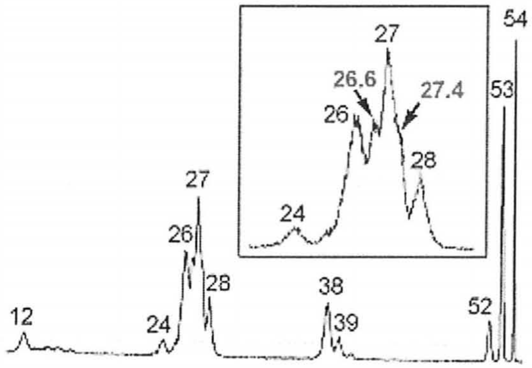

Figure 3.16. NR mass spectrum of m/z 54 ions generated from ionized diaminomaleonitrile. Inset displays an enlarged picture of the m/z 23–29 region.

3.5. A mechanistic proposal for the formation of ethenediimine ions (7) and aminocyanocarbene ions (8) from DAMN in different energy regimes.

The peaks in the MI and the CID spectra (not shown) of the DAMN molecular ion ($M^{\bullet+}$) and the prominent m/z 81 dissociation ion show that the m/z 54 ions are presumably generated according to Scheme 3.17.

As shown, the DAMN molecular ion undergoes a 1,3-H shift before losing HCN to yield m/z 81 **DAMN-1** ions. Thereafter, the **DAMN-1** ions could simply lose HNC to generate m/z 54 ions of connectivity matching ion **8**. However, a closer look at this loss shows that an intermediate is generated which is a hydrogen-bridged radical cation (**DAMN-2a**) [23]. Given that **DAMN-2a** could flip between rotamers via a low energy barrier at 318 kcal/mol, the generation of **DAMN-2b** makes two interesting reaction pathways accessible; proton transport catalysis (PTC) [24,25] and *quid-pro-quo* catalysis (QPQ) [26].

In the PTC pathway, the HNC molecule in the **DAMN-2b** geometry abstracts a proton from the amino nitrogen and donates it to the cyano nitrogen to produce **DAMN-4** which consists of ion **7** in complex with HNC. In the same manner, the QPQ pathway involves the same initial abstraction to yield a HC=NH$^+$ but instead of donating the proton from the CH moiety as in the PTC pathway, this pathway entails the back-donation of a proton from the NH moiety. This process yields **DAMN-3** which consists of ion **7** in complex with HCN. Both these reaction pathways are competitive processes with negligible barriers. However, comparing the dissociation of **DAMN-3** into ion **7** +

HCN to that of **DAMN-4** into ion **7** + HNC, the former dissociation reaction is energetically preferred. This is due to the fact that HCN is the lower energy neutral isomer.

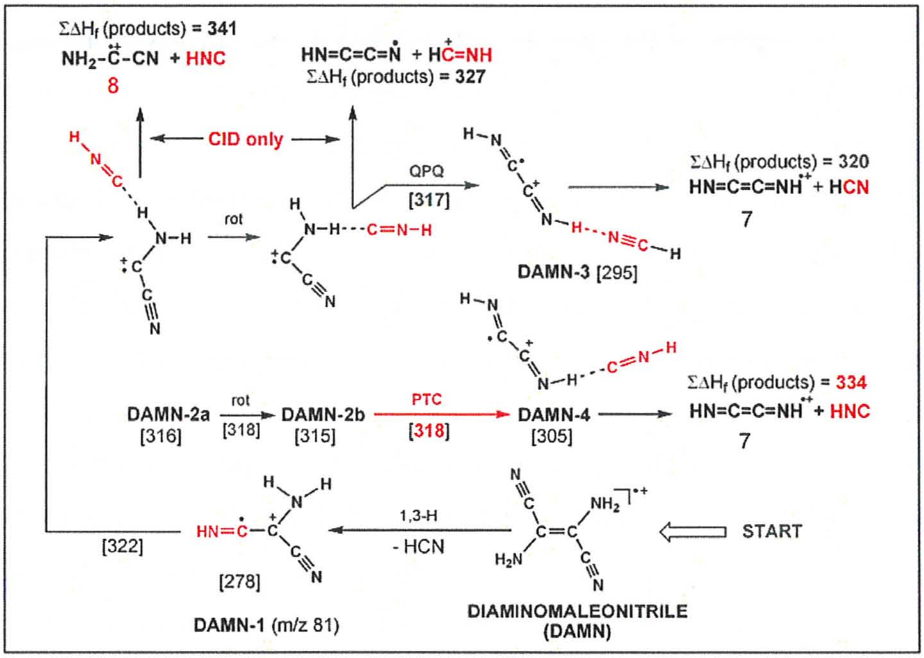

Scheme 3.17. CBS-QB3 (values in square brackets) results showing the generation of ions **7** and **8** from ionized DAMN in different energy regimes. All values are in kcal/mol derived at 298 K.

The computational results of Scheme 3.17 predict that the *m/z* 81 ions from DAMN would rather undergo a remarkable QPQ reaction pathway to generate ion **7** in an energy deficient regime. Both, the ion and the neutral undergo isomerization in this process. At elevated energy levels however, both ion **8** (*m/z* 54) and the $HC{=}NH^+$ (*m/z* 28) ion may possibly be co-generated.

The above proposal also holds true for *m/z* 54 ions generated from *m/z* 81 ions in the source as observed in the *m/z* 54 CID and NR spectra from DAMN. Table 4 lists the enthalpies of formation of the species shown in Scheme 3.17 along with their respective transition states and dissociation products.

3.6. The NR-CID mass spectra of $HN{=}C{=}C{=}NH^{\bullet+}$ *and* $NH_2\text{-}C\text{-}C{\equiv}N^{\bullet+}$.

As discussed in Sections 3.2 and 3.3, analysis of the *m/z* 54 CID spectra corresponding to ions **7** and **8** reveal that these ionic species are distinguishable and do not readily interconvert. The respective NR mass spectra of ions **7** and **8** display prominent survivor peaks at *m/z* 54 suggesting the stability of their neutral counterparts in the gas phase. However, it is not inconceivable that reionized species giving rise to the survivor peak seen in the NR spectra is due to isomeric or isobaric impurities. Therefore, to eliminate the likelihood of the generation of such impurities, the reionized *m/z* 54 species were subjected to collision induced dissociations with O_2 in the 3ffr of the instrument to generate NR-CID spectra. Provided the reionized species maintained their atom connectivity, the NR-CID spectrum should closely resemble the CID spectrum [22] discussed in Section 3.2.

Figs. 3.10b and 3.12b display the acquired NR-CID spectra of reionized ions **7** and **8**. In comparison to the respective CID spectra of Figs. 3.10a and 3.12a, the NR-CID spectra match very closely with regards to peaks and relative intensities confirming isomeric and isobaric purity. In line with this, previously discussed structurally characteristic peaks at *m/z* 15 for ion **7** and *m/z* 16 for ion **8** are clearly seen in the respective NR-CID spectra. Therefore, the neutral counterparts of the ethenediimine ion (**7**) and the aminocyanocarbene ion (**8**) are stable species in the rarefied gas phase.

Conclusions

From the combined results of tandem mass spectrometric experiments and CBS-QB3/APNO theoretical calculations, it is concluded that the ionic and neutral forms of ethenediimine (**7**) and aminocyanocarbene (**8**) are stable gas phase species in the microsecond timeframe of the NRMS experiment. One dissociation pathway of the metastable *m/z* 81 diaminomaleonitrile ions involves a remarkable *quid-pro-quo* (QPQ) catalysis that results in the loss of HCN from the hydrogen-bridged radical cation $[HNC{\cdots}H_2N\text{-}C\text{-}C{\equiv}N]^{\bullet+}$.

References

[1] A. Carrington, D.A. Ramsay, *Molecules in interstellar space*. The Royal Society, London, 1982.
[2] W.M. Irvine, F.P. Schloerb, Astrophys. J. 282 (1984) 516.
[3] J.P. Ferris, P.C. Joshi, E.H. Edelson, J.G. Lawless, J. Mol. Evol. 11 (1978) 293.
[4] J.P. Ferris, W.J. Hagan Jr., Tetrahedron. 40 (1984) 1093.
[5] R.A. Evans, P. Lorencak, T-K. Ha, C. Wentrup. J. Am. Chem. Soc. 113 (1991) 7261.
[6] C. Wentrup, P. Lorencak, A. Maquestiau, R. Flammang, Chem. Phys. Lett. 137 (1987) 241.
[7] R.A. Evans, S.M. Lacombe, M.J. Simon, G. Pfister-Guillouzo, C. Wentrup, J. Phys. Chem. 96 (1992) 4801.
[8] R.E. Moser, J.M. Fritsch, T.L. Westman, R.M. Kliss, C.N. Matthews, J.Am. Chem. Soc. 89 (1967) 5673.
[9] F. Freeman, M. Gomarooni, Int. J. Quant. Chem. 106 (2006) 2379.
[10] P.C. Burgers, J.K. Terlouw, in : M.E. Rose (Ed.), Specialist Periodical Reports: Mass Spectrometry, vol. 10, The Royal Society of Chemistry, London, 1989, p. 44 (Chapter 2).
[11] R. Flammang, Y. Van Haverbeke, S. Laurent, M. Barbieux-Flammang, M.W. Wong, C. Wentrup, J. Phys. Chem. 98 (1994) 5801.
[12] C. Lifshitz, E.D. Bergmann, U. Sheinok, Israel J. Chem. 6 (1968) 827.
[13] S.N. Bose, R.J.H. Davies, D.R. Boyd, Biomed. Mass Spectrom. 4 (1977) 305.
[14] R. Flammang, L. Gallez, Y. Van Haverbeke, M.W. Wong, C. Wentrup, Rapid Commun. Mass Spectrom. 10 (1996) 232.
[15] A.D. Boese, J.M.L. Martin, J. Chem. Phys. 121 (2004) 3405.
[16] H.F. van Garderen, P.J.A. Ruttink, P.C. Burgers, G.A. McGibbon, and J.K. Terlouw, Int. J. Mass Spectrom. Ion Proc. 121 (1992) 159.
[17] J.L. Holmes, C. Aubry, P.M. Mayer. Assigning Structures to Ions in Mass Spectrometry, CRC Press, Boca Raton, 2007.
[18] J.A. Montgomery, Jr, M.J. Frisch, J.W. Ochterski, and G.A. Petersson, J. Chem. Phys. 112, (2000) 6532.
[19] J.W. Ochterski, G.A. Petersson, J.A. Montgomery, Jr., J. Chem. Phys. 104 (1996) 2598.
[20] M. J. Frisch et al. Gaussian 03 (Revisions C.02 and D.01), Gaussian, Inc., Wallingford CT, 2004.
[21] G.A. McGibbon, C.A. Kingsmill, J.K. Terlouw, P.C. Burgers, Int. J. Mass Spectrom. Ion Proc. 121 (1992) R11.
[22] G.A. McGibbon, C.A. Kingsmill, J.K. Terlouw, Chem. Phys. Lett. 222 (1994) 129.
[23] P.C. Burgers, J.K. Terlouw, in: N.M.M. Nibbering (Ed.), Encyclopedia of Mass Spectrometry, vol. 4, Elsevier, Amsterdam, 2005, p. 173.
[24] C.Y. Wong, P.J.A. Ruttink, P.C. Burgers, J.K. Terlouw, Chem. Phys. Lett. 390 (2004) 176.
[25] C.Y. Wong, P.J.A. Ruttink, P.C. Burgers, J.K. Terlouw, Chem. Phys. Lett. 387 (2004) 204.
[26] K.J. Jobst, P.C. Burgers, P.J.A. Ruttink, J.K. Terlouw, Int. J. Mass Spectrom. 254 (2006) 127.

Appendix to Chapter 3

Table 1a. Energetic data [a] derived from **CBS-QB3** and **CBS-APNO** calculations for minima of stable ionic isomers of $C_2H_2N_2$ and their connecting transition states.

Ionic species	**CBS-QB3 E(total)** [0K]	**QB3 ZPE**	**QB3 $\Delta_fH^0_0$**	**QB3 $\Delta_fH^0_{298}$**	**APNO $\Delta_fH^0_{298}$**
1	-186.191984	22.6	304.1	302.8	302.7
2a	-186.202316	22.0	297.6	296.7	296.3
2b	-186.195574	21.8	301.8	300.9	299.1
3a	-186.159687	23.4	324.3	323.0	323.8
3b	-186.160496	23.6	323.8	322.4	323.3
4	-186.189889	22.3	305.4	304.3	305.3
5a	-186.181675	22.1	310.5	309.4	309.8
5b	-186.181132	22.3	310.9	309.7	310.1
6	-186.205889	22.6	295.3	294.1	294.5
7a	-186.214811	22.2	289.7	288.8	288.6
7b	-186.216134	22.4	288.9	287.9	285.7
8	-186.204802	23.8	296.0	294.8	294.9
9	-186.173970	21.8	315.4	314.1	314.4
HBRC-1	-186.172894	20.7	316.0	315.4	315.2
TS **1** → **2**	-186.123165	18.6	347.2	346.3	345.3
TS **2a** → **9**	-186.165356	21.4	320.8	319.3	317.9
TS **2** → **HBRC-1**	-186.133423	20.4	340.8	340.3	341.4
TS **3a** → **5a**	-186.123460	21.8	347.1	345.5	346.1
TS **3b** → **4**	-186.089026	18.9	368.7	367.6	367.0
TS **5a** → ***m/z*** **53**	-186.131936	17.4	341.7	340.8	340.4
TS **5a** → **6**	-186.124516	18.4	346.4	345.2	[b]
TS **5a** → ***m/z*** **28**	-186.125661	20.4	345.7	345.0	344.1
TS **5a** → **8**	-186.115557	19.0	352.0	351.0	350.2
TS **5b** → **8**	[c]	-	-	-	-
TS **6** → ***m/z*** **53**	-186.135252	17.4	339.7	338.7	339.1
TS **6** → **7b**	-186.139189	18.8	337.2	336.4	335.4
TS **7a** → **6**	[d]	-	-	-	-
TS **9** → **6**	-186.176238	21.3	313.9	312.5	[e]
TS **8** → ***m/z*** **53**	-186.128390	17.5	344.0	343.0	344.0
TS 7 → ***m/z*** **53**	[b]	-	-	-	338.3

[a] $E_{(total)}$ in Hartrees, all other components, including the ZPE scaled by 0.99, are in kcal/mol. [b] The desired transition state could not be found. [c] The desired transition state optimizes to TS **5a** → **8**. [d] The desired transition state optimizes to TS **6** → **7b**. [e] The desired transition state optimizes to **2a**.

Table 1b. Energetic data [a] derived from **BMK/CBSB7** and **B3LYP/CBCB7** calculations (with their respective discrepancies relative to corresponding CBS-QB3 values) for minima of stable ionic isomers of $C_2H_2N_2$ and their connecting transition states. Note that all discrepancies have been calculated taking the zero-point energies into consideration.

Ionic species	**$\Delta_fH^0_{298}$ (QB3)**	**$\Delta_fH^0_{298}$ (BMK)** [b]	**Discrepancy** $\Delta_fH^0_{298}$ (BMK-QB3)	**$\Delta_fH^0_{298}$ (B3LYP)** [b]	**Discrepancy** $\Delta_fH^0_{298}$ (B3LYP-QB3)
1	302.8	-	-	-	-
2a	296.7	292.4	**-4.3**	291.1	**-6.2**
2b	300.9	298.4	**-2.5**	296.5	**-5.2**
3a	323.0	323.5	**0.5**	321.4	**-0.8**
3b	322.4	327.0	**4.6**	320.8	**-0.6**
4	304.3	301.3	**-3.0**	298.6	**-6.0**
5a	309.4	309.4	**0.0**	307.6	**-2.3**
5b	309.7	309.7	**0.0**	307.8	**-2.3**
6	294.1	294.8	**0.7**	293.8	**-0.3**
7a	288.8	[c]	-	282.7	**-6.5**
7b	287.9	286.3	**-1.6**	281.8	**-6.4**
8	294.8	295.2	**0.4**	289.5	**-4.1**
9	314.1	[d]	-	313.2	**-1.8**
HBRC-1	315.4	321.7	**6.3**	321.2	**3.9**
TS **1** → **2**	346.3	345.6	**-0.7**	343.2	**-3.1**
TS **2a** → **9**	319.3	316.2	**-3.1**	317.4	**-1.9**
TS **2** → **HBRC-2**	340.3	346.0	**5.7**	341.8	**1.5**
TS **3a** → **5a**	345.5	343.4	**-2.1**	344.4	**-1.1**
TS **3b** → **4**	367.6	366.7	**-0.9**	364.4	**-3.2**
TS **5a** → ***m/z* 53**	340.8	343.8	**3.0**	338.7	**-2.1**
TS **5a** → **6**	345.2	346.4	**1.2**	339.9	**-5.3**
TS **5a** → ***m/z* 28**	345.0	351.6	**6.6**	347.0	**2.0**
TS **5a** → **8**	351.0	351.5	**0.5**	347.4	**-3.6**
TS **6** → ***m/z* 53**	338.7	343.7	**5.0**	338.8	**0.1**
TS **6** → **7b**	336.4	335.4	**-1.0**	331.7	**-4.7**
TS **9** → **6**	312.5	313.3	**0.8**	312.2	**-0.3**
TS **7** → ***m/z* 53**	[e]	340.9	-	-	-
TS **8** → ***m/z* 53**	343.0	346.5	**3.5**	339.8	**-3.2**

[a] $E_{(total)}$ in Hartrees, all other components, including the ZPE scaled by 0.99, are in kcal/mol. [b] The CBS-QB3 $\Delta_fH^0_{298}$ of **1** is used as the value of reference. [c] The desired minimum optimizes to a 1st order saddle point. [d] The desired minimum optimizes to **6**. [e] The desired transition state could not be found.

Table 2. Energetic data [a] derived from **CBS-QB3** and **CBS-APNO** calculations for selected minima of stable neutral isomers of $C_2H_2N_2$ and their connecting transition states.

Ionic species	CBS-QB3 E(total) [0K]	QB3 ZPE	QB3 $\Delta_fH^0_0$	QB3 $\Delta_fH^0_{298}$	APNO $\Delta_fH^0_{298}$
N5a	-186.581318	24.5	59.7	58.2	58.3
N5b	-186.582492	24.6	59.0	57.5	57.7
N6	No minimum	-	-	-	-
N7a	-186.518834	23.2	98.9	97.7	97.5
N7b	-186.517408	23.1	99.8	98.7	99.2
N8	-186.537042	24.6	87.5	86.1	86.1
TS **N5a** → **N5b**	-186.540876	22.7	85.1	83.7	84.3
TS **N5b** → **N8**	-186.458389	20.0	136.8	135.6	135.8
TS **N7a** → **N7b**	-186.491778	22.0	115.9	114.7	114.1
TS **N7a** → **N8**	-186.419764	20.0	161.1	159.4	155.8
TS **N5a** → **HCN + HNC**	-186.443606	19.6	146.1	144.8	143.9
TS **N7a** → **2 HNC**	-186.483945	20.3	120.8	120.0	119.4
TS **N7a** → **HCN + HNC**	-186.439735	19.5	148.5	147.4	[b]
TS **N7b** → **2 HNC**	-186.486378	20.5	119.3	118.3	117.9

[a] $E_{(total)}$ in Hartrees, all other components, including the ZPE scaled by 0.99, are in kcal/mol. [b] The desired transition state could not be found.

Table 3. Energetic data for various dissociation products of ionized and neutral $C_2H_2N_2$ derived from **CBS-QB3/CBS-APNO** calculations [a].

Species	CBS-QB3 E(total) [0 K]	QB3 $\Delta_fH^0_0$	QB3 $\Delta_fH^0_{298}$	APNO $\Delta_fH^0_{298}$
HCNCN$^+$ + H$^\bullet$	-	**351.2**	**351.2**	**350.9**
CNCNH$^+$ + H$^\bullet$	-	**351.3**	**351.6**	**352.0**
HNCCN$^+$ + H$^\bullet$	-	**335.9**	**336.0**	**336.2**
HNCCN$^\bullet$ + H$^\bullet$	-	**152.9**	**153.1**	**152.9**
HCNCN$^+$	-185.617054	299.6	299.1	298.8
CNCNH$^+$	-185.616887	299.7	299.5	299.9
HNCCN$^+$	-185.641405	284.3	283.9	284.1
HNCCN$^\bullet$	-185.932872	101.3	101.0	100.8
H$^\bullet$	-0.499818	51.6	52.1	52.1
HCNH$^+$ + CN$^\bullet$	-	**332.8**	**332.8**	**333.1**
HCNH$^+$	-93.558686	227.0	226.2	226.8
CN$^\bullet$	-92.587607	105.8	106.6	106.3
HCN$^{\bullet+}$ + HCN	-	**377.7**	**377.6**	**378.6**
HNC$^{\bullet+}$ + HCN	-	**355.6**	**355.5**	**356.0**
HCN + HCN	-	**63.6**	**63.4**	**64.0**
HCN + HNC	-	**77.7**	**77.7**	**78.5**
HNC + HNC	-	**91.8**	**92.0**	**93.0**
HCN$^{\bullet+}$	-92.787025	345.9	345.9	346.6
HNC$^{\bullet+}$	-92.822241	323.8	323.8	324.0
HCN	-93.287537	31.8	31.7	32.0
HNC	-93.265114	45.9	46.0	46.5

[a] $E_{(total)}$ in Hartrees, all other components, including the ZPE scaled by 0.99, are in kcal/mol.

Table 4. Energetic data [a] derived from **CBS-QB3** calculations for minima of stable ionic isomers of diaminomaleonitrile (**DAMN**), their connecting transition states and dissociation products.

Ionic species	**CBS-QB3 E(total)** [0K]	**QB3 ZPE**	**QB3 $\Delta_fH^0_0$**	**QB3 $\Delta_fH^0_{298}$**
DAMN-1	-279.568616	36.7	279.9	277.5
DAMN-2a	-279.508171	34.0	317.8	316.3
DAMN-2b	-279.509855	34.1	316.8	315.1
DAMN-3	-279.542324	32.9	296.4	295.1
DAMN-4	-279.526485	33.1	306.3	305.0
TS **DAMN-1 → 2a**	-279.498528	34.7	323.9	322.1
TS **DAMN-2a → 2b**	-279.504710	33.4	320.0	318.1
TS **DAMN-2b → 3**	-279.506009	34.0	319.2	317.3
TS **DAMN-2b → 4**	-279.504469	34.1	320.2	318.4
$HNCCNH^{\bullet+}$ + HCN	-	-	**320.7**	**319.6**
$HNCCNH^{\bullet+}$ + HNC	-	-	**334.8**	**333.9**
$NH_2CCN^{\bullet+}$ + HNC	-	-	**341.9**	**340.8**
$HNCCNH^{\bullet+}$	-186.216134	-	288.9	287.9
$NH_2CCN^{\bullet+}$	-186.204802	-	296.0	294.8
HCN	-93.287537	-	31.8	31.7
HNC	-93.265114	-	45.9	46.0
$HNCCN^{\bullet}$ + $HCNH^{+}$	-	-	**328.3**	**327.2**
$HNCCN^{\bullet}$	-185.932872	-	101.3	101.0
$HCNH^{+}$	-93.558686	-	227.0	226.2

[a] $E_{(total)}$ in Hartrees, all other components, including the ZPE scaled by 0.99, are in kcal/mol.

Figure 3.18. Selected optimized geometries (CBSB7 basis set) of stable intermediates and transition states involved in the isomerization and dissociation of ionized and neutral $C_2H_2N_2$.

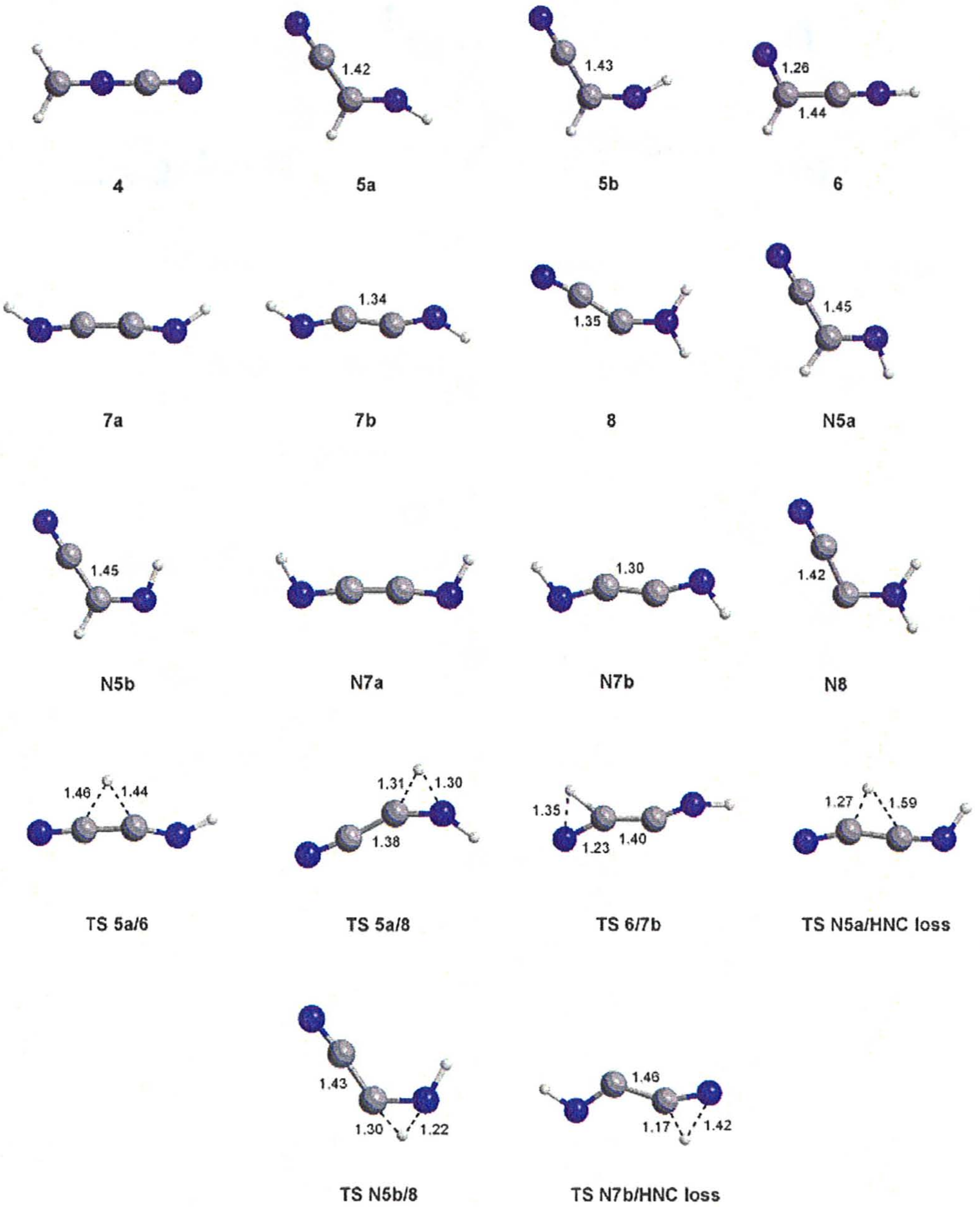

Figure 3.19. Selected optimized geometries (CBSB7 basis set) of stable intermediates and transition states involved in the isomerization and dissociation of ionized diaminomaleonitrile (**DAMN**).

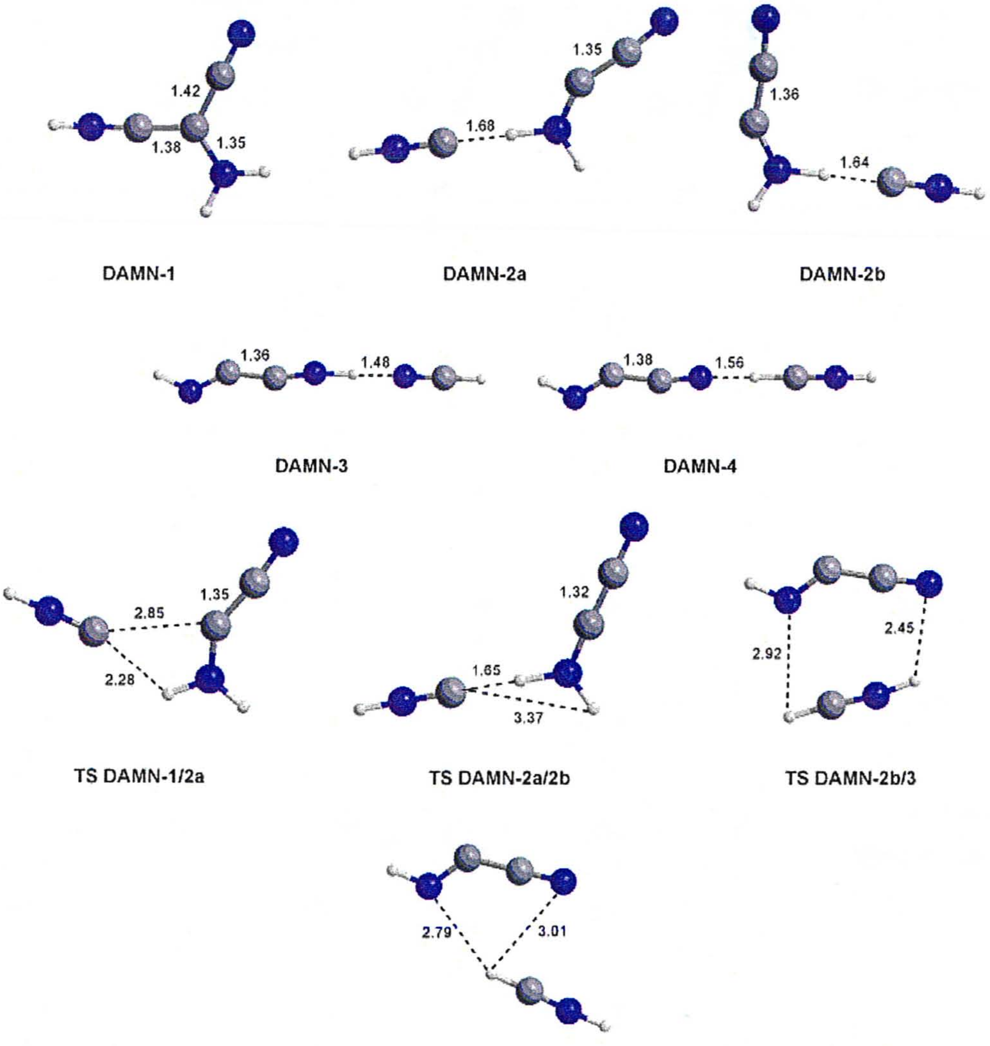

DAMN-1 **DAMN-2a** **DAMN-2b**

DAMN-3 **DAMN-4**

TS DAMN-1/2a **TS DAMN-2a/2b** **TS DAMN-2b/3**

TS DAMN-2b/4

Chapter 4

The generation and characterization of the HC≡N dimer ion HC=N-N=CH$^{\bullet+}$ and its nitrene isomer HC=N-C(=N)H$^{\bullet+}$ by tandem mass spectrometry and computational chemistry

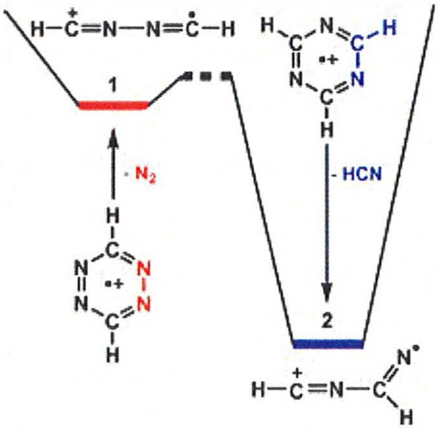

In a previous study [K.J.Jobst, M.R.Hanifa, J.K.Terlouw, Chem. Phys. Lett. 462(2008)152], we have shown that the HNC dimer ion, HN=C=C=NH$^{\bullet+}$, has a neutral counterpart in the rarefied gas phase. A similar study was performed to examine the stability of the ionic and neutral forms of the HCN dimer, HC=N-N=CH.

Ionized *s*-tetrazine was proposed to generate HC=N-N=CH$^{\bullet+}$ following N_2 loss. A mechanistic analysis using the CBS-QB3/APNO model chemistries confirmed that this ion was generated. However, this ion possessed sufficient internal energy to undergo rearrangement into a more stable nitrene ion, HC=N-C(=N)H$^{\bullet+}$. The nitrene isomer was separately generated from *s*-triazine following HCN loss. Collision-induced dissociation (CID) characteristics were used to identify these ionic species.

Neutralization-reionization experiments interestingly reveal that the neutral forms of either of the HCN dimer ions are not viable species in the gas phase despite the stability of their ionic counterparts. All experimental results are in agreement with our computational results.

The work described here has been published previously in an article under a different title : Karl J. Jobst, M. Ruzni Hanifa, Paul J.A. Ruttink and Johan K. Terlouw. Chem. Phys. Lett. 473 (2009) 257-262.

1. Introduction

Both, HCN and HNC are widely distributed in the universe [1]. HCN, $(CN)_2$ and H-C≡C-C≡N have been identified in the atmosphere of Titan [2,3]. HCN and/or $CN^{\bullet}$ have been detected in comets such as Halley and the asteroid Chiron [4]. Therefore, the characterization of covalent dimers of [H,C,N] including the ionic and neutral forms of $C_2H_2N_2$ is of profound prebiotic and astrochemical interest [5,6].

To date, two $C_2H_2N_2$ isomers; CH_2=N-C≡N (*N*-cyanomethanimine) and HN=C(H)-C≡N (*C*-cyanomethanimine or iminoacetonitrile), have been generated and probed using various spectroscopic methods in an earlier study. The results revealed that the ions and the neutral counterparts of the respective $C_2H_2N_2$ species were stable species in the rarefied gas phase [4,5,7]. Additionally, we have shown in a previous study (see Chapter 3) that two other $C_2H_2N_2$ isomers, HN=C=C=NH (ethenediimine) and H_2N-C-C=N (aminocyanocarbene), can be generated as stable ions and neutrals in the gas phase [8].

An earlier study by Nenner and co-workers [9] used threshold photoelectron-photoion coincidence techniques (TPEPICO) in conjunction with synchrotron radiation in the vacuum UV (9-22 eV) to study the dissociation chemistry of the *s*-tetrazine ion. The results of the study [9] reported the generation of a $C_2H_2N_2^{\bullet+}$ fragment following the loss of N_2. The connectivity of the ion generated was not verified. However, a closer look at the structure of *s*-tetrazine reveals that the loss of N_2 could interestingly generate the elusive linear HCN dimer ion, $HC=N-N=CH^{\bullet+}$ (**1**). In line with this, the results of our combined computational and tandem mass spectrometry study reveal that the *s*-tetrazine ion does in fact yield the dimer ion **1**. However, model chemistry calculations show that this ion, despite being a local minimum on the $C_2H_2N_2$ potential energy surface, is generated in the dissociation of *s*-tetrazine with sufficient internal energy to readily interconvert into the more stable nitrene isomer, $HC=N-C(=N)H^{\bullet+}$ (**2**). Another precursor studied, *s*-triazine, is also found to yield a prominent signal at *m/z* 54 corresponding to the connectivity of the nitrene isomer. The characterization of this $C_2H_2N_2^{\bullet+}$ fragment from *s*-triazine supports the proposed dissociation chemistry of *s*-tetrazine. Finally, the neutralization-reionization (NR) mass spectra [10] acquired in this study demonstrate that both the $C_2H_2N_2^{\bullet+}$ species (**1** and **2**) do not have stable neutral counterparts in the rarefied gas phase. A separate theoretical study on the neutral $C_2H_2N_2$ potential energy surface did not show local minima for the neutral counterparts of ions **1** and **2** in agreement with our experimental observations.

2. Experimental and Theoretical Methods

The mass spectrometric experiments were performed on the VG Analytical ZAB-R mass spectrometer of BE_1E_2 geometry (E = electric sector, B = magnet). Typically, electron ionization conditions (70 eV) and an accelerating potential of 8 kV are used [11]. Metastable ion (MI) mass spectra were recorded in the second field free region (2ffr); collision induced dissociation (CID) mass spectra were recorded in the 2ffr and 3ffr using oxygen or helium as the collision gas. Neutralization-reionization (NR) mass spectra were recorded using *N*,*N*-dimethylaniline as the reducing agent and oxygen gas for reionization in the 2ffr. All kinetic energy releases (KER) (corrected $T_{0.5}$ values) reported were acquired using standard procedures [12]. The details of this instrument and the acquisition of the NR mass spectra have been previously explained [11].

All solid samples were introduced into the instrument via a heated direct insertion probe. The HCN trimer *s*-triazine (research grade) was obtained from Sigma-Aldrich and used without further purification. Samples of *s*-tetrazine were prepared as outlined by J. Sauer and co-workers [13]. The reagents used for the synthesis were commercially available (Sigma-Aldrich) and of research grade.

All computational values were obtained using CBS-QB3 and the computationally more demanding CBS-APNO model chemistries [14,15]. These calculations were performed using the Gaussian 03 Revision C.02 and D.01 suite of programs on SHARCNET [16]. The resulting total energies and enthalpies of formation ($\Delta_fH^0_{298}$ in kcal/mol) for the minima and connecting transition states (TS) of various ions and neutrals are presented in Tables 1 and 2. Theoretical enthalpies for all relevant dissociation products are presented in Table 3. Schemes 4.2-4.6 show mechanistic proposals for the generation of various pertinent ions including those corresponding to *m/z* 54. Detailed geometries of selected species are displayed in the Appendix, Figures

4.9, 4.10, and 4.11. The identity of local minima and connecting transition states (TS) were confirmed by frequency analysis.

3. Results and Discussion

3.1. The structure of the m/z 54 ions generated from s-tetrazine.

The mass spectrum of *s*-tetrazine, see Fig. 4.1, displays a significant peak at *m/z* 54 presumably corresponding to the ionic HCN dimer, $HC{=}N{-}N{=}CH^{\bullet +}$ (**1**).

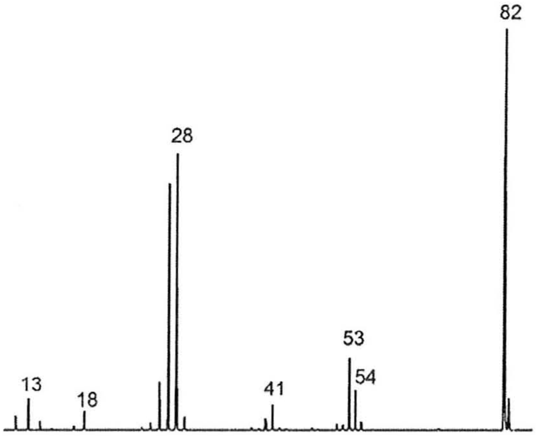

Figure 4.1. 70 eV EI mass spectrum of *s*-tetrazine.

The proposed fragmentation pathway studied in Scheme 4.2 shows that this ion can be generated from the parent ion following a ring-opening and subsequent N_2 loss.

The observed dissimilarity in the collision-induced dissociation (CID) spectrum of the *m/z* 54 ions from *s*-tetrazine (see Fig. 4.3a) in comparison to those from other $C_2H_2N_2^{\bullet +}$ ions that have been previously characterized is indicative of a formerly unseen connectivity. In the same vein, the low mass region of the spectrum seen in Fig. 4.3a shows a weak but structure diagnostic peak at *m/z* 13 corresponding to the -CH fragment of the HCN dimer ion (**1**). Previously studied $C_2H_2N_2$ isomers such as $CH_2{=}N{-}C{\equiv}N$ (*N*-cyanomethanimine), $HN{=}C{=}C{=}NH$ (ethenediimine) and $NH_2{-}C{-}C{=}N$ (aminocyanocarbene) exhibit structure-diagnostic signals at *m/z* 14, 15 and 16 respectively. In addition, comparison of the CID spectrum corresponding to $HN{=}C(H){-}C{\equiv}N$ (*C*-cyanomethanimine or iminoacetonitrile) to the spectrum in Fig. 4.3a reveals that the *m/z* 53:28 ratio in the former is relatively higher than that seen in the latter (~20:1 vs. ~1:2).

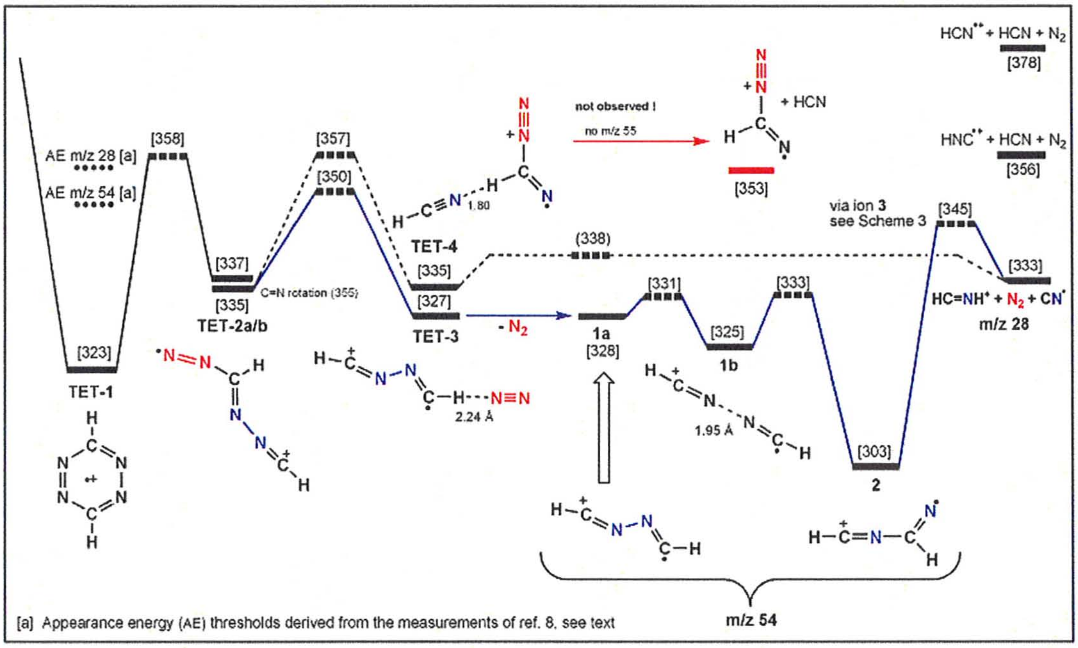

Scheme 4.2. Theoretical prediction of the formation of the *m/z* 54 and *m/z* 28 ions from metastable *s*-tetrazine ions (**TET-1**). All values are in kcal/mol derived at 298 K. The values in square brackets and round brackets refer to enthalpies of formation obtained using the CBS-APNO and CBS-QB3 model chemistries.

As previously stated, the generation of ion **1** from ionized *s*-tetrazine is adequately substantiated by the theoretical calculations of Scheme 4.2. The scheme shows that the *s*-tetrazine ion (**TET-1**) initially undergoes a ring-opening step via cleavage of a C-N bond. This step is associated with a transition state (TS) at 358 kcal/mol. Next, the C-N_2 bond in the ring-opened structure, **TET-2**, is elongated to rearrange into **TET-3**. This resulting structure is a hydrogen-bridged radical cation (HBRC) [17]. When the enthalpy of formation of this HBRC is compared to that of its dissociation products, HC=N-N=$CH^{\bullet+}$ (**1**) + N_2, the hydrogen bridge is noted to provide a minor stabilization energy of ~1 kcal/mol.

With respect to the isomerization threshold **TET-1** → **2**, the **TET-3** ions are generated with ~30 kcal/mol of internal energy. A significant portion of this internal energy (~15 kcal/mol) is redistributed as translational energy in the dissociation reaction of the HBRC involving the loss of N_2. This is observed in the measurement of a sizeable kinetic energy release ($T_{0.5}$ = 600 meV) from the wide dish-shaped *m/z* 54 peak in the MI spectrum of **TET-1** (not shown).

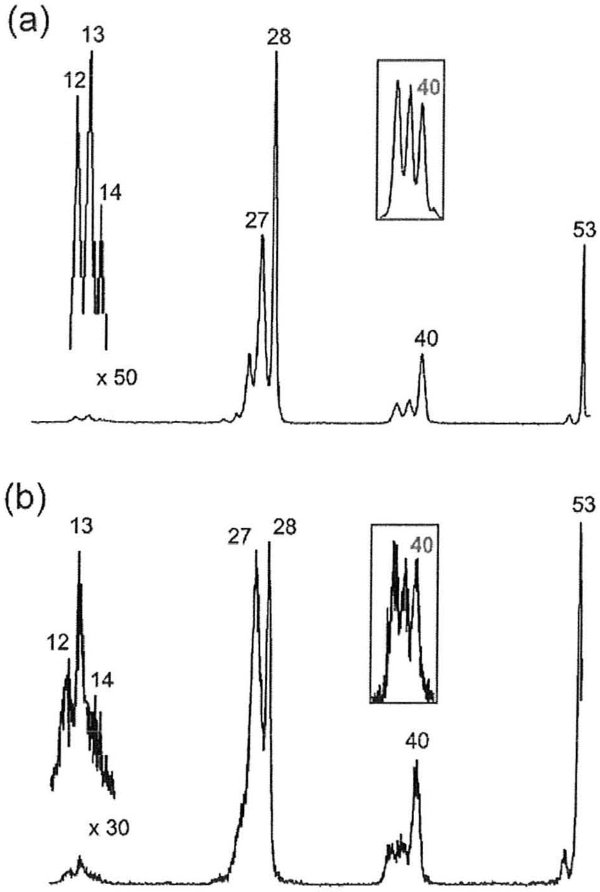

Figure 4.3. (a,b) CID (O_2) mass spectra of *m/z* 54 ions generated from *s*-tetrazine in the source and from metastable molecular ions. Insets show partial CID (He) spectra of *m/z* 38-40 region.

In regards to the appearance energy (AE) of the $C_2H_2N_2^{\bullet+}$ ion from *s*-tetrazine, Nenner and co-workers [9] published a value of 10.2 eV. Using this value, the dissociation threshold level is found to be at 349 kcal/mol. Note that this threshold is obtained using the reported AE and the enthalpy of formation for neutral *s*-tetrazine (115 kcal/mol) obtained from the CBS-APNO model chemistry at 298 K. The CBS-APNO value was used instead of the approximate value reported by Lias et al. [18] (111 kcal/mol) or the value used by Nenner et al. [9] (102 kcal/mol). Nevertheless, when compared to the theoretical threshold of 358 kcal/mol, there exists a discrepancy of about 9 kcal/mol.

In spite of this, there is little likelihood that there exists an alternative fragmentation of the *s*-tetrazine ion (**TET-1**) involving the loss of N_2. Given the planes of symmetry in **TET-1**, the only other ring-opening mechanism entails the cleavage of the N-N bond. Model chemistry calculations reveal that this process is associated with a high energy barrier leading to a three-body dissociation into $HCN^{\bullet+}$ + HCN + N_2. A reaction scan at the B3LYP/CBSB7 level of theory shows that the associated TS lies at 384 kcal/mol. Similarly, the generation of the ylide-ion (**TET-5**) from **TET-1**, see Table 1, is associated with an even higher energy barrier. The TS corresponding to the 1,2-H shift is found to lie at 415 kcal/mol. Therefore, the path involving **TET-2** is, energetically, the most feasible way to generate $C_2H_2N_2^{\bullet+}$ ions.

Ions **TET-2** can also be used to rationalize the generation of the *m/z* 28 fragment ions ($HC{=}NH^+$) reported by Nenner et al. [9]. Theory predicts that this pathway involves an intermediate (**TET-4**) which is another HBRC formed from the elongation of the N-NCH bond in **TET-2** followed by the migration of the HCN moiety. One may envisage **TET-4** to readily dissociate yielding HCN and the corresponding *m/z* 55 fragment ion. However, computations reveal that this dissociation (353 kcal/mol) does not occur, see Scheme 4.2. Instead, the HCN moiety abstracts a proton via a low energy barrier at 338 kcal/mol to undergo a three-body dissociation to form $HC{=}NH^+$ + $CN^\bullet$ + N_2. The experimental study by Nenner et al. [9] concluded that the *m/z* 28 ions are primarily generated from the $C_2H_2N_2^{\bullet+}$ species by the consecutive process : **TET-1** (*m/z* 82) → *m/z* 54 → *m/z* 28. In line with these observations, the base peak in the *m/z* 54 CID spectrum (see Fig. 4.3a) corresponds to *m/z* 28. By the same token, Scheme 4.2 shows that both, the consecutive and three-body dissociation mechanisms, share the transition state, TS **TET-1/2,** at 358 kcal/mol. This raises the possibility of the two mechanisms becoming competitive in a narrow band of energies close to the onset for *m/z* 28 generation. In this context, according to the studies of Nahon et al. [19], we note that a pure three-body dissociation mechanism illustrates the dissociation of *neutral* *s*-tetrazine.

Following the loss of N_2, Scheme 4.2 shows that the enthalpy of formation of ion **1a** is 328 kcal/mol. Although this ion is a local minimum on the ionic $C_2H_2N_2^{\bullet+}$ potential energy surface, it is seen that an excess energy of only 3 kcal/mol results in the elongation of the central N-N bond to yield a more stable (325 kcal/mol) long-bonded species (**1b**). In an energy-rich regime, ion **1b** serves as an intermediate in its isomerization into a much more stable nitrene isomer, $HC{=}N{-}C({=}N)H^{\bullet+}$ (**2**). This process proceeds via a 1,2-HCN shift at 333 kcal/mol. Therefore, to predict that a majority of the ions **1a/b** generated readily converts into ion **2** is reasonable. To support this, the presence of a protruding N atom in the structure of ion **2** rationalizes the exaggerated N atom loss generating a peak at *m/z* 40 in the *m/z* 54 helium CID spectrum (Fig. 4.3a inset).

In the same vein, when oxygen is used as the collision gas, the *m/z* 54 CID spectrum displays a peak at *m/z* 40 which is comparatively much higher in intensity. This is referred to as the 'Oxygen effect' and has been tentatively explained by Aubry et al. [20]. We reported the same effect in a previous study on the viability of the HNC dimer, $HN{=}C{=}C{=}NH^{\bullet+}$ [8,21]. In the case of the HNC dimer however, there is no exposed N atom. Therefore, the prominent peak at *m/z* 40 in the *m/z* 54 oxygen CID spectrum substantially decreased in intensity when the collision gas was replaced with helium.

In conclusion, the experimental observations agree with the theoretical predictions that a majority of the *m/z* 54 ions generated in the source of the instrument isomerizes into the more stable nitrene ion **2** before collisions. However, the dissociation behavior of ion **2** was studied to explore the possibility of a minority of source-generated ions retaining their initial connectivity. Section 3.2 explains the generation of such low energy ions by the dissociative ionization of *s*-triazine.

3.2. The structure of the m/z 54 ions generated from s-triazine.

s-Triazine is another precursor molecule that displays a sizeable peak at *m/z* 54 in its mass spectrum corresponding to ions of elemental composition $C_2H_2N_2^{\bullet+}$ (see Fig. 4.4).

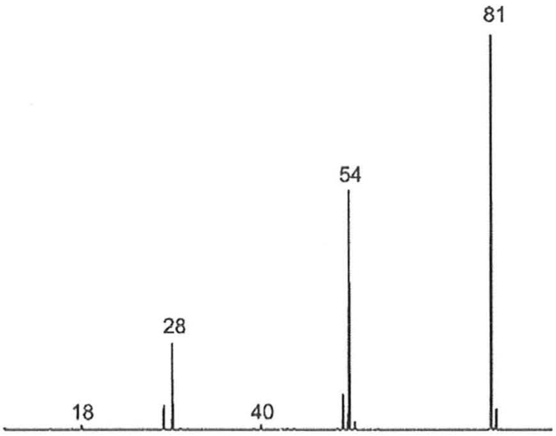

Figure 4.4. 70 eV EI mass spectrum of *s*-triazine.

Theoretical calculations, see Scheme 4.5, show that the *m/z* 54 ions derived from the parent *s*-triazine ion (**TRI-1**) correspond to the nitrene ion, HC=N-C(=N)H$^{\bullet+}$ (**2**). Unlike in the case of *s*-tetrazine, the *m/z* 54 ion **2** obtained from *s*-triazine is generated at the dissociation threshold. The lowest energy fragmentation pathway for the generation of ion **2** is as follows; **TRI-1** → **TRI-3** → **2** + HCN. It is likely that the elongation of the C-NCH bond in **TRI-3** could lead to various HBRCs (**TRI-4/5**) and ion-dipole complexes. However, as shown in the scheme, there are no interfering high energy barriers and **2** + HCN is generated at threshold. This is further supported by the small kinetic energy release measured for the reaction involving HCN loss ($T_{0.5} \leq 1$ meV).

One may envision the dissociating HCN molecule from **TRI-5** to engage in a process coined proton-transport catalysis (PTC) [22,23] to generate an isomeric ion **3**, HC=N-C=NH$^{\bullet+}$. However, when computationally probed, we find that the barrier for this assisted 1,2-H shift is well above the dissociation threshold at 345 kcal/mol. An unassisted 1,2-H shift on the HBRC, **TRI-4**, to yield the connectivity corresponding to ion **3** is also unlikely due to an associated high energy barrier : the 1,2-H shift in ion **2** to yield ion **3** is associated with a TS that is at 345 kcal/mol (see Scheme 4.6). In addition, another 1,2-H shift in ion **2** yielding a different isomer, H-C-N(H)-C≡N$^{\bullet+}$, was also probed and found to be associated with a high energy barrier. In comparison, the resulting (as yet uncharacterized) carbene ion is approximately 20 kcal/mol higher in energy.

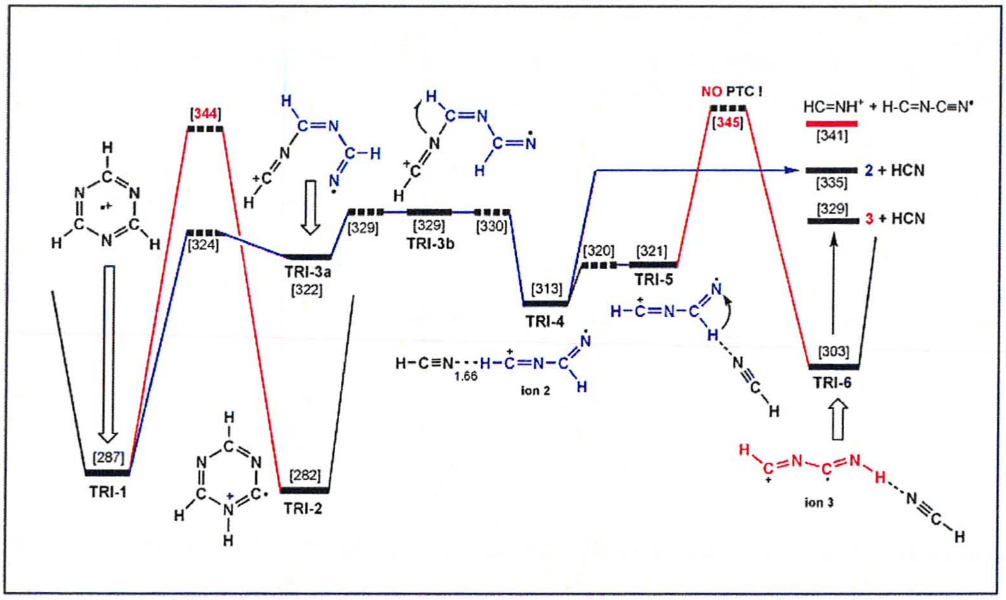

Scheme 4.5. Proposed mechanism for the generation of *m/z* 54 ions from metastable *s*-triazine ions (**TRI-1**). All values are in kcal/mol derived at 298 K using the CBS-APNO model chemistry.

Thus, all studies performed on the $C_2H_2N_2^{\bullet+}$ fragment generated from parent metastable (low-energy) *s*-triazine ions reveal that its connectivity corresponds to ion **2** and should be isomerically pure.

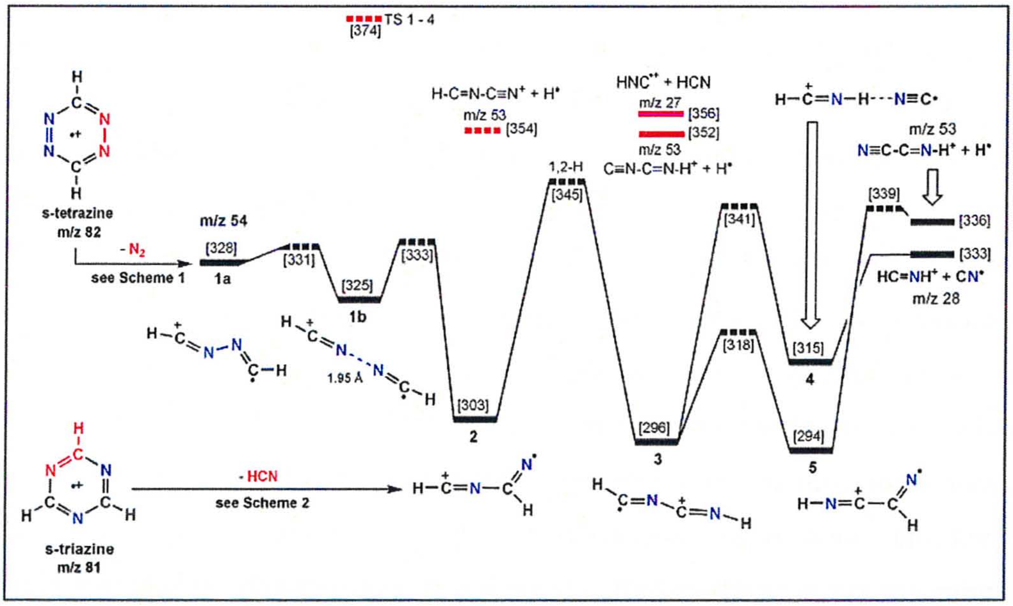

Scheme 4.6. Proposed mechanism for the generation of *m/z* 53 ions and *m/z* 28 ions from the metastable $C_2H_2N_2^{\bullet+}$ ions **1** and **2**. All values are in kcal/mol derived at 298 K using the CBS-APNO model chemistry.

3.3. The dissociation characteristics of the m/z 54 ions generated from s-triazine vs. s-tetrazine.

Analysis of the MI spectra corresponding to *m/z* 54 from both *s*-triazine (ion **2**) and *s*-tetrazine (ions **1/2**) shows that the spectra from both precursors contain peaks that are consistent with losses of $H^•$ and $CN^•$. In addition, the relative intensities corresponding to these losses from both precursors have a similar ratio (1.7). The main difference between the precursors is that the dissociations from *s*-triazine are associated with smaller KER values relative to those from *s*-tetrazine ($T_{0.5}$ = 25 vs. 40 meV for loss of $CN^•$, 120 vs. 160 meV for loss of $H^•$).

Examining these respective dissociations individually, Scheme 4.6 shows that ion **2** must initially isomerize into ion **3** ($HC{=}N{-}C{=}NH^{•+}$) via a 1,2-H shift at 345 kcal/mol before transforming into the HBRC, $HC{=}N{\bullet\bullet}H{\bullet\bullet}N{=}C^{•+}$ (**4**), and losing $CN^•$. Similarly, for $H^•$ loss, ion **2** isomerizes into ion **3** as before, but it then undergoes a 1,2-HNC shift to generate ion **5**, $HN{=}C{-}C({=}N)H^{•+}$, prior to $H^•$ loss. The associated reverse activation barrier for this process is small.

The *m/z* 53 ion generated has the structure, $HN{=}C{=}C{=}N^+$, corresponding to the global minimum on the $C_2HN_2^+$ potential energy surface [24].

In the case of the HCN dimer ion **1**, it is reasonably expected to isomerize into ion **2** and dissociate in the same fashion as discussed above. This is important because the 1,2-H shift TS connecting the minima, **1** and **4**, lies much too high in energy at 374 kcal/mol, see Scheme 4.6. Thus, as all the barriers for interconversion are well below the dissociation thresholds (including that for $H^•$ loss from any of the intermediates, see Table 2) for the metastable ions **2** and **1**, the fragmentation scheme discussed above is energetically reasonable. These results also lead us to infer that the differences between the MI and oxygen CID *m/z* 54 spectra from *s*-triazine and *s*-tetrazine (see Figs. 4.3 and 4.7) are not indicative of the co-generation of ions **1** from **TET-1**. Instead, the reason for differences such as higher KER values and more intense *m/z* 28 peaks (for the $C_2H_2N_2^{•+}$ fragment) from *s*-tetrazine, is that the corresponding ions **2** are generated at a greater energy threshold translating to higher internal energy content. This observation is in comparison to the *m/z* 54 ions from *s*-triazine that are generated at the dissociation threshold.

In spite of this, a comparison of the *m/z* 54 helium CID spectra in the region *m/z* 38 – 40 (see Fig. 4.3a and 4.7a insets) from both precursor molecules shows that the peak at *m/z* 40 in the spectrum from *s*-triazine is noticeably more intense. This difference is characteristic of the connectivity of the species and is consistent with the theoretical prediction of the isomeric purity of ions **2** generated from *s*-triazine. In other words, this is indicative of a minor fraction of *m/z* 54 ions generated from *s*-tetrazine retaining their initial connectivity (**1**).

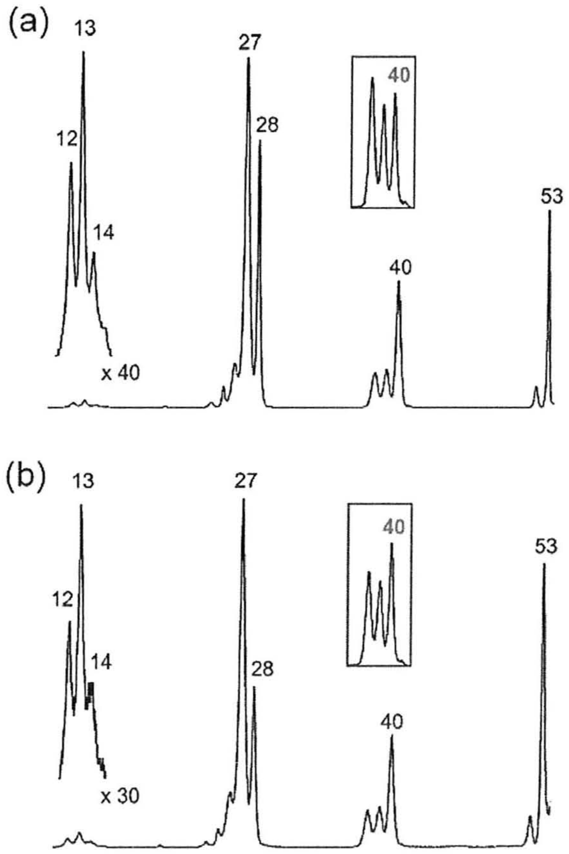

Figure 4.7. (a,b) CID (O_2) mass spectra of *m/z* 54 ions generated from *s*-triazine in the source and from metastable molecular ions. Insets show partial CID (He) spectra of *m/z* 38-40 region.

The spectra of the *m/z* 54 ions generated from both metastable molecular ions, Figs. 4.3b and 4.7b, show the same pattern. However, a more prominent peak at *m/z* 40 in the *m/z* 54 oxygen CID spectrum from metastable *s*-triazine ions (Fig. 4.7b) relative to that from the low energy *m/z* 54 ions generated in the source (Fig. 4.7a) illustrates the lower tendency of the latter ions **2** to isomerize into **1**. Therefore, the *m/z* 40 peak in the *m/z* 54 CID spectra is a structure diagnostic peak and its relative intensity is linked to the extent of co-generation of ions **1** from ionized *s*-tetrazine.

3.4. The NR mass spectra of m/z 54 ions generated from s-triazine vs. s-tetrazine.

Figs. 4.8a and 4.8b show the NR spectra of *m/z* 54 ions **1/2** generated from *s*-tetrazine and *s*-triazine respectively.

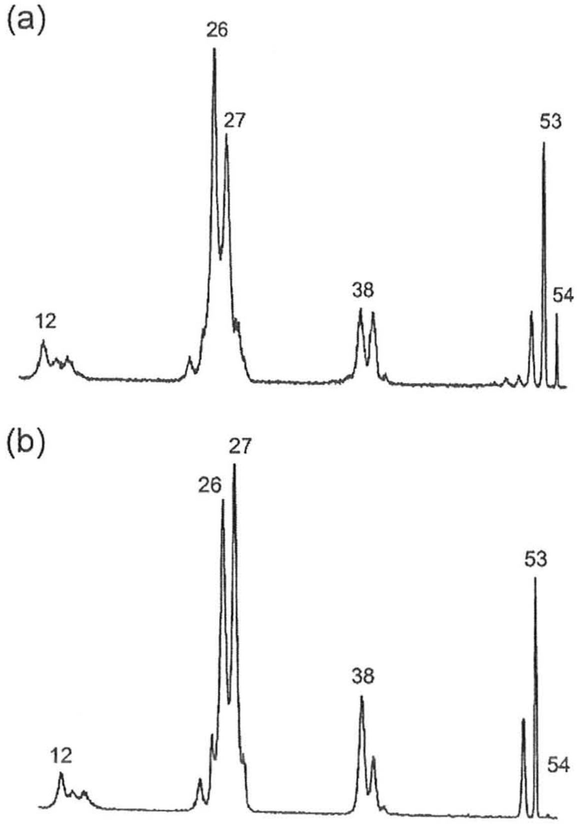

Figure 4.8. NR mass spectra of the *m/z* 54 ions generated from (a) *s*-tetrazine and (b) *s*-triazine.

The NR spectrum from *s*-triazine (Fig. 4.8b) does not display a *survivor* peak at *m/z* 54 implying that the neutral counterpart of ion **2** is not stable in the gas phase. This observation is in agreement with model chemistry calculations on the neutral potential energy surface that failed to locate a local minimum for the neutral **2**N. Instead, computations revealed that the species dissociates into two HCN molecules. This dissociation rationalizes the intense *m/z* 27 and 26 peaks seen in Fig. 4.8b.

In contrast to the NR mass spectrum acquired from *s*-tetrazine (Fig. 4.8a), one may propose that the presence of a relatively low intense *survivor* peak at *m/z* 54 is indicative of the stable neutral counterpart (**1**N) of a minority of ions **1** co-generated with ions **2**. When this possibility was theoretically probed, **1**N was not a minimum either. A more in-depth look [25] reveals that ~60% of the displayed *survivor* peak (Fig. 4.8a) derives from ^{13}C and ^{15}N neutral isotopologues of the *m/z* 53 ion, $H\text{-}C{=}N\text{-}C{=}N^{+}$. The remaining fraction of the *survivor* peak possibly originates from an isobaric impurity linked to the weak signals at *m/z* 51 and 52.

In conclusion, the absence of a survivor *m/z* 54 peak in the NR spectra confirms that the neutral counterparts of either of the ions **1**, $HC{=}N\text{-}N{=}CH^{\bullet+}$, or **2**, $HC{=}N\text{-}C({=}N)H^{\bullet+}$, are not stable species in the rarefied gas phase. These results are in perfect agreement with the model chemistry calculations.

Conclusion

Ionized *s*-tetrazine is shown to eliminate N_2 and yield the HCN dimer, $HC{=}N\text{-}N{=}CH^{\bullet+}$ (**1**). The ion is a stable species in the gas phase but it is generated with an elevated internal energy content that enables it to readily isomerize into the more stable nitrene isomer, $HC{=}N\text{-}C({=}N)H^{\bullet+}$ (**2**). Ionized *s*-triazine is shown to independently generate isomerically pure ion **2**. Analysis of the results of neutralization-reionization experiments leads to the conclusion that the neutral counterparts of ions **1** and **2** are not stable species in the rarefied gas phase. Simultaneous theoretical findings (CBS-QB3/APNO) convincingly agree with our experimental observations.

References

[1] A. Carrington, D.A. Ramsay, *Molecules in interstellar space*. The Royal Society, London, 1982.
[2] D.F. Strobel. Planet Space Sci. 30 (1982) 839.
[3] D.F. Strobel. Int. Rev. Phys. Chem. 3 (1983) 145.
[4] R.A. Evans, S.M. Lacombe, M.J. Simon, G. Pfister-Guillouzo, C. Wentrup, J. Phys. Chem. 96 (1992) 4801, and references cited therein.
[5] R.A. Evans, P. Lorencak, T-K. Ha, C. Wentrup. J. Am. Chem. Soc. 113 (1991) 7261.
[6] F. Pichieri, Chem. Phys. Lett. 353 (2002) 383, and references cited therein.
[7] C. Wentrup, P. Lorencak, A. Maquestiau, R. Flammang, Chem. Phys. Lett. 137 (1987) 241.
[8] K.J. Jobst, M.R. Hanifa, J.K. Terlouw, Chem. Phys. Lett. 462 (2008) 152.
[9] I. Nenner, O. Dutuit, M. Richard-Viard, P. Morin, A.H. Zewail, J. Am. Chem. Soc. 110 (1988) 1093.
[10] J.L. Holmes, C. Aubry, P.M. Mayer, Assigning Structures to Ions in Mass Spectrometry, CRC Press, Boca Raton, 2007 (Chapter 1).
[11] H.F. van Garderen, P.J.A. Ruttink, P.C. Burgers, G.A. McGibbon, and J.K. Terlouw, Int. J. Mass Spectrom. Ion Proc. 121 (1992) 159.
[12] J.L. Holmes, C. Aubry, P.M. Mayer. Assigning Structures to Ions in Mass Spectrometry, CRC Press, Boca Raton, 2007.
[13] J. Sauer, D.K. Heldmann, J. Hetzenegger, J. Krauthan, H. Sichert, J. Schuster, Eur. J. Org. Chem. 12 (1998) 2885.
[14] J.A. Montgomery Jr., M.J. Frisch, J.W. Ochterski, G.A. Petersson, J. Chem. Phys. 112 (2000) 6532.
[15] J.W. Ochterski, G.A. Petersson, J.A. Montgomery Jr., J. Chem. Phys. 104 (1996) 2598.
[16] M.J. Frisch et al., GAUSSIAN 03 (Revisions C.02 and D.01), Gaussian Inc., Wallingford, CT, 2004.
[17] P.C. Burgers, J.K. Terlouw In: N.M.M. Nibbering, Editor, *Encyclopedia of Mass Spectrometry* Volume 4, Elsevier, Amsterdam (2005), p. 173.
[18] S.G. Lias, J.E. Bartmess, J.F. Liebman, J.L. Holmes, R.O. Levin, W.G. Maillard, J. Phys. Chem. Ref. Data 17 (Suppl. 1) (1988).
[19] L. Nahon, P. Morin, M. Larzilliere, I. Nenner, J. Chem. Phys. 96 (1992) 3628.
[20] C. Aubry, J.L. Holmes, J. Am. Soc. Mass Spectrom. 12 (2001) 23.
[21] R. Flammang, Y. Van Haverbeke, S. Laurent, M. Barbieux-Flammang, M.W. Wong, C. Wentrup, Rapid Commun. Mass Spectrom. 98 (1996) 232.
[22] C.Y. Wong, P.J.A. Ruttink, P.C. Burgers, J.K. Terlouw, Chem. Phys. Lett. 390 (2004) 176.
[23] C.Y. Wong, P.J.A. Ruttink, P.C. Burgers, J.K. Terlouw, Chem. Phys. Lett. 387 (2004) 204.
[24] S. Petrie, J. Phys. Chem. A 102 (1998) 7835.
[25] L.N. Heydorn, C.Y. Wong, R. Srinivas, J.K. Terlouw, Int. J. Mass Spectrom. 225 (2003) 11.

Appendix to Chapter 4

Table 1. Energetic data [a] derived from **CBS-QB3** and **CBS-APNO** calculations for minima of stable ionic isomers of *s*-Tetrazine (**TET-1**) and *s*-Triazine (**TRI-1**), and their connecting transition states.

Ionic species	**CBS-QB3 E(total)** [0K]	**QB3 ZPE**	**QB3 $\Delta_fH^0_0$**	**QB3 $\Delta_fH^0_{298}$**	**APNO $\Delta_fH^0_{298}$**
TET-1N	-295.889970	31.8	116.8	113.4	115.4
TET-1	-295.561583	31.5	323.0	319.5	322.7
TET-2a	-295.533987	28.9	340.3	338.0	337.2
TET-2b	-295.537651	28.8	338.0	335.8	334.6
TET-3	-295.551859	26.2	329.1	328.2	327.1
TET-4 [b]	-295.536281	26.6	338.9	337.7	334.6
TET-5	-295.499268	31.8	362.1	358.7	363.0
TS **TET-1** → **2a**	-295.504592	28.4	358.7	355.7	357.6
TS **TET-1** → **5** [c]	-295.410190	25.9	418.0	415.1	403.3
TS **TET-2a** → **2b**	-295.506236	28.0	357.7	355.3	352.8
TS **TET-2a** → **TET-3**	-295.516775	27.2	351.1	349.0	350.0
TS **TET-2b** → **TET-4**	-295.505434	26.6	358.2	356.3	356.6
TS **TET-4** → ***m/z* 28**	-295.535989	23.0	339.0	338.2	[d]
TRI-1N	-279.923786	40.4	57.0	53.3	54.4
TRI-1	-279.555934	39.0	287.9	284.4	286.5
TRI-2	-279.559382	40.4	285.8	282.2	282.1
TRI-3a	-279.498316	35.7	324.1	321.8	322.0
TRI-3b	-279.487429	35.4	330.9	328.7	329.4
TRI-4	-279.512221	33.5	315.4	313.9	312.9
TRI-5 [b]	-279.501468	33.6	322.1	320.8	320.5
TRI-6	-279.528590	33.2	305.1	303.6	303.4
TS **TRI-1** → **2**	-279.460773	34.7	347.7	344.5	344.2
TS **TRI-1** → **3a**	-279.494357	35.6	326.6	323.8	324.1
TS **TRI-3a** → **3b**	-279.488455	35.2	330.3	327.6	329.2
TS **TRI-3b** → **4**	-279.486518	34.3	331.5	329.5	329.7
TS **TRI-4** → **5**	-279.501593	33.5	322.0	320.4	320.4
TS **TRI-5** → **6**	-279.461997	30.8	346.9	345.4	344.8

[a] $E_{(total)}$ in Hartrees, all other components, including the ZPE scaled by 0.99, are in kcal/mol. [b] The CBS-QB3 hydrogen-bridged geometry was converted to an ion-dipole geometry by the CBS-APNO model chemistry. [c] The CBS-QB3 closed-ring transition state geometry generated was converted to an open-ring structure by the CBS-APNO model chemistry. [d] The desired transition state was not found.

Table 2. Energetic data [a] derived from **CBS-QB3** and **CBS-APNO** calculations for pertinent minima of stable ionic isomers of $C_2H_2N_2$ and their connecting transition states.

Ionic species	CBS-QB3 E(total) [0K]	QB3 ZPE	QB3 $\Delta_fH^0_0$	QB3 $\Delta_fH^0_{298}$	APNO $\Delta_fH^0_{298}$
1a	-186.149466	22.2	330.7	329.5	328.0
1b	-186.158698	21.1	324.9	324.4	324.8
2	-186.191984	22.6	304.1	302.8	302.7
3a	-186.202316	22.0	297.6	296.7	296.3
3b	-186.195574	21.8	301.8	300.9	299.1
4	-186.172894	20.7	316.0	315.4	315.2
5	-186.205889	22.6	295.3	294.1	294.5
TS **1a** → **1b**	-186.143924	20.2	334.2	333.2	331.4
TS **1b** → **2**	-186.143005	20.6	334.8	333.9	333.4
TS **1** → **4**	-186.079898	17.5	374.3	374.1	373.9
TS **2** → **3**	-186.123165	18.6	347.2	346.3	345.3
TS **3** → **4**	-186.133423	20.4	340.8	340.3	341.4
TS **3a** → **5**	-186.165356	21.4	320.8	319.3	317.9
TS **2** → ***m/z* 53**	-186.110145	17.4	355.4	354.4	354.1
TS **5** → ***m/z* 53**	-186.135252	17.4	339.7	338.7	339.1

[a] $E_{(total)}$ in Hartrees, all other components, including the ZPE scaled by 0.99, are in kcal/mol.

Table 3. Energetic data for various dissociation products of ionized *s*-Tetrazine derived from CBS-QB3/CBS-APNO calculations [a].

Species	*m/z*	CBS-QB3 E(total) [0 K]	QB3 $\Delta_fH^0_0$	QB3 $\Delta_fH^0_{298}$	APNO $\Delta_fH^0_{298}$
$HC(=N)NN^{\bullet+}$ + HCN	**55**		**352.7**	**351.4**	**352.7**
$HC(N)NN^{\bullet+}$		-202.226685	320.9	319.7	320.7
HCN		-93.287537	31.8	31.7	32.0
1a + N_2	**54**		**331.5**	**330.3**	**329.2**
1b + N_2			**325.7**	**325.2**	**325.6**
$HCNC(=N)H^{\bullet+}$ + N_2			**304.9**	**303.6**	**303.9**
1a		-186.149466	330.7	329.5	328.0
1b		-186.158698	324.9	324.4	324.8
$HCNC(=N)H^{\bullet+}$		-186.191984	304.1	302.8	302.7
N_2		-109.398466	0.8	0.8	1.2
$HCNNC^+ + H^\bullet + N_2$	**53**		**392.3**	**392.6**	**393.6**
$HCNCN^+ + H^\bullet + N_2$			**352.0**	**352.0**	**352.1**
$CNCNH^+ + H^\bullet + N_2$			**352.1**	**352.4**	**353.2**
$HNCCN^+ + H^\bullet + N_2$			**336.7**	**336.8**	**337.4**
$HCNNC^+$		-185.552726	339.9	339.7	340.3
$HCNCN^+$		-185.617054	299.6	299.1	298.8
$CNCNH^+$		-185.616887	299.7	299.5	299.9
$HNCCN^+$		-185.641405	284.3	283.9	284.1
$H^\bullet$		-0.499818	51.6	52.1	52.1
$HCNH^+ + NNCN^\bullet$	**28**		**350.7**	**349.9**	**344.0**
$HCNH^+ + HCNCN^\bullet$			**341.7**	**340.5**	**341.5**
$HCNH^+ + CN^\bullet + N_2$			**333.6**	**333.6**	**334.3**
$HCNH^+$		-93.558686	227.0	226.2	226.8
$NNCN^\bullet$ [b]		-201.958782	123.7	123.7	117.2
$HCNCN^\bullet$		-185.911712	114.7	114.3	114.7
$CN^\bullet$		-92.587607	105.8	106.6	106.3
$HCN^{\bullet+}$ + HCN	**27**		**377.7**	**377.6**	**378.6**
$HNC^{\bullet+}$ + HCN			**355.6**	**355.5**	**356.0**
$HCN^{\bullet+}$		-92.787025	345.9	345.9	346.6
$HNC^{\bullet+}$		-92.822241	323.8	323.8	324.0

[a] $E_{(total)}$ in Hartrees, all other components, including the ZPE scaled by 0.99, are in kcal/mol. [b] The CBS-APNO optimized geometry is bent to a greater degree in comparison to that from the CBS-QB3 model chemistry. The remarkable divergence of the calculated enthalpies is reflected in the optimized geometries. Note that this radical is thermodynamically unstable with respect to its dissociation products; $N_2 + CN^\bullet$.

Figure 4.9. Selected optimized geometries (CBSB7 basis set) of stable intermediates and transition states involved in the isomerization and dissociation of ionized $C_2H_2N_2$.

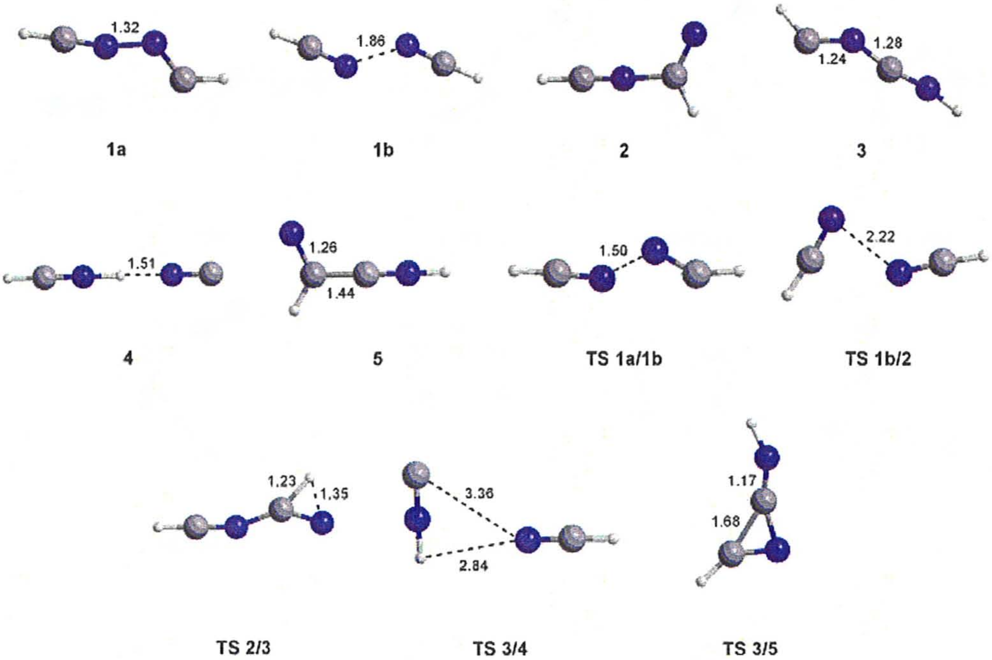

Figure 4.10. Selected optimized geometries (CBSB7 basis set) of stable intermediates and transition states involved in the isomerization and dissociation of ionized *s*-tetrazine (**TET-1**).

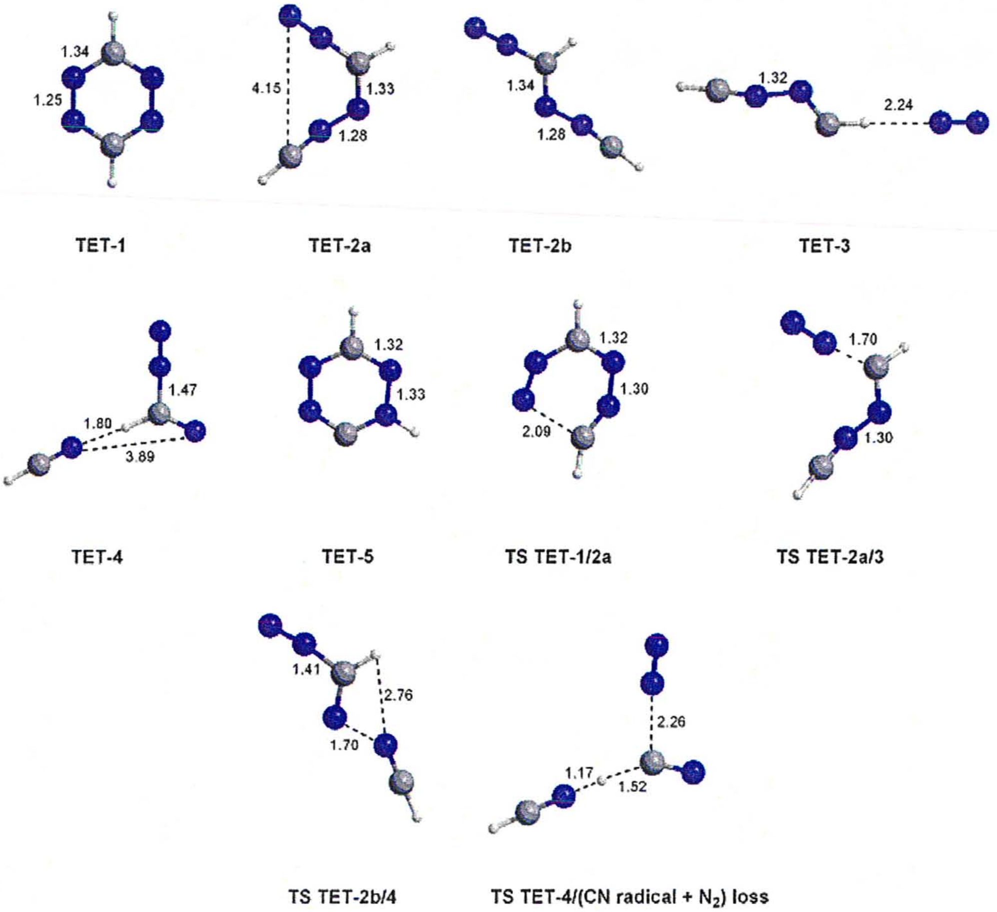

TET-1 **TET-2a** **TET-2b** **TET-3**

TET-4 **TET-5** **TS TET-1/2a** **TS TET-2a/3**

TS TET-2b/4 **TS TET-4/(CN radical + N_2) loss**

Figure 4.11. Selected optimized geometries (CBSB7 basis set) of stable intermediates and transition states involved in the isomerization and dissociation of ionized s-triazine (**TRI-1**).

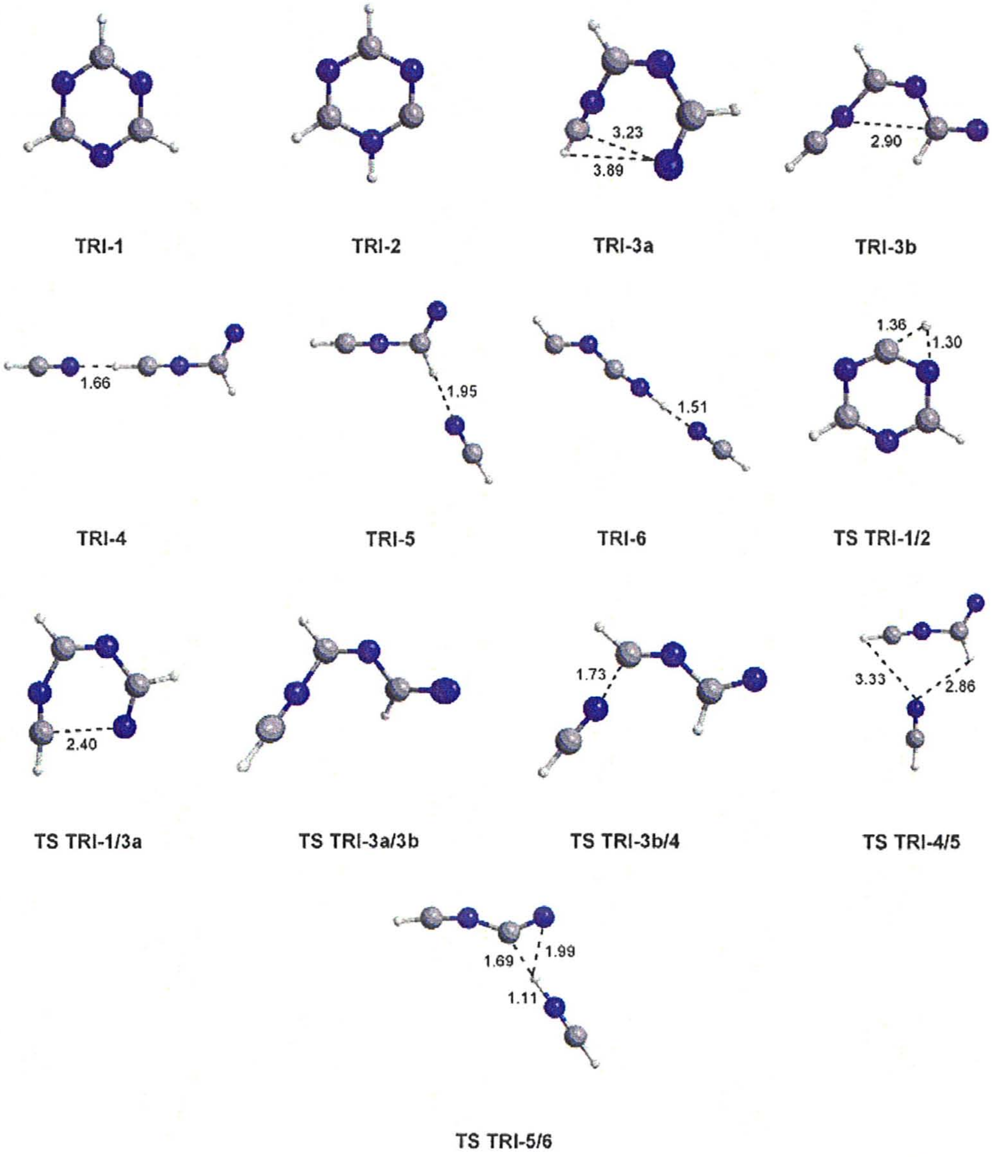

TRI-1 **TRI-2** **TRI-3a** **TRI-3b**

TRI-4 **TRI-5** **TRI-6** **TS TRI-1/2**

TS TRI-1/3a **TS TRI-3a/3b** **TS TRI-3b/4** **TS TRI-4/5**

TS TRI-5/6

Chapter 5

Methylated analogues of the dimers of HCN and HNC : Combined model chemistry and tandem mass spectrometry studies.

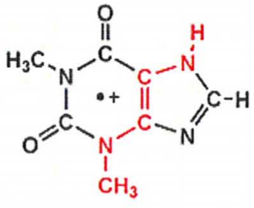

theophylline

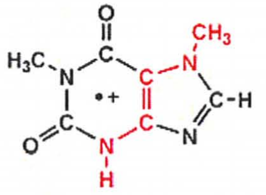

paraxanthine

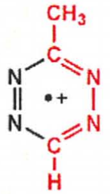

s-methyltetrazine

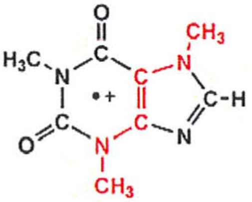

caffeine

This chapter primarily describes the characterization of ionized isomers of *N*-methylethenediimine $CH_3N{=}C{=}C{=}NH^{\bullet+}$ (**1**) and *N,N*-dimethylethenediimine $CH_3N{=}C{=}C{=}NCH_3^{\bullet+}$ (**A1**) respectively. Ionized theophylline and paraxanthine are shown to generate the former ion (**1**) corresponding to *m/z* 68. Using experimental observations, we will show that theophylline generates ions **1** in admixture with its 1,4-H shift isomeric ions **2**. In contrast, ions **1** generated from paraxanthine are shown to be isomerically pure. Neutralization-reionization experiments, together with theoretical calculations, will be used to reveal that the neutral counterpart **N2** is relatively more kinetically stable than **N1**. The connectivity of the *m/z* 68 ions generated from *s*-methyltetrazine, initially presumed to correspond to the $CH_3\text{-}C{=}N\text{-}N{=}CH^{\bullet+}$ ion (**6a**), will be theoretically shown to generate a complex mixture of isomers including **6a**. Both, experiment and theory show that nearly all of the isomers generated have no stable neutral counterpart in the rarefied gas phase.

Ionized caffeine is proposed to generate the *m/z* 82 *N,N*-dimethylethenediimine ion $CH_3N{=}C{=}C{=}NCH_3^{\bullet+}$ (**A1**). A mechanistic analysis using model chemistry calculations revealed that ion **A1** is co-generated with its 1,4-H shift isomer (**A2**) at the same threshold. In the form of ions, interconversion is shown to be energetically too demanding relative to the predominant $CH_3^{\bullet}$ loss pathway. However, as stable neutrals, interconversion takes place more readily generating a mixture of stable isomeric species giving rise to a strong 'survivor' peak in the NR spectra.

1. Introduction

In the past few decades, there have been several reports acknowledging the importance of gas phase ion-molecule reactions in the generation of relatively more complex molecules in the interstellar medium (ISM) [1-4]. $CH_3C{\equiv}N$ is one such molecule. It has been proposed that $CH_3C{\equiv}N$ is generated under interstellar conditions by the rapid radiative association of CH_3^+ with $HC{\equiv}N$ followed by electron dissociative recombination [1]. In addition, it is also considered to be important [5,6] in the formation of larger molecules and perhaps even primitive biological systems.

As pointed out in Chapters 3 and 4, both $HC{\equiv}N$ and $HN{\equiv}C$ are ubiquitous in molecular clouds and comets [7]. Similarly, $CH_3C{\equiv}N$ (acetonitrile) is a well established interstellar species [8-11] predominantly detected in interstellar space using radio frequencies. Despite the first detection of $CH_3C{\equiv}N$ in the interstellar medium in 1971 [8], its was only more recently in 2005 that the iso-nitrile $CH_3N{\equiv}C$ was confirmed by Remijan et al. [12] to exist in the hot core known as the Large Molecule Heimat located in Sagittarius B2(N) [Sgr B2(N)-LMH] [13].

Therefore, in line with the studies of Chapters 3 and 4, the characterization of covalently bound [H,C,N] and [CH_3,C,N] species is of considerable astrochemical and prebiotic interest. Further, it would also be interesting to study the family of covalently bound [CH_3,C,N] dimers to understand the effects of additional methyl groups on reactivity. As these species are studied in the context of interstellar chemistry, both neutral and ionic species are probed.

Previous studies reporting the isomerization and dissociation chemistries of any pertinent or relevant species discussed could not be found. Therefore, in this study, using tandem mass spectrometry based experiments and model chemistry calculations (CBS-QB3/APNO), we report the stability and reactivity of the :

(i) *N*-methylethenediimine ion $CH_3N{=}C{=}C{=}NH^{\bullet+}$ (**1**) generated from theophylline and paraxanthine respectively. The results reveal that source generated ions from ionized theophylline yield both, ion **1** and its 1,4-H shift isomeric ion (**2**). However, metastably generated parent *m/z* 95 fragment ions are found to yield only ion **2**. Neutralization-reionization (NR) mass spectrometry [14] reveals that the neutral counterpart of ion **1** is only marginally stable whereas **N2** is associated with a greater kinetic stability. This is in agreement with theoretical results. Paraxanthine is found to generate only $CH_3N{=}C{=}C{=}NH^{\bullet+}$ (**1**) ions.

(ii) $CH_3\text{-}C{=}N\text{-}N{=}CH^{\bullet+}$ ion (**6a**) generated from *s*-methyltetrazine. The results show that the *m/z* 68 ions generated are part of a relatively more complex mixture. Theory reveals that none of the ions generated have a neutral counterpart except ion **11**. This is probably the minor 'survivor' peak observed in the NR experiments.

(iii) *N,N*-dimethylethenediimine ion $CH_3N{=}C{=}C{=}NCH_3^{\bullet+}$ (**A1**) generated from caffeine. Similar to theophylline, theoretical calculation show that ion **A1** is generated in admixture with its 1,4-H shift isomeric ion (**A2**). Both, theory and NR experiments suggest that the respective ionic species have stable neutral counterparts in the gas phase. However, at elevated energies, they can easily interconvert providing no information in regards to the dissociation chemistry of any individual neutral species generated.

2. Experimental and Theoretical Methods

The mass spectrometric experiments were performed on the VG Analytical ZAB-R mass spectrometer of BE_1E_2 geometry (E = electric sector, B = magnet) using an electron ionization source (70 eV) at an accelerating voltage of 8 kV [15].

The metastable ion (MI) spectra were recorded in the second field free region (2ffr) and the collision-induced dissociation (CID) spectra were recorded in the 2ffr and 3ffr. For all collision experiments, oxygen was used as the collision gas. Neutralization-reionization (NR) mass spectra were acquired using *N,N*-dimethylaniline as the reducing agent and oxygen gas for reionization. Kinetic energy release or KER values (corrected

$T_{0.5}$ values) were measured following standard procedures [14]. Features of the instrument and the measurement of NR mass spectra have been previously outlined [15].

Solid samples of theophylline, paraxanthine and caffeine were introduced into the mass spectrometer via a direct insertion solid probe. All three precursor molecules listed were obtained from Sigma-Aldrich and used without further purification. Samples of N-D labeled theophylline for MI experiments were achieved by repeated exchange with commercially available D_2O. The sample of *s*-methyltetrazine used was prepared by modifying a procedure outlined by J. Sauer and co-workers [16] intended to generate *s*-tetrazine. In the procedure followed, both, acetamidine hydrochloride [CH_3-$C(NH_2)$=NH.HCl] and formamidine acetate [NH_2-CH=NH.$CH_3C(=O)OH$] were added to the reaction mixture in a 1:1 ratio instead of only the latter. This was done to introduce the methyl moiety and hence, generate *s*-methylteterazine. However, the product consisted of a mixture of *s*-methyltetrazine and the dimethyl analogue as discussed in Section 3.5. The reagents used for the synthesis were purchased from Sigma-Aldrich and of research grade.

The optimized geometries of pertinent ions and neutrals and their respective enthalpies of formation were probed using the standard CBS-QB3 and the computationally more challenging CBS-APNO model chemistries [17,18]. All relevant calculations were executed using the Gaussian 03 Revision C.02 and D.01 suite of programs on SHARCNET [19]. The calculated absolute energies and enthalpies of formation ($\Delta_f H^0_{298}$ in kcal/mol) for the minima and connecting transition states (TS) of ions and neutrals are presented in Tables 1a, 2a-b and 3a-b (see Appendix). Schemes 5.2-5.20 illustrate mechanistic proposals for the generation of various ions of interest and their respective dissociation and isomerization behaviour. Theoretical enthalpies of formation of important dissociation products are presented in Tables 1b-c, 2c and 3c. Detailed geometries of selected species are given in the Appendix, Figures 5.21-5.23. The identity of all local minima and connecting TS were confirmed by frequency analysis.

3. Results and Discussion

3.1. The generation of m/z 68 ions from theophylline and paraxanthine.

3.1.1. Proposed atom connectivity of the m/z 68 ions generated from both precursor molecules

The 70 eV EI mass spectra of both, theophylline [20] and paraxanthine [21], exhibit a significant peak at *m/z* 68 corresponding to ions of elemental composition $C_3H_4N_2$, see Fig. 5.1.

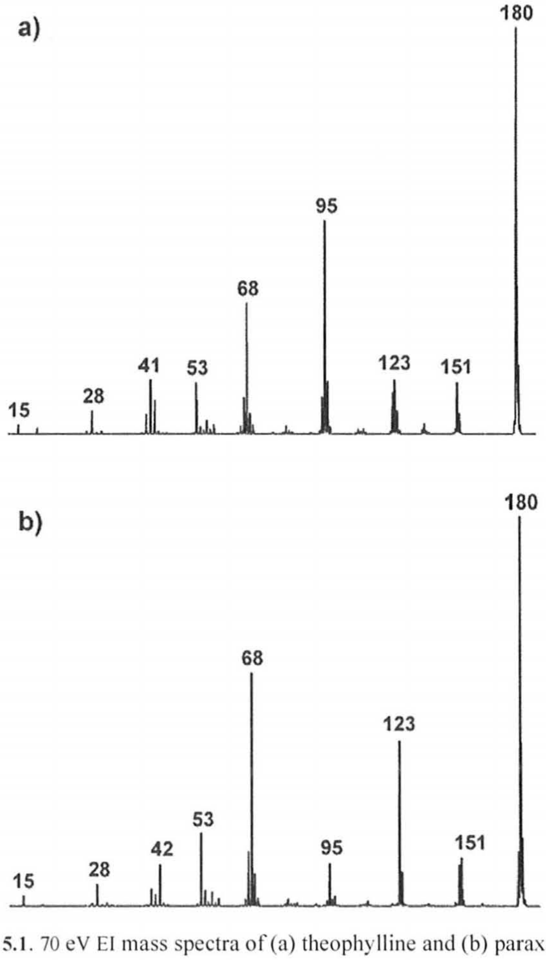

Figure 5.1. 70 eV EI mass spectra of (a) theophylline and (b) paraxanthine.

In the case of theophylline, Scheme 5.2 reveals a proposed fragmentation scheme for the generation of the *m/z* 68 ion. As shown, the *m/z* 180 molecular ion is expected to undergo consecutive losses of $CH_3N{=}C{=}O$ and CO respectively to generate the ion corresponding to the prominent *m/z* 95 peak in the mass spectrum, see Fig. 5.1a.

Thereafter, the *m/z* 95 fragment can undergo HC≡N loss to generate the *m/z* 68 *N*-methylethenediimine ion, $CH_3N{=}C{=}C{=}NH^{\bullet+}$ (**1**). However, given the depicted conformer of the *m/z* 95 ion, a 1,4-H shift prior to HC≡N loss is just as conceivable yielding the an isomer of ion **1**, $CH_2{=}N{-}C{=}C(H){-}NH^{\bullet+}$ (**2**). Hence, the isomeric purity of the *m/z* 68 ions generated from theophylline needs to be probed.

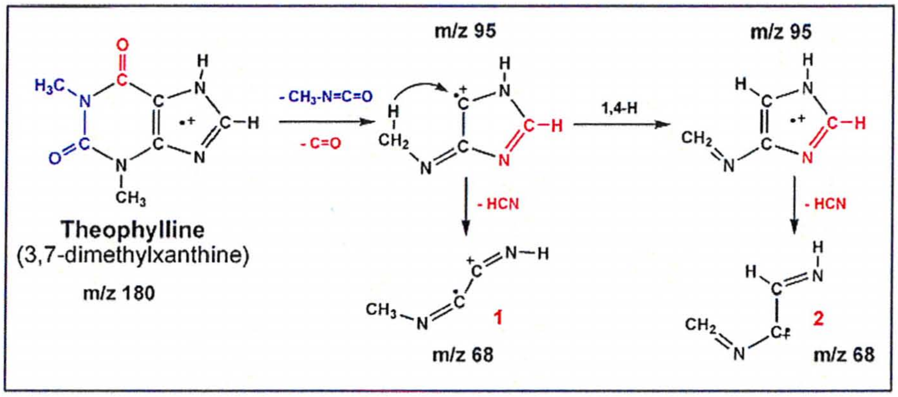

Scheme 5.2. Proposed fragmentation pathway for the generation of ions **1** and **2** from ionized theophylline.

Paraxanthine is another precursor molecule known to generate a sizeable peak at *m/z* 68 [21], see Fig. 5.1b. As illustrated in Scheme 5.3, the first step in the relevant fragmentation pathway involves the loss of $CH_3N{=}C{=}O$ from the *m/z* 180 molecular ion to generate the intense peak at *m/z* 123, see Fig. 5.1b. The neighbouring intense peak at a lower *m/z* value in the mass spectrum of paraxanthine corresponds to *m/z* 95. Scheme 5.3 shows that the corresponding fragment ion is resulted from the loss of CO from *m/z* 123. This ion can then undergo subsequent HC≡N loss to generate ion **1** (*N*-methylethenediimine), $CH_3N{=}C{=}C{=}NH^{\bullet+}$.

However, Scheme 5.3 also reveals that the *m/z* 123 ion can alternatively lose HC≡N to generate a fragment corresponding to *m/z* 96. The resulting ion can then undergo CH_2N loss following a 1,4-H shift to generate the isobaric $HN{=}C(H){-}C{=}C{=}O^+$ ion. This *m/z* 68 ionic species is a confirmed stable gas-phase species [22]. In spite of this, a comparison of the peak intensities corresponding to *m/z* 95 and 96 in the mass spectrum suggests that a vast majority of the *m/z* 68 ions derive from the *m/z* 95 fragment. Nonetheless, the isobaric purity of the *m/z* 68 species giving rise to the corresponding intense peak in the mass spectrum, see Fig. 5.1b, will be investigated.

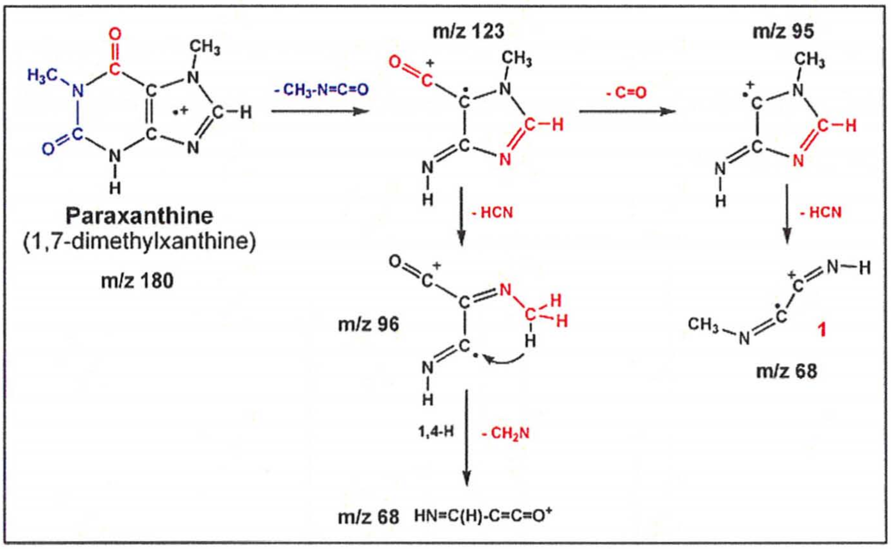

Scheme 5.3. Proposed fragmentation pathway for the generation of ion **1** from ionized paraxanthine.

3.1.2. Characterization of the $C_3H_4N_2^{\bullet+}$ ions generated using MI and CID mass spectrometry.

The MI spectrum of the *m/z* 68 ion presumably corresponding to $CH_3N{=}C{=}C{=}NH^{\bullet+}$ (**1**) generated from theophylline is shown in Fig. 5.4. Prominent peaks corresponding to losses of $CH_3^{\bullet}$ and HN≡C give rise to peaks at *m/z* 53 and 41 respectively. Note that the spectrum also displays a peak at *m/z* 48.5 for which the corresponding species is at this point uncertain.

To help understand the connectivity and the dissociation chemistry of the *m/z* 68 ions studied, we will use the CBS-QB3 potential energy diagram of Scheme 5.5, which summarizes our theoretical calculations on the deuterated counterparts of ions **1** and **2**. The reason for the theoretical study on the deuterated potential energy surface (PES) is to further understand the chemistry of the pertinent species by comparison to experiments performed on deuterated theophylline.

Scheme 5.5 reveals that the deuterated ion **1** (**1**D) lies in a deep potential well on the PES corresponding to $DC_3H_3N_2^{\bullet+}$. The closest dissociation thresholds for the exceptionally stable ion correspond to $H^{\bullet}$ loss at 316 kcal/mol and $CH_3^{\bullet}$ loss at 320 kcal/mol respectively. The latter dissociation rationalizes the peak at *m/z* 53 in Fig. 5.4. However, the former reaction that is expected to generate a prominent peak at *m/z* 67 is observed to yield a peak of lower intensity. The corresponding $H^{\bullet}$ loss reaction scan has not been theoretically probed. The computed dissociation threshold together with the minor peak in the MI spectrum suggests the loss of $H^{\bullet}$ to be associated with a barrier larger than 320 kcal/mol.

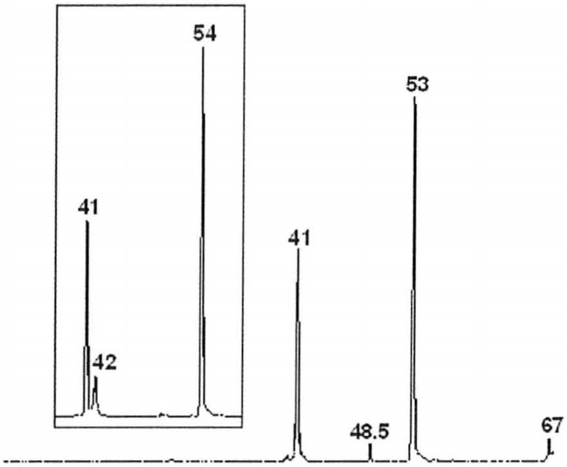

Figure 5.4. 2ffr MI mass spectrum of *m/z* 68 ions generated from theophylline. Inset shows corresponding MI mass spectrum of *m/z* 69 ions generated from deuterated theophylline.

Theoretical findings reveal that the threshold corresponding to $CH_3N{\equiv}C^{\bullet+}$ + $DN{\equiv}C$ (potentially giving rise to the peak at *m/z* 41) lies substantially higher at 350 kcal/mol ! In line with this, the isomerization threshold corresponding to the generation of the 1,4-H shift isomer (**2**D) from **1**D is also relatively higher at 330 kcal/mol. Therefore, within a narrow band of energies, theory predicts that ion **1** could dissociate only via $CH_3^{\bullet}$ loss generating a solitary peak at *m/z* 53 in the MI spectrum. Therefore, the appearance of a sizeable peak at *m/z* 41 in the *m/z* 68 MI spectrum, see Fig. 5.4, is indicative of the co-generation of another isomer presumably ion **2**. The generation of other 1,2-H and 1,3-H shift isomers from ion **1** are found to be associated with much higher energy barriers (~10 kcal/mol higher than the 1,4-H shift) leading to ions **5**D and **3**D respectively, see Table 1a.

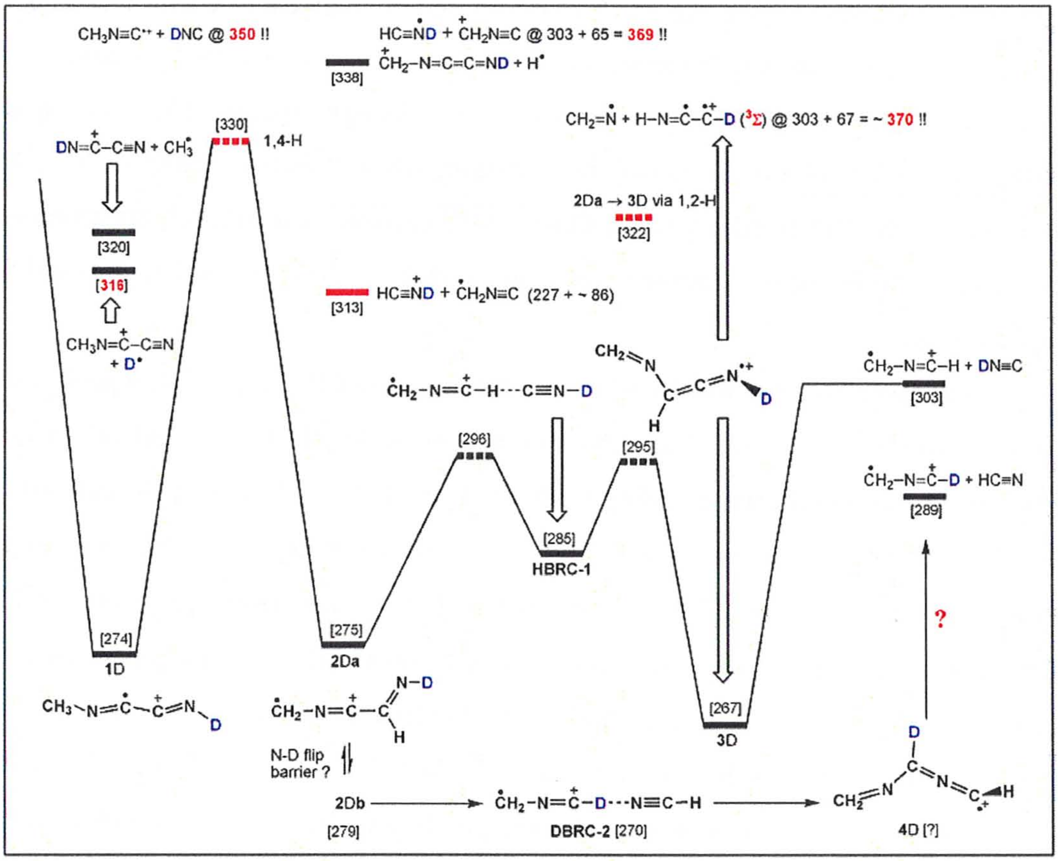

Scheme 5.5. Theoretical prediction of the dissociation behaviour of the *m/z* 68 ions **1** and **2** generated from both, theophylline and paraxanthine. All values are in kcal/mol derived at 298 K using the CBS-QB3 model chemistry.

The calculations of Scheme 5.5 reveal that ion **2Da** is a local minimum on the PES. In addition, the scheme also shows that the elongation of the C-C bond in ion **2Da** is associated with an accessible transition state at 296 kcal/mol generating a hydrogen-bridged radical cation, **HBRC-1**. Thereafter, the DN≡C moiety in **HBRC-1** migrates and forms a bond with the carbene of the $CH_2N{=}C{-}H^{\bullet+}$ moiety to generate ion **3D**. This isomerization takes place at the same threshold as that for the formation of **HBRC-1**. In this context, direct isomerization **2Da** → **3D** is associated with a high energy barrier, see Scheme 5.5. Finally, ion **3D** readily undergoes DN≡C loss to generate *m/z* 41 $CH_2N{=}C{-}H^{\bullet+}$ ions at a dissociation threshold of 303 kcal/mol. In contrast, as HC≡N is the lower energy neutral isomer, Scheme 5.5 displays the attractive dissociation threshold corresponding to $CH_2N{=}C{-}D^{\bullet+}$ + HC≡N to be relatively lower at 289 kcal/mol. The uninvestigated pathway, see Scheme 5.5, is proposed to involve a mechanism analogous to the generation of the above mentioned *m/z* 41 ions. Elongation of the C-C bond in the isomer ion **2Db** is expected to generate a deuterium-bridged species. The resulting ion (**DBRC-2**) consists of a HC≡N moiety instead of the DN≡C moiety in **HBRC-1**. Next, the migration of the HC≡N moiety to the $CH_2N{=}C{-}D^{\bullet+}$ carbene generates ion **4D** which can then undergo direct bond cleavage to result in HC≡N loss. We note that ion **4D** could not be optimized.

However, the only way by which ion **2Da** can lose $CH_3^{\bullet}$ to generate a peak at *m/z* 53 is to overcome the 1,4-H shift barrier at 330 kcal/mol. This is unlikely as the dissociation threshold corresponding to $HC{\equiv}ND^+ + CH_2N{\equiv}C^{\bullet}$ lies at ~313 kcal/mol. In conclusion, the peaks at *m/z* 53 and 41 in the *m/z* 68 MI spectrum, see Fig. 5.4, should therefore correspond to $CH_3^{\bullet}$ loss from ion **1** and HN≡C loss from ion **2** respectively. Clarifying this proposal, the MI spectrum of *m/z* 69 $DC_3H_3N_2^{\bullet+}$ ions generated from deuterated theophylline, see Fig. 5.4 inset, displays peaks at *m/z* 54 and *m/z* 41 corresponding to the generation of $DN{=}C{-}C{\equiv}N^+$ ($CH_3^{\bullet}$ loss) and $CH_2N{=}C{-}H^{\bullet+}$ (DN≡C loss) respectively. The peak at *m/z* 42 corresponding to HC≡N loss is much lower in intensity indicative of a reaction associated with a larger barrier relative to DN≡C loss.

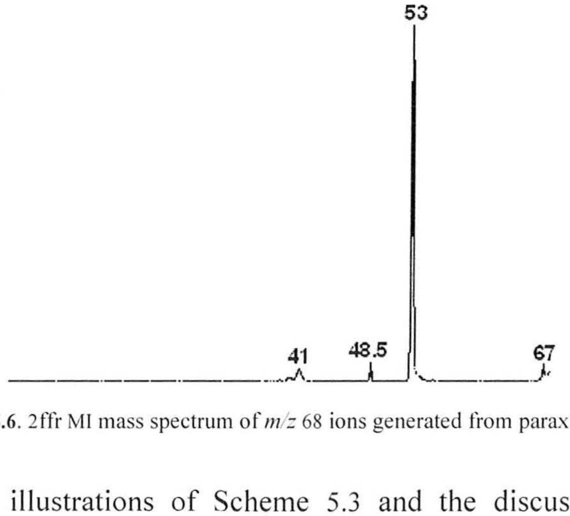

Figure 5.6. 2ffr MI mass spectrum of *m/z* 68 ions generated from paraxanthine.

Consistent with the illustrations of Scheme 5.3 and the discussion above, the MI spectrum of *m/z* 68 ions generated from paraxanthine, see Fig. 5.6, displays only one significant dissociation peak corresponding to $CH_3^{\bullet}$ loss from ion **1**. This observation suggests that the *m/z* 68 ions generated from paraxanthine are isomerically pure ions **1**. Similar to the MI spectrum in Fig. 5.4, the unconfirmed peak at *m/z* 48.5 is observed in this MI spectrum as well.

The *m/z* 68 CID spectra generated from theophylline and paraxanthine are shown in Figs. 5.7a and 5.7b respectively.

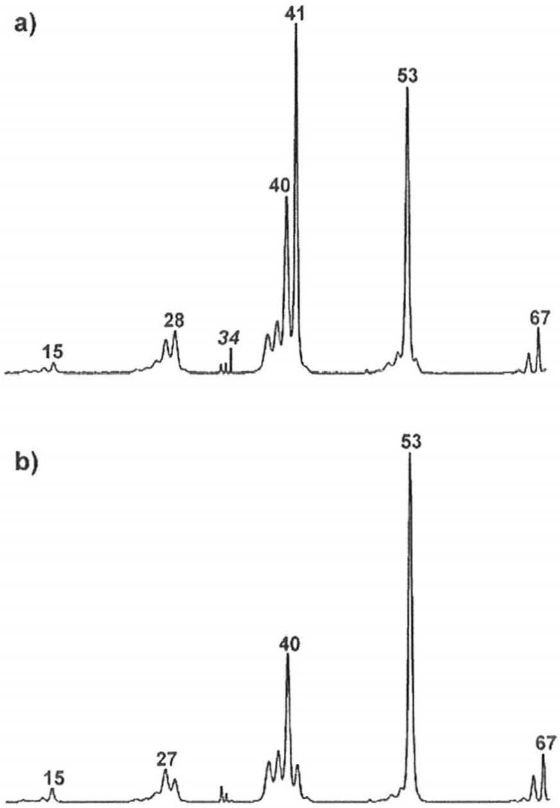

Figure 5.7. CID (O_2) mass spectra of *m/z* 68 ions generated from (a) theophylline and (b) paraxanthine. The peak at *m/z* 34 in (a) corresponds to the doubly-charged species.

A comparison of the *m/z* 68 MI and CID spectra generated from paraxanthine (Figs. 5.6 and 5.7b) shows that the prominent peaks at *m/z* 53 and 40 in the CID spectrum (Fig. 5.7b) correspond to a metastable reaction and a collision induced dissociation of ion **1**. The peak at *m/z* 40 does not correspond to the generation of $CH_2N{\equiv}C^+$ ($HC{\equiv}ND^\bullet$ loss) as the dissociation threshold lies significantly high at 369 kcal/mol, see Scheme 5.5. Therefore, it is likely that the *m/z* 40 fragment ion is generated from a step-wise consecutive process from ion **1**. To support this, the *m/z* 67 MI spectrum (not shown) displays a significant peak at *m/z* 40. According to ref. [14], $CH_2N{\equiv}C^+$ is more stable than $CH_2C{\equiv}N^+$ and less stable than *cyclic*-NC(H)C(H)- by about 3.5 kcal/mol each. As the intensity of the peak at *m/z* 40 indicates much greater stability, the connectivity of the corresponding ion has to be that of a different $C_2H_2N^+$ isomer, most probably $HCCNH^+$. The remaining peaks at *m/z* 67 and 27 in the *m/z* 68 CID spectrum (Fig. 5.7b) are generated due to losses of $H^\bullet$ and $CH_3N{\equiv}C$ respectively.

The prominent peaks in the *m/z* 68 CID spectrum generated from theophylline, see Fig. 5.7a, correspond to *m/z* 67, 53, 41, 40 and 28. The less intense narrow peak at *m/z* 34 corresponds to the doubly charged species and the peak at *m/z* 15 is indicative of the –NH connectivity in ions **1** and **2**. Comparing the MI and CID spectra from both precursor molecules (Figs. 5.4, 5.6, 5.7a and 5.7b), it is apparent that the peaks at *m/z* 67, 53 and 41 are metastably generated corresponding to losses of $H^\bullet$, $CH_3^\bullet$ and $HN{\equiv}C$ respectively.

The reversed ratio of peak intensities corresponding to *m/z* 53 and 41 in the CID spectrum is expected. The observation is rationalized by the difference in the dissociation thresholds corresponding to *m/z* 53 (320 kcal/mol) and *m/z* 41 (303 kcal/mol), see Scheme 5.5. The peak at *m/z* 40 in the spectrum represents the collision induced dissociation of ion **1** seen in the CID spectrum of Fig. 5.7b. Finally, the *m/z* 28 peak in the spectrum of Fig. 5.7a corresponds to the generation of $HC{\equiv}NH^+$.

The *m/z* 68 CID spectrum displayed in Fig. 5.7a displays the dissociation chemistry of the source generated *m/z* 68 ions from theophylline. In contrast to the co-generation of source generated ions **1** and **2**, we propose the *m/z* 68 ion that is metastably generated from the *m/z* 95 fragment to correspond only to ion **2**. The reason for this is that the source generated *m/z* 95 ions possess sufficient internal energy to overcome the barrier associated with the generally less energy demanding 1,4-H shift. In order to verify this proposal, we acquired the CID spectrum of *m/z* 68 ions that are metastably generated from the *m/z* 95 fragment ions of theophylline, see Fig. 5.8a.

When compared to the CID spectrum of Fig. 5.7a, the experimental observations are found to be consistent with our proposal. These confirmative observations include the presence of dissociation reaction peaks describing the behaviour of ion **2** and the absence of the intense peak at *m/z* 53 in Fig. 5.8a corresponding to $CH_3^\bullet$ loss from ion **1**.

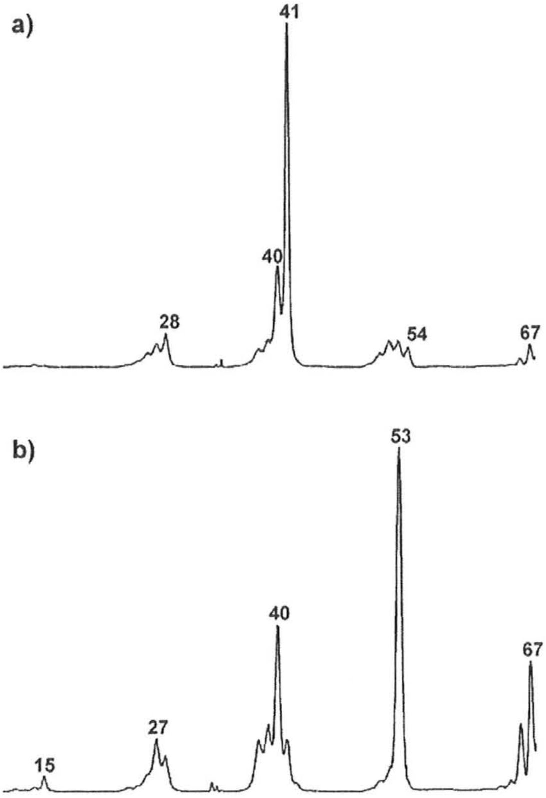

Figure 5.8. CID (O_2) mass spectra of *m/z* 68 ions generated from metastable *m/z* 95 fragment ions of (a) theophylline and (b) paraxanthine.

The analogous CID spectrum of *m/z* 68 ions metastably generated from *m/z* 95 ions of paraxanthine was also acquired, see Fig. 5.8b. When this spectrum was compared to that of source generated *m/z* 68 ions from paraxanthine (Fig. 5.7b), the peaks and their relative intensities matched closely proving both sources generated the same ion (**1**).

3.1.3. Isomerization reactions of the neutral counterparts of ions 1 (N1) and 2 (N2).

Model chemistry calculations of the neutral PES connecting the singlet-state neutral counterparts of ions **1** and **2** reveal a behaviour that is similar to that of the ions, see Scheme 5.9. Triplet states were not considered. The scheme shows that the neutral counterpart of ion **1** referred to as **N1** lies at an energy level that is c. 8 kcal/mol higher in energy relative to the combined enthalpies of $CH_3N{\equiv}C$ and $HN{\equiv}C$. The transition state (TS) for the direct bond cleavage of **N1** to generate $CH_3N{\equiv}C$ + $HN{\equiv}C$ lies relatively higher at 114 kcal/mol. The TS associated with the 1,4-H shift in **N1** to yield **N2** did not optimize. However, the energy corresponding to the activated complex is probably quite high inhibiting the interconversion of **N1** into **N2**. Provided the high energy barriers of the reactions discussed and that any other reaction pathway has a greater activation energy, **N1** is kinetically stable.

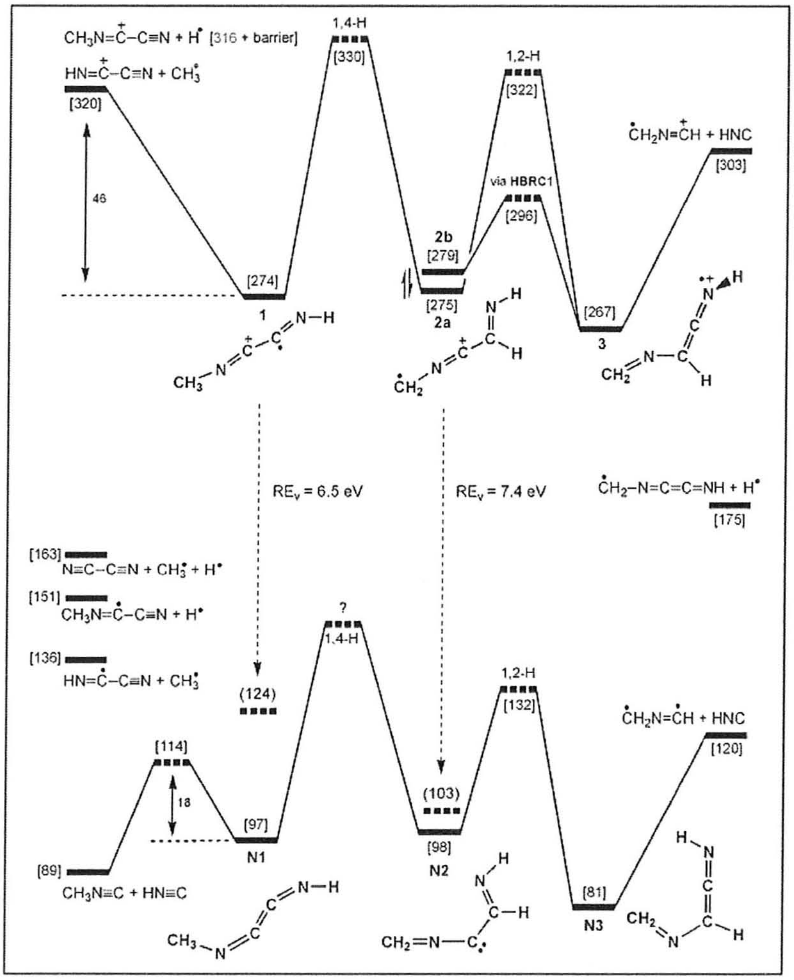

Scheme 5.9. CBS-QB3 results showing the dissociation and isomerization chemistry of ions **1-3** and their neutral counterparts **N1-N3**. Vertical recombination energies (REv) shown are in eV. All values are in kcal/mol derived at 298 K.

N2 is also shown to reside in a potential energy well at 98 kcal/mol providing sizeable kinetic stability, see Scheme 5.9. At elevated energies, these neutrals can interconvert via a 1,2-H shift at 132 kcal/mol into the relatively more stable **N3** species (81 kcal/mol). **N3** can then undergo direct bond cleavage to yield $CH_2N{\equiv}C\text{-}H$ + HN≡C.

The NR process involves a charge transfer that is a vertical Frank-Condon process. Provided resonant charge exchange occurs, an estimate of the internal energy content of the neutral generated can be obtained by subtracting the associated vertical recombinant energy (REv) from its adiabatic ionization energy (IEa). As **N2** species are generated with c. 5 kcal/mol of excess internal energy (IEa-REv), it is highly improbable that these species would either isomerize or dissociate. In contrast, **N1** species are generated with ~30 kcal/mol of internal energy facilitating its dissociation into $CH_3N{\equiv}C$ + $HN{\equiv}C$. The experimental results of the next section (Section 3.1) support this point.

3.1.4. The NR mass spectra of ions 1 and 2.

In general, NR spectra could display peaks from several sources. These sources include dissociation products of reionized species and reionized neutral dissociation products of neutralized species. This explains the general similarity between CID and NR spectra.

The *m/z* 68 NR spectra generated from theophylline and paraxanthine are shown in Figs. 5.10a and 5.10b respectively. The peaks at *m/z* 68 in the two spectra strongly suggest that ions **1** and **2** 'survived' the neutralization process.

The *m/z* 68 'survivor' peak seen in the NR spectrum from paraxanthine (Fig. 5.10b) is relatively much lower in intensity. Of the remaining peaks in the spectrum, there are five peaks that correspond to non-integral values. By comparison to the *m/z* 68 MI and CID (Figs. 5.6 and 5.7b), the presence of these peaks only in the NR spectrum indicates the generation of dissociation products from **N1**. One set of two peaks corresponds to *m/z* 27.4 and 26.6, see Fig. 5.10b inset (i). The second set of three peaks corresponds to 41.4, 40.5 and 39.6, see Fig. 5.10b inset (ii). The first set of peaks is proposed to be 'horns' of a wide dish-shaped peak [14] centered at *m/z* 27. The width of a peak is generally a measure of the kinetic energy release (T_h) associated with the dissociation products generated. In the same vein, the measured kinetic energy release (T_h) is proportional to the reverse energy barrier of the corresponding dissociation reaction. Therefore, the wide peak centered at *m/z* 27 describes the generation of $HN{\equiv}C$ in the reaction, **N1** → $HN{\equiv}C$ + $CH_3N{\equiv}C$, associated with a sizeable reverse barrier of 25 kcal/mol. Therefore, experimental observations are consistent with the theoretical predictions discussed in Section 3.1.3.

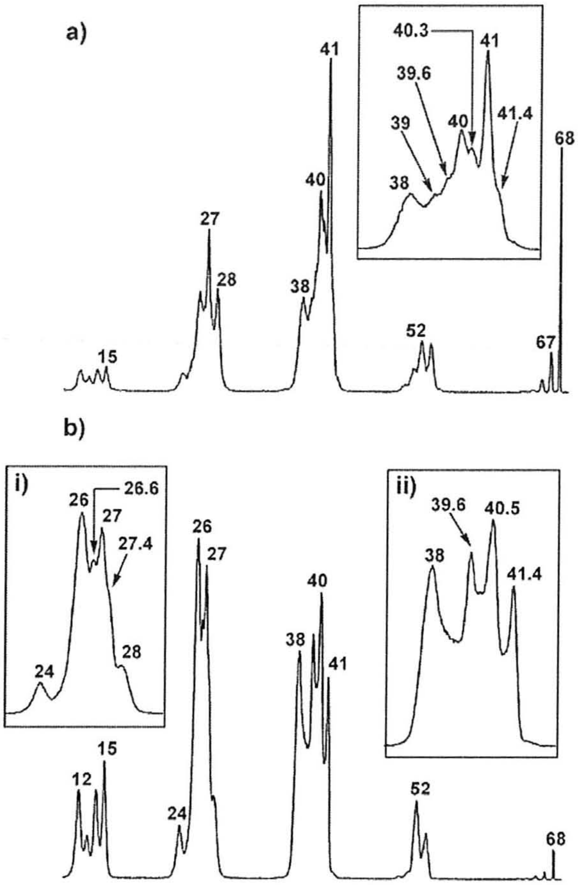

Figure 5.10. NR mass spectra of *m/z* 68 ions generated from (a) theophylline and (b) paraxanthine. Insets show expanded views of the (i) *m/z* 24–28 and (ii) *m/z* 38–41 regions.

The presence of a minor 'survivor' peak in the NR spectrum (Fig. 5.10b) is indicative of the kinetic stability of the **N1** species generated. However, as a fraction of the species generated possesses elevated internal energies, the reaction, **N1** → $HN{\equiv}C + CH_3N{\equiv}C$, takes place liberating a significant amount of kinetic energy.

The second set of peaks in the NR spectrum from paraxanthine is proposed to be 'horns' of two adjacent dish-shaped peaks centered at *m/z* 41 and 40 respectively. The peak at *m/z* 41 corresponds to the generation of $CH_3N{\equiv}C$ in the above mentioned reaction. As for the *m/z* 40 peak, the calculations of Scheme 5.9 on the neutral PES do not reveal a dissociation reaction that would rationalize the peak. Therefore, the *m/z* 40 peak is most likely describing the reaction, $CH_3N{\equiv}C \rightarrow CH_2N{\equiv}C^\bullet + H^\bullet$, which is possibly associated with a significant reverse barrier.

The *m/z* 68 'survivor' peak in the NR spectrum from theophylline (Fig. 5.10a) is much higher in intensity describing the kinetic stability of the co-generated neutrals, **N1** and **N2**. We note that the *m/z* 38 – 41 region contains signals at *m/z* 41.4, 40.5 and 39.6 describing the dissociation of **N1**. In comparison to the identical peaks seen in the *m/z* 68 NR spectrum from paraxanthine (Fig. 5.10b), the intensity of these peaks is lower. This is further evidence for our proposal that ions **1** are generated in admixture with ions **2** from theophylline.

3.2. The structure of m/z 68 ions generated from s-methyltetrazine.

As noted in the Experimental section, *s*-methyltetrazine was synthesized according to an analogous procedure used to synthesize *s*-tetrazine reported in Chapter 4. Hence, *s*-methyltetrazine is a mono-methyl analogue of *s*-tetrazine and is presumed to have very similar dissociation chemistry. As acetamidine hydrochloride [CH_3-$C(NH_2)$=NH.HCl] and formamidine acetate [NH_2-CH=NH.CH_3C(=O)OH] were introduced in 1:1 ratio during the synthesis, the final product is expected to be a mixture of *s*-methyltetrazine and 1,4-dimethyltetrazine. The EI mass spectrum of the product is shown in Fig. 5.11.

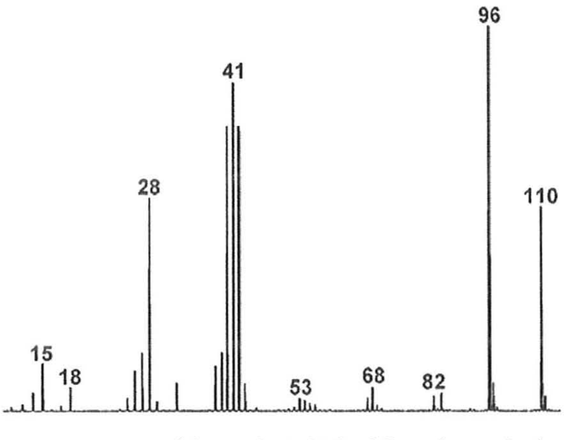

Figure 5.11. 70 eV EI mass spectrum of the product obtained from the synthesis of *s*-methyltetrazine.

The presence of intense peaks at *m/z* 96 and 110 is consistent with the mixture. These peaks correspond to *s*-methyltetrazine and 1,4-dimethyltetrazine ions respectively. Among the other peaks, a fairly intense peak at *m/z* 68 in the spectrum presumably corresponds to the ion, CH_3-C=N-N=$CH^{\bullet+}$ (**6a**). We note that this ion has been chronologically labeled due to the fact that this species and any of its isomers belong to the same PES as *N*-methylethenediimine (**1**).

The proposed dissociation mechanism for the generation of ion **6a** from *s*-methyltetrazine is shown in Scheme 5.13a. CBS-QB3 calculations predict that ion **6a** can be generated from the parent ion via N_2 loss following ring-opening. Confirming this proposal, the *m/z* 96 MI spectrum (Fig. 5.12) displays a solitary, intense dish-shaped peak [14] at *m/z* 68.

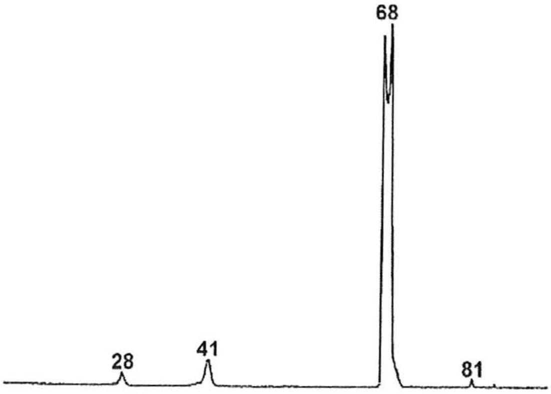

Figure 5.12. 2ffr MI mass spectrum of *m/z* 96 ions generated from *s*-methyltetrazine.

The width of the peak corresponds to a measured kinetic energy release (T_h) of c. 7 kcal/mol. From the calculations of Scheme 5.13a, the intermediate species, **HBMT-1**, are generated with ~30 kcal/mol of internal energy from which ~7 kcal/mol is redistributed as kinetic energy in the dissociation products, **6a** + N_2.

Scheme 5.13a reveals that the parent *s*-methyltetrazine ion (**MTET-1**) can either cleave the CH_3C-N or the HC-N bond to generate two species consisting of a terminal –N_2 group. Both intermediates are found to be local minima on the $C_3H_4N_4^{\bullet+}$ PES. The first cleavage listed yields **MTET-3a** and is the lower energy reaction with a TS at 332 kcal/mol. The HC-N bond cleavage in the parent ion with an energy barrier at 338 kcal/mol, generates **MTET-4a**. Thereafter, by elongating the C-N_2 bond, both species are capable of generating the HBRC species (**HBMT-1**) consisting of ion **6a** in complex with N_2. The hydrogen bridge between ion **6a** and N_2 in **HBMT-1** is noted to provide ~1 kcal/mol of stabilization energy. In comparison, see Scheme 5.13a, the reaction, **MTET-4a** → **HBMT-1**, is associated with a lower energy barrier relative to the reaction,

MTET-3a → **HBMT-1**. Therefore, despite a relatively higher energy ring-opening step, **MTET-4a** is proposed to be the intermediate involved in the generation of **HBMT-1** and therefore ion **6a**. In addition, a B3LYP/CBSB7 reaction scan reveals that the interconversion, **MTET-3a** → **4a**, is unlikely as the TS lies at 352 kcal/mol.

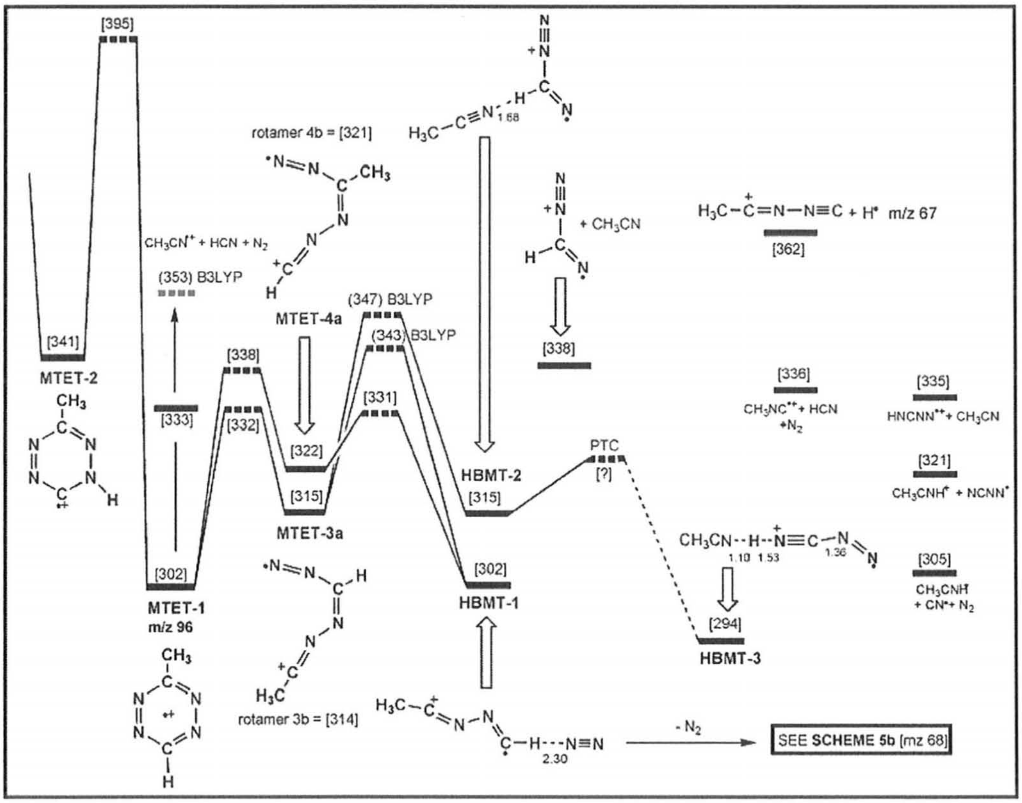

Scheme 5.13a. Mechanistic proposal for the formation of *m/z* 68 ions from low-energy *s*-methyltetrazine ions (**MTET-1**). Numbers in square brackets refer to 298 K enthalpies (in kcal/mol) derived from CBS-QB3 calculations.

An alternative ring-opening reaction involving the cleavage of the N-N bond in **MTET-1** is found to lead to a three-body dissociation associated with a high energy barrier to generate $CH_3C{\equiv}N^{\bullet+}$ + $HC{\equiv}N$ + N_2. A reaction scan at the B3LYP/CBSB7 level of theory places the TS at 353 kcal/mol. A considerably higher energy reaction is the 1,2-H shift on **MTET-1** to generate the ylide-ion (**MTET-2**). The associated TS lies at 395 kcal/mol.

Further, Scheme 5.13a shows that **MTET-3a** could undergo CH_3CN-N bond cleavage followed by the migration of the $CH_3C{\equiv}N$ moiety to generate a different

HBRC, **HBMT-2**. A B3LYP/CBSB7 reaction scan reveals that the TS lies at 347 kcal/mol. It is conceivable that **HBMT-2** could readily dissociate via $CH_3C{\equiv}N$ loss before or after undergoing proton transport catalysis (PTC) [23,24] to generate an ion at *m/z* 55, see Scheme 5.13a. Although the TS for the PTC reaction leading to **HBMT-3** (see Table 2a) did not optimize, this fragment ion is not observed in the *m/z* 96 MI spectrum (Fig. 5.12).

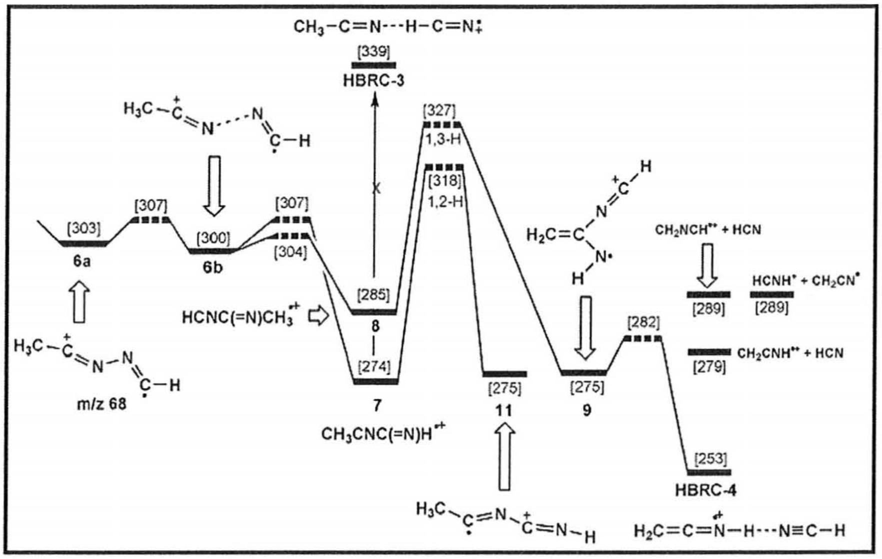

Scheme 5.13b. Theoretical prediction of the dissociation behaviour of the *m/z* 68 ions **6a** generated from *s*-methyltetrazine. Numbers in square brackets refer to enthalpies in kcal/mol derived at 298 K using the CBS-QB3 model chemistry.

Following the loss of N_2, ion **6a** is theoretically predicted to reside in a shallow minimum on the PES, see Scheme 5.13b. A mere 4 kcal/mol of excess energy leads to the elongation of the N-N bond to yield a marginally more stable long-bonded ion (**6b**). At this isomerization threshold, ion **6b** serves only as an intermediate in the generation of significantly more stable ions **7** and **8**. Ion **7** is the result of a 1,2-$CH_3C{\equiv}N$ shift at 307 kcal/mol and **8** is the product of a 1,2-$HC{\equiv}N$ shift at 304 kcal/mol. Therefore, within a narrow band energies, theory predicts that *s*-methyltetrazine generates a mixture of ions **6a**, **6b**, **7** and **8**. As ion **7** is ~10 kcal/mol more stable than ion **8**, we predict a majority of the source-generated *m/z* 68 ions to rearrange into ion **7**. Both ions contain an exposed N atom. The direct isomerization, **6a** → **7**, is unlikely as it is associated with a relatively higher energy TS at 344 kcal/mol, see Table 2b. In this context, it is conceivable that an elongation of CH_3CN-C bond in ion **7** could generate **HBRC-3**, see Scheme 5.13b. However, computations revealed that it is a higher energy species not favouring its generation.

The *m/z* 68 MI and CID spectra from *s*-methyltetrazine are displayed in Figs. 5.14a and 5.14b. The MI spectrum shows two prominent peaks at *m/z* 41 and 28 which are intensified in the CID spectrum. The mechanism for the generation of these peaks is discussed below. The peak at *m/z* 67 corresponding to $H^•$ loss is also metastably generated. The *m/z* 68 CID spectrum shows a structure-diagnostic peak at *m/z* 14, see Fig. 5.14b inset, indicative of the protruding N atom characteristic of co-generated ions **7** and **8**.

The theoretical calculations of Scheme 5.13b show that ion **8** can undergo a 1,3-H shift to generate ion **9**. This ion can thereafter elongate the C-NCH bond to form the hydrogen-bridged species, **HBRC-4**, and then dissociate. However, as the resulting ions are generated at a threshold of 327 kcal/mol, the ions possess sufficient energy to readily dissociate into $CH_2C{=}NH^{•+}$ + HC≡N; and $HC{\equiv}NH^+$ + $CH_2C{\equiv}N^•$ respectively. These two dissociations give rise to the peaks at *m/z* 41 and 28 in Figs. 5.14a and 5.14b. Other 1,3-H and 1,5-H shifts from ion **6a** going to ions **10** and **12** respectively were associated with much higher energy barriers, see Table 2b. The 1,4-H shift isomer (**13**) of ion **6a** is found to be a local minimum on the PES at 325 kcal/mol. However, the TS for the pertinent reaction was not optimized. In this context, a 1,2-H shift at 318 kcal/mol in ion **7** is found to yield a stable isomer, ion **11**, that is likely to be generated. Other stable ions discovered but most probably not generated include the product (**14**) of the 1,3-H shift in ion **8** at 374 kcal/mol which could further undergo CH_2C-NH bond cleavage to generate **HBRC-5**, see Table 2b. Further, we note that a PTC reaction in ion **6b** may lead to an interesting mechanism. Unfortunately, the attempted reaction scan was not successful.

The NR spectrum of *m/z* 68 ions generated from *s*-methyltetrazine is shown in Fig. 5.14c. A weak 'survivor' peak is indicative of the stability of a minor component of the mixture of *m/z* 68 ions generated. Model chemistry calculations predict that none of the ions **6a**, **6b**, **7** or **8** have stable neutral counterparts on the neutral PES. Instead, these geometries optimized to a $CH_3C{\equiv}N{\cdots}HC{\equiv}N$ dipole-dipole complex at 45 kcal/mol. Only low energy ion that is found to have a stable neutral counterpart is ion **11** at 107 kcal/mol (i.e. probable minor contributor to 'survivor' peak) albeit a shallow minimum on the PES. A mere 2 kcal/mol of energy leads to its dissociation into $CH_3C{\equiv}N + HN{\equiv}C$ at 65 kcal/mol, see Table 2b. Given that $CH_3C{\equiv}N$ dissociates via $H^{\bullet}$ loss, these findings justify the intense peaks seen in the NR spectrum at *m/z* 40 and 27 respectively.

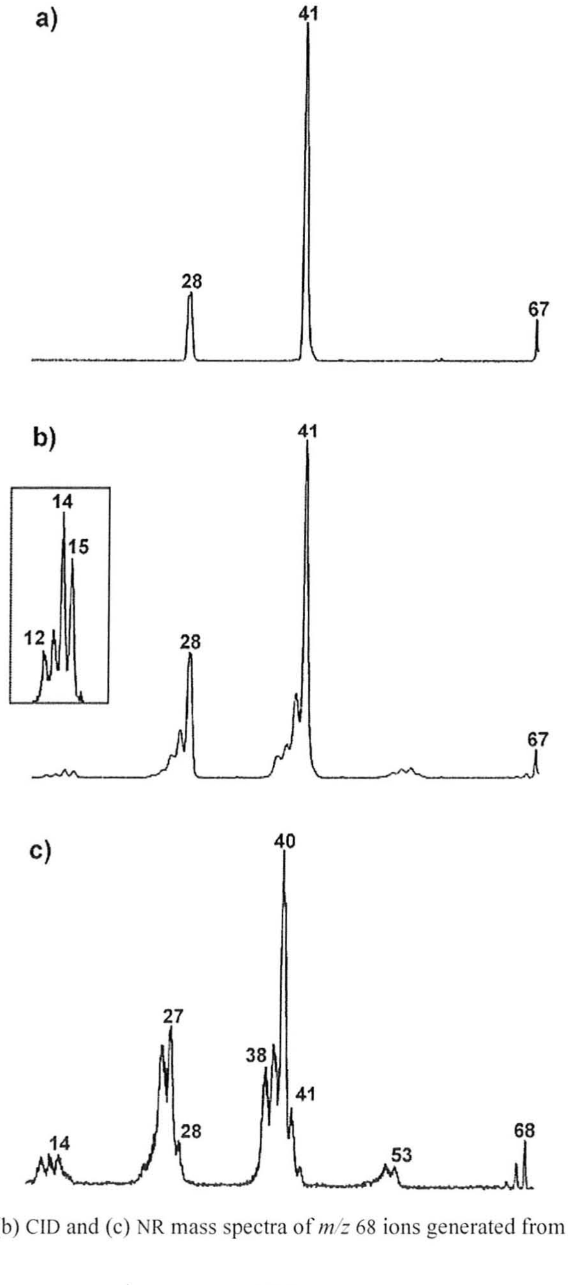

Figure 5.14. (a) MI (b) CID and (c) NR mass spectra of *m/z* 68 ions generated from *s*-methyltetrazine.

3.3. The structure of m/z 82 ions generated from caffeine.

The mass spectrum of caffeine, see Fig. 5.15, shows a prominent peak at *m/z* 82 most likely corresponding to the *N,N*-dimethylethenediimine ion, $CH_3N{=}C{=}C{=}NCH_3^{\bullet +}$ (**A1**). The connectivity corresponds to a dimer of aceto-iso-nitrile, $CH_3N{\equiv}C$.

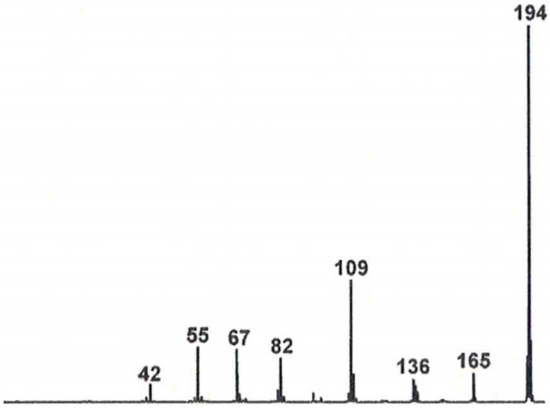

Figure 5.15. 70 eV EI mass spectrum of caffeine.

Scheme 5.16 displays a proposed fragmentation scheme for the generation of the *m/z* 82 ion from caffeine.

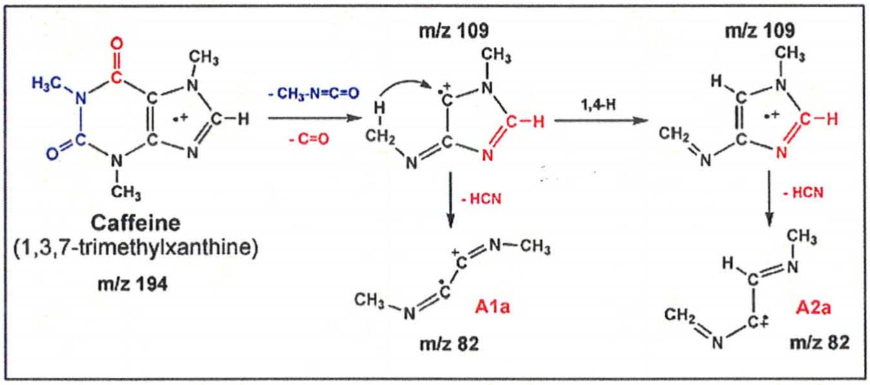

Scheme 5.16. Proposed fragmentation pathway for the generation of ions **A1a** and **A2a** from ionized caffeine.

The scheme is virtually identical to that showing the fragmentation scheme of theophylline (Scheme 5.2) to generate the corresponding *m/z* 68 ion. Here, the *m/z* 194 molecular ion is expected to undergo consecutive losses of $CH_3N{=}C{=}O$ and CO to yield an ion corresponding to the considerably intense *m/z* 109 peak in the mass spectrum, see Fig. 5.15. Similar to theophylline, the *m/z* 109 fragment ion can lose $HC{\equiv}N$ to generate the *m/z* 82 ion, $CH_3N{=}C{=}C{=}NCH_3^{\bullet+}$ (**A1**). However, given the depicted conformer of the *m/z* 109 ion, one may envisage a 1,4-H shift prior to HC≡N loss to generate an isomer of ion **A1**, $CH_2{=}N{-}C{=}C(H){-}CH_3^{\bullet+}$ (**A2**). Hence, the *m/z* 82 ions generated from caffeine may not be isomerically pure.

The CBS-QB3 theoretical investigation of the depicted proposed fragmentation pathway is displayed in Scheme 5.17a. The structure presumed to correspond to the parent *m/z* 109 ion generated is used as the reference, **P1a**. The first step in the generation of ion **A1** involves the ring-opening step via cleavage of the CH_3NC-NCH bond in **P1a** to generate **P2**. The associated TS lies at 318 kcal/mol. As **P2** is only marginally stable, it only serves as an intermediate in the interconversion to generate the more stable ion-dipole complex, **P3**. This ion can then readily dissociate into ion **A1** + HC≡N. Another lower energy pathway found to yield the same dissociation products is a one-step process involving the cleavage of the CH_3N-CH bond in **P1a** to generate **P3** that can consequently dissociate and generate ion **A1**. This step is associated with an energy barrier of only 16 kcal/mol placing the TS lower at 311 kcal/mol.

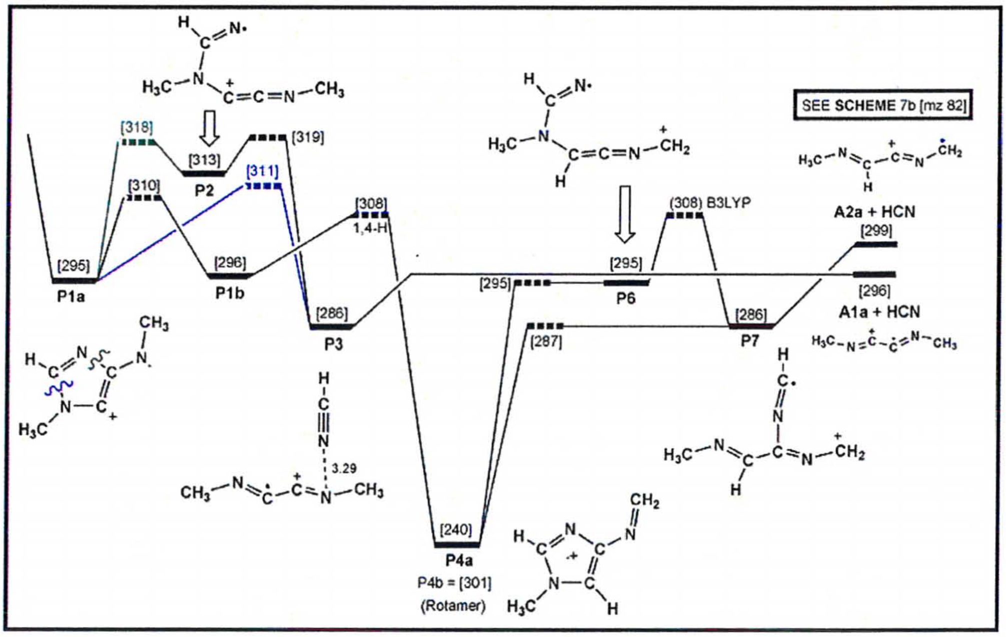

Scheme 5.17a. Mechanistic proposal for the formation of *m/z* 82 ions from low-energy *m/z* 109 ions (**P1a**). Numbers in square brackets refer to 298 K enthalpies (in kcal/mol) derived from CBS-QB3 calculations.

In contrast, further investigation reveals that the *m/z* 109 ion can also generate the 1,4-H shift isomer, $CH_2=N-C=C(H)-CH_3^{\bullet+}$ (**A2**). In this scenario, the first step involves a 180° rotation about the CC-NCH_3 bond at 310 kcal/mol in **P1a** to generate the corresponding rotamer, **P1b**. The resulting geometry is then favourable for a 1,4-H shift at 308 kcal/mol to yield yet another ring-structure, **P4a**. Thereafter, the lowest energy pathway involves the cleavage of the $CH_3N-C(N)H$ bond at 287 kcal/mol in **P4a** to generate a ring-opened structure, **P7**. Finally, **P7** can readily dissociate via HC≡N loss to generate ion **A2**. Therefore, the separate generation of ions **A1** and **A2** respectively, are competitive processes presumably yielding a mixture of the two *m/z* 82 ions. Other reactions such as, **P2** → **P4b** and **P3** → **P5b**, are found to be associated with much higher energy barriers, see Table 3a.

Consistent with theory, the *m/z* 109 MI spectrum, see Fig. 5.18, displays an intense peak at *m/z* 82 corresponding to the ions **A1** and **A2**. Other peaks in the spectrum include those at *m/z* 108, 94 and 55. The *m/z* 108 and 94 peaks correspond to $H^\bullet$ loss and $CH_3^\bullet$ loss respectively. The peak at *m/z* 55 most probably corresponds to a second consecutive HC≡N loss from the *m/z* 109 fragment ion. In other words, the peak at *m/z* 55 most likely is a result of HC≡N loss from the *m/z* 82 fragment ion.

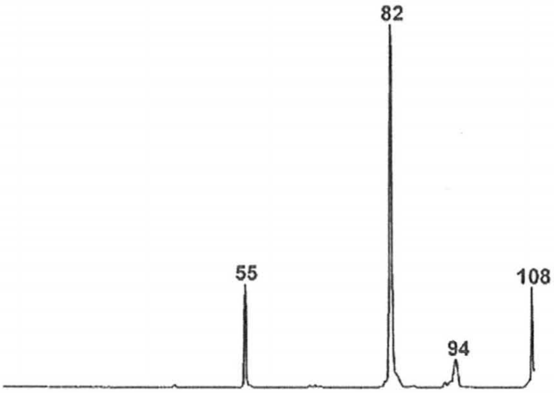

Figure 5.18. 2ffr MI mass spectrum of *m/z* 109 ions generated from caffeine.

According to the CBS-QB3 calculations of Scheme 5.17b, both ions, **A1** and **A2**, reside in deep potential energy wells at 264 and 267 kcal/mol respectively. The lowest reaction threshold relative to the remarkably stable ion **A1** corresponds to its dissociation via $CH_3^\bullet$ loss. This dissociation threshold lies at 300 kcal/mol. Isomerization thresholds corresponding to 1,2-H, 1,3-H, 1,4-H and 1,5-H shifts in **A1a** leading to **A3a**, **A4a**, **A2a** and **A5** respectively are significantly higher (≥15 kcal/mol) relative to $CH_3N{=}C{=}C{=}N^+$ + $CH_3^•$, see Table 3b. In the same context, the energy barrier for 1,2-CH_3 shift in **A1a** to yield **A6** is also higher at 315 kcal/mol, see Table 3b. Hence, the only reaction observed from ion **A1** should be the generation of *m/z* 67 ions involving $CH_3^•$ loss.

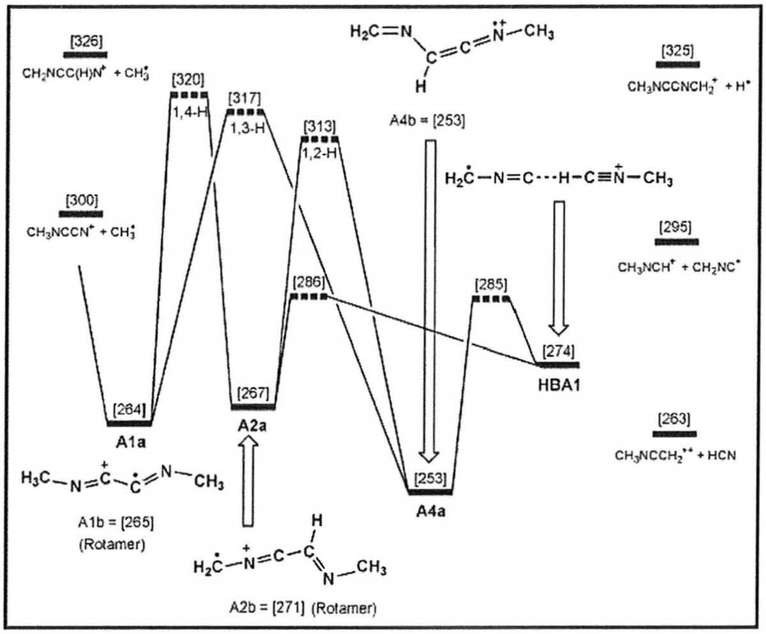

Scheme 5.17b. Theoretical investigation of the dissociation behaviour of the *m/z* 82 ions **A1a** generated from caffeine. Numbers in square brackets refer to enthalpies in kcal/mol derived at 298 K using the CBS-QB3 model chemistry.

However, as previously mentioned, ions **A2** are generated in admixture with ions **A1**. Of the three reaction mechanisms studied on ion **A2**, the lowest energy pathway involves the elongation of the C-C bond at 286 kcal/mol in ion **A2** to generate the hydrogen-bridged species, **HBA1**. Another pathway studied for the reaction, **A2** → **HBA1**, included a relatively more stable 1,2-H shift intermediate ion **A4**. However, this pathway is unlikely due to a high energy TS between **A2** and **A4**, see Table 3b. Upon formation of **HBA1**, its dissociation leads to the *m/z* 42 $CH_3N{=}CH^+$ ion via $CH_2N{\equiv}C^•$ loss at a dissociation threshold that lies at 295 kcal/mol. It is unlikely that a large fraction of ions **A2** would isomerize into ions **A1** due to the significantly large energy barrier for the 1,4-

H shift at 320 kcal/mol. However, this reaction would be favoured over $CH_3^\bullet$ loss as the corresponding dissociation threshold lies at 326 kcal/mol, see Scheme 5.17b.

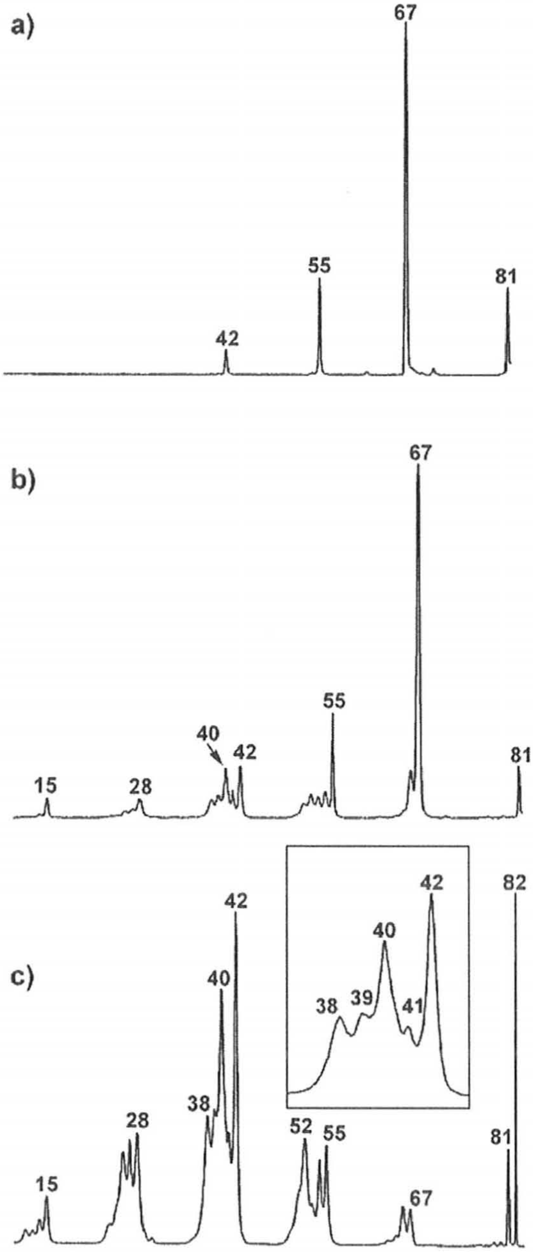

Figure 5.19. (a) MI (b) CID and (c) NR mass spectra of *m/z* 82 ions generated from caffeine.

The *m/z* 82 MI and CID spectra generated from caffeine are displayed in Figs. 5.19a and 5.19b. Prominent peaks in the MI spectrum correspond to *m/z* 81, 67, 55 and 42.

Dissociation via $H^\bullet$ loss explains the *m/z* 81 peak. The intense *m/z* 67 peak is consistent with the dissociation of ion **A1** involving $CH_3^\bullet$ loss. In line with the interpretation of the *m/z* 109 MI spectrum (Fig. 5.18), the *m/z* 55 peak seen in this spectrum is due to HC≡N loss from ion **A2** most likely generating the ion, $CH_3N{=}C{=}CH_2^{\bullet+}$. The generation of this ion could not be theoretically probed. However, this dissociation threshold is computed to be at 263 kcal/mol which is relatively lower than the threshold corresponding to $CH_3N{=}CH^+$ (*m/z* 42) + $CH_2N{\equiv}C^\bullet$. The difference in the threshold levels is consistent with the difference in intensities of the *m/z* 55 and 42 peaks respectively. The presence of peaks corresponding to the dissociation of both ions confirms our proposal of the co-generation of ions **A1** and **A2**. The *m/z* 82 CID, see Fig. 5.19b, displays relatively less intense peaks at *m/z* 40, 28 and 15 in addition to the already discussed MI peaks. The ion giving rise to the peak at *m/z* 40 is at this point uncertain. However, the peak at *m/z* 28 possibly corresponds to $HC{\equiv}NH^+$ and the *m/z* 15 peak is indicative of the $-CH_3$ connectivity of ions **A1** and **A2**.

The *m/z* 82 NR spectrum generated from caffeine is displayed in Fig. 5.19c. An intense signal at *m/z* 82 is strongly indicative of the co-generated ions **A1** and **A2** having survived the NR process. Consistent with this observation, CBS-QB3 calculations indicate that the neutral counterparts of both ions, **A1**N and **A2**N, are local minima on the neutral $C_4H_6N_2$ PES. Scheme 5.20 displays the dissociation chemistry of the neutrals, **A1**N and **A2**N. Unlike on the ionic PES, the scheme reveals that, at elevated energies, **A1**N**a** can interconvert via 1,4-H shift into **A2**N**a** instead of losing $CH_3^\bullet$. In line with this, at the same threshold, **A2**N**a** can also interconvert into the relatively more stable **A4**N**a**. The difference between the respective isomerization and dissociation threshold levels is ~3 kcal/mol. This prediction is observed in the NR spectrum (Fig. 5.19c) from the low intensity peak at *m/z* 67. Other 1,2-H, 1,3-H or 1,5-H shifts in **A1**N**a** to generate **A3**N**a**, **A4**N**a** and **A5**N**a** respectively are unlikely as the corresponding transition states lie at least 10 kcal/mol above the 1,4-H shift threshold, see Table 3b. The scheme also shows that **A2**N**a** can undergo a 1,2-$CH_2N{\equiv}C$ shift to generate **A7**N. The associated TS lies at 120 kcal/mol. It is at this point uncertain how this species may play a role in the generation of any of the other NR peaks. However, as there are no tell-tale dish-shaped peaks in the NR spectrum, see Fig. 5.19c inset, and that the ions can freely communicate with each other, it is really difficult to deduce any characteristic behaviour of any one neutral isomer.

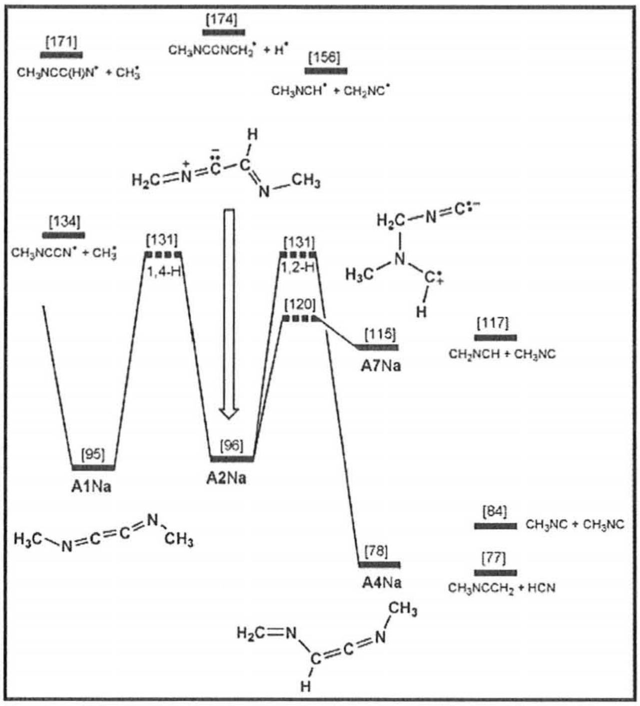

Scheme 5.20. CBS-QB3 results showing the dissociation and isomerization chemistry of the neutral species **A1Na**. All enthalpy values are in kcal/mol derived at 298 K.

Conclusion

Both, theophylline and paraxanthine are shown to generate the *m/z* 68 *N*-methylethenediimine ion $CH_3N{=}C{=}C{=}NH^{\bullet+}$ (**1**) by dissociative ionization. Theory shows that the latter precursor molecule yields isomerically pure ions **1**. In contrast, theophylline is shown to co-generate the 1,4-H shift isomeric ion (**2**) from the parent *m/z* 95 fragment ion. The neutral counterpart of ion **1** and **2** are found to be kinetically stable from the NR experiments. **N1** is relatively less stable than **N2**. Ionized *s*-methyltetrazine is also shown to yield an isomeric *m/z* 68 ion, $CH_3\text{-}C{=}N\text{-}N{=}CH^{\bullet+}$ (**6a**). However, as the ion is generated at elevated internal energies, theory shows that ion **6a** would readily isomerize into multiple other ions resulting in a mixture. A majority of this mixture do not have stable neutral counterparts in the gas phase. Finally, ionized caffeine is revealed to generate the *N,N*-dimethylethenediimine ion $CH_3N{=}C{=}C{=}NCH_3^{\bullet+}$ (**A1**) corresponding to *m/z* 82. Similar to theophylline, caffeine is shown to co-generate the 1,4-H shift isomer **A2** at the same threshold. The resulting ion does not readily interconvert with **A1**. In contrast, the neutral counterparts of these ions are found to be interconvertible stable species in the rarefied gas phase

References

[1] A.G.G.M. Tielens, S.B. Charnley. Origins Life Evol. Biosphere. 27 (1997) 23.

[2] E. Herbst, W. Klemperer. Astrophys. J. 185 (1973) 505.

[3] W.T. Huntress, Jr., V.G. Anicich. Astrophys. J. 208 (1976) 237.

[4] E. Herbst. Annu. Rev. Phys. Chem. 46 (1995) 27.

[5] H. Wincel, R.H. Fokkens, N.M.M. Nibbering. Rapid Commun. Mass Spectrom. 14 (2000) 135.

[6] A.H. Delsemme. Origins Life Evol. Biosphere. 14 (1984) 51.

[7] F. Pichieri. Chem. Phys. Lett. 353 (2002) 383 and references cited therein.

[8] D. Buhl, C. Ponnamperuma. Origins Life Evol. Biosphere. 3 (1971) 157.

[9] S. Green. Annu. Rev. Phys. Chem. 32 (1981) 103.

[10] L.E. Snyder. Origins Life Evol. Biosphere. 27 (1997) 115.

[11] L.E.B. Johansson, C. Andersson, J. Ellder, P. Friberg, A. Hjalmarson, B. Hoglund, W.M. Irvine, H. Olofsson, G. Rydbeck. Astron. Astrophys. 130 (1984) 227.

[12] A.J. Remijan, J.M. Hollis, F.J. Lovas, D.F. Plusquellic, P.R. Jewell. Astrophys. J. 632 (2005) 333.

[13] D.M. Mehringer, L.E. Snyder, Y. Miao, F.J. Lovas. ApJ. 480 (1997) L71.

[14] J.L. Holmes, C. Aubry, P.M. Mayer. Assigning Structures to Ions in Mass Spectrometry, CRC Press, Boca Raton, 2007.

[15] H.F. van Garderen, P.J.A. Ruttink, P.C. Burgers, G.A. McGibbon, J.K. Terlouw. Int. J. Mass Spectrom. Ion Proc. 121 (1992) 159.

[16] J. Sauer, D.K. Heldmann, J. Hetzenegger, J. Krauthan, H. Sichert, J. Schuster. Eur. J. Org. Chem. 12 (1998) 2885.

[17] J.A. Montgomery, Jr, M.J. Frisch, J.W. Ochterski, and G.A. Petersson, J. Chem. Phys. 112, (2000) 6532.

[18] J.W. Ochterski, G.A. Petersson, J.A. Montgomery, Jr., J. Chem. Phys. 104 (1996) 2598.

[19] M. J. Frisch et al. Gaussian 03 (Revisions C.02 and D.01), Gaussian, Inc., Wallingford CT, 2004.

[20] M. Culea, N. Palibroda, M. Chiriac, Z. Moldovan. Biol. and Environ. Mass Spectrom. 19 (1990) 360.

[21] K.K. Midha, S. Sved, R.D. Hossie, I.J. McGilveray. Biol. Mass Spectrom. 4 (2005) 172.

[22] R. Flammang, Y.V. Haverbeke, M.W. Wong, A. Ruhmann, C. Wentrup. J. Phys. Chem. 98 (1994) 4814.

[23] C.Y. Wong, P.J.A. Ruttink, P.C. Burgers, J.K. Terlouw, Chem. Phys. Lett. 390 (2004) 176.

[24] C.Y. Wong, P.J.A. Ruttink, P.C. Burgers, J.K. Terlouw, Chem. Phys. Lett. 387 (2004) 204.

Appendix to Chapter 5

Table 1a. Energetic data [a] derived from **CBS-QB3** calculations for minima of stable ionic and neutral isomers of *N*-methylethenediimine (**1**) and their connecting transition states.

Ionic species	CBS-QB3 E(total) [0K]	QB3 ZPE	QB3 $\Delta_fH^0_0$	QB3 $\Delta_fH^0_{298}$
1	-225.458030	40.0	275.7	273.6
2a	-225.455516	40.2	277.3	274.6
2b	-225.449478	40.1	281.1	278.5
3	-225.468159	40.3	269.3	266.7
5	-225.425528	40.7	291.9	289.2
HBRC-1	-225.441356	36.5	286.2	284.5
HBRC-2	-225.463758	37.0	272.1	270.4
TS **1** → **2**	-225.366151	37.5	333.3	330.1
TS **2** → **3**	-225.379860	36.6	324.7	322.1
TS **2** → **HBRC-1**	-225.422976	36.8	297.7	295.9
TS **3** → **5**	-225.358232	36.2	338.3	336.1
TS **3** → **HBRC-1**	-225.423487	37.4	297.4	295.2
Neutral Species				
N1a	-225.739378	40.8	99.1	96.5
N1b	-225.738127	40.9	99.9	97.3
N2a	-225.736608	40.7	100.9	98.1
N2b	-225.737498	40.8	100.3	97.6
N3	-225.763380	40.9	84.1	81.2
TS **N1a** → HNC loss	-225.712382	38.6	116.1	113.7
TS **N2** → **N3**	-225.682802	37.7	134.6	131.6

[a] $E_{(total)}$ in Hartrees, all other components, including the ZPE scaled by 0.99, are in kcal/mol.

Table 1b. Energetic data for various dissociation products of ionized *N*-methylethenediimine (**1**) derived from **CBS-QB3** calculations [a].

Species	*m/z*	CBS-QB3 E(total) [0 K]	QB3 $\Delta_fH^0_0$	QB3 $\Delta_fH^0_{298}$
CH_3NCCN^+ + $H^\bullet$	**67**	-	**317.4**	**316.1**
CH_2NCCNH^+ + $H^\bullet$		-	**339.6**	**338.3**
CH_3NCCN^+		-224.891330	265.8	264.0
CH_2NCCNH^+		-224.856383	288.0	286.2
$H^\bullet$		-0.499818	51.6	52.1
$HNCCN^+$ + $CH_3^\bullet$	**53**	-	**320.6**	**319.5**
$HNCCN^+$		-185.641344	284.3	283.9
$CH_3^\bullet$		-39.744795	36.3	35.6
$CH_2NCH^{\bullet+}$ + HNC	**41**	-	**304.7**	**303.3**
$CH_2NCH^{\bullet+}$ + HCN		-	**290.6**	**289.0**
$CH_3NC^{\bullet+}$ + HNC		-	**351.0**	**349.5**
$CH_2NCH^{\bullet+}$		-132.141540	258.7	257.2
$CH_3NC^{\bullet+}$		-132.072590	305.0	303.4
HNC		-93.265114	46.0	46.1
HCN		-93.287537	31.9	31.8
CH_2NC^+ + $HCNH^\bullet$	**40**	-	**370.6**	**369.2**
$HNCCH^+$ + $CH_2N^\bullet$		-	**382.5**	**381.2**
$CH_3CCH^{\bullet+}$ + N_2		-	**287.8**	**286.4**
CH_2NC^+		-131.492274	304.1	303.6
$HNCCH^+$		-131.459958	324.4	324.0
$CH_3CCH^{\bullet+}$		-116.040279	287.0	285.6
$HCNH^\bullet$		-93.814547	66.5	65.6
$CH_2N^\bullet$		-93.827908	58.1	57.2
N_2		-109.398466	0.8	0.8
$HCNH^+$ + $CH_2NC^\bullet$	**28**	-	**314.0**	**312.6**
$HCNH^+$		-93.558626	227.0	226.2
$CH_2NC^\bullet$		-131.837990	87.0	86.4

[a] $E_{(total)}$ in Hartrees, all other components, including the ZPE scaled by 0.99, are in kcal/mol.

Table 1c. Energetic data for various dissociation products of neutral *N*-methylethenediimine (**N1**) derived from **CBS-QB3** calculations [a].

Species	**CBS-QB3** **E(total)** [0 K]	**QB3** **$\Delta_fH^0_0$**	**QB3** **$\Delta_fH^0_{298}$**
$CH_3NCCN^{\bullet}$ + $H^{\bullet}$	-	**152.7**	**150.5**
$CH_2NCCNH^{\bullet}$ + $H^{\bullet}$	-	**175.6**	**174.5**
$CH_3NCCN^{\bullet}$	-225.155374	101.1	98.4
$CH_2NCCNH^{\bullet}$	-225.117615	124.0	122.4
$H^{\bullet}$	-0.499818	51.6	52.1
$HNCCN^{\bullet}$ + $CH_3^{\bullet}$	-	**137.3**	**136.3**
$HNCCN^{\bullet}$	-185.933354	101.0	100.7
$CH_3^{\bullet}$	-39.744795	36.3	35.6
NCCN + $CH_3^{\bullet}$ + $H^{\bullet}$	-	**162.4**	**162.5**
NCCN	-185.393902	74.5	74.8
CH_2NCH + HNC	-	**122.0**	**120.4**
CH_3NC + HNC	-	**89.9**	**88.5**
CH_2NCH	-132.437680	76.0	74.3
CH_3NC	-132.488986	43.9	42.4
HNC	-93.265114	46.0	46.1

[a] $E_{(total)}$ in Hartrees, all other components, including the ZPE scaled by 0.99, are in kcal/mol.

Table 2a. Energetic data [a] derived from **CBS-QB3** and **CBS-APNO** calculations for minima of stable ionic isomers of ionized methyltetrazine (**MTET-1**) and their connecting transition states.

Ionic species	CBS-QB3 E(total) [0K]	QB3 ZPE	QB3 $\Delta_fH^0_0$	QB3 $\Delta_fH^0_{298}$	APNO $\Delta_fH^0_{298}$
MTET-1	-334.808935	48.3	306.1	301.5	[b]
MTET-2	-334.746542	48.6	345.3	340.8	343.6
MTET-3a	-334.789394	46.5	318.4	315.0	314.2
MTET-3b	-334.791908	46.4	316.8	313.5	312.4
MTET-4a	-334.777837	45.9	325.6	322.2	320.4
MTET-4b	-334.779843	46.1	324.4	320.9	318.7
HBMT-1	-334.812839	43.7	303.7	301.7	301.0
HBMT-2	-334.791120	43.5	317.3	314.9	315.6
HBMT-3	-334.824522	43.7	296.3	293.9	294.0
TS **MTET-1** → **2**	-334.661274	42.7	398.8	394.7	[c]
TS **MTET-1** → **3a**	-334.761569	45.7	335.8	331.7	329.8
TS **MTET-1** → **4a**	-334.751866	45.0	341.9	337.8	335.8
TS **MTET-3a** → **HBMT-1**	[c]	-	-	-	-
TS **MTET-4a** → **HBMT-1**	-334.764266	44.0	334.2	330.9	327.5

[a] $E_{(total)}$ in Hartrees, all other components, including the ZPE scaled by 0.99, are in kcal/mol.
[b] The desired geometry could not be optimized. [c] The desired transition state could not be found.

Table 2b. Energetic data [a] derived from **CBS-QB3** and **CBS-APNO** calculations for minima of stable isomers of **6a** and their connecting transition states.

Ionic species	CBS-QB3 E(total) [0K]	QB3 ZPE	QB3 $\Delta_fH^0_0$	QB3 $\Delta_fH^0_{298}$	APNO $\Delta_fH^0_{298}$
6a	-225.410967	39.7	305.0	302.6	301.5
6b	-225.416660	38.4	301.4	299.7	[b]
7	-225.456674	40.0	276.3	273.9	273.8
8	-225.438637	40.1	287.6	285.0	283.7
9	-225.454528	39.9	277.7	274.7	273.6
10	-225.373255	39.7	328.7	326.2	325.2
11	-225.455642	39.5	277.0	274.8	272.3
N11	-225.723117	39.7	109.3	106.9	-
12 [c]	-225.428298	39.7	294.1	291.5	291.2
13	-225.374386	39.1	328.0	325.3	325.9
14	-225.365552	40.7	333.5	330.6	330.8
HBRC-3	-225.354899	35.8	340.2	339.0	[b]
HBRC-4	-225.491016	36.7	254.8	252.9	252.1
HBRC-5	-225.463758	37.0	271.9	270.2	268.1
TS **6a** → **6b**	-225.404671	37.8	309.0	306.7	305.3
TS **6a** → 7	-225.344318	38.0	346.8	344.2	344.2
TS **6b** → 7	-225.403861	37.8	309.5	307.3	305.8
TS **6b** → **8**	-225.408530	38.0	306.5	304.3	[d]
TS **6a** → **10**	-225.285624	34.9	383.7	380.9	378.4
TS **6b** → **12**	-225.345794	36.9	345.9	342.6	340.2
TS 7 → **11**	-225.387111	36.2	320.0	317.8	316.1
TS **8** → **9**	-225.371352	36.8	329.9	326.8	324.8
TS **8** → **14**	-225.296578	35.2	376.8	374.0	377.1
TS **9** → **HBRC-4**	-225.443900	37.7	284.3	281.8	280.0
TS **10** → **HBRC-4**	[d]	-	-	-	-
TS **14** → **HBRC-5**	-225.338740	37.0	350.3	348.2	346.2
TS *N11* → **HNC loss**	-225.719113	39.2	111.9	109.3	-

[a] $E_{(total)}$ in Hartrees, all other components, including the ZPE scaled by 0.99, are in kcal/mol. [b] The CBS-APNO model chemistry optimized the CBS-QB3 geometry **6b** into that of **8**. [c] The staggered geometry generated by CBS-QB3 was converted to an eclipsed geometry by the CBS-APNO model chemistry. [d] The desired transition state could not be found.

Table 2c. Energetic data for various dissociation products of ionized **6a** derived from **CBS-QB3/CBS-APNO** calculations [a].

Species	**CBS-QB3** **E(total)** [0 K]	**QB3** $\Delta_fH^0_0$	**QB3** $\Delta_fH^0_{298}$	**APNO** $\Delta_fH^0_{298}$
$CH_3CNNC^+ + H^\bullet + N_2$		**363.4**	**362.4**	**362.7**
CH_3CNNC^+	-224.817985	311.8	310.3	310.6
$H^\bullet$	-0.499818	51.6	52.1	52.1
$HC(=N)NN^{\bullet+} + CH_3CN$		**341.1**	**338.2**	**338.3**
$HC(=N)NN^{\bullet+}$	-202.226685	320.9	319.7	320.7
CH_3CN	-132.526594	20.2	18.5	17.6
$HNCNN^{\bullet+} + CH_3CN$		**337.8**	**335.2**	**335.5**
$HNCNN^{\bullet+}$	-202.231939	317.6	316.7	317.9
$CH_3CNH^+ + NNCN^\bullet$		**323.6**	**321.1**	**313.4**
CH_3CNH^+	-132.822286	199.9	197.4	196.2
$NNCN^\bullet$ [b]	-201.958782	123.7	123.7	117.2
$CH_3CNH^+ + CN^\bullet + N_2$		**306.5**	**304.8**	**303.7**
$CN^\bullet$	-92.587607	105.8	106.6	106.3
$CH_3NC^{\bullet+} + HCN + N_2$		**337.7**	**336.0**	**335.5**
$CH_3NC^{\bullet+}$	-132.072585	305.1	303.5	302.3
HCN	-93.287537	31.8	31.7	32.0
$CH_3CN^{\bullet+} + HCN + N_2$		**334.8**	**333.4**	-
$CH_3CN^{\bullet+}$	-132.077129	302.2	300.9	[c]
$CH_2CNH^{\bullet+} + HCN$		**280.1**	**278.6**	**277.8**
$CH_2CNH^{\bullet+}$	-132.163079	248.3	246.9	245.8
$CH_2NCH^{\bullet+} + HCN$		**290.5**	**289.0**	**287.8**
$CH_2NCH^{\bullet+}$	-132.146421	258.7	257.3	255.8
$HCNH^+ + CH_2CN^\bullet$		**290.2**	**288.8**	**288.9**
$HCNH^+$	-93.558686	227.0	226.2	226.8
$CH_2CN^\bullet$	-131.875867	63.2	62.6	62.1

[a] $E_{(total)}$ in Hartrees, all other components, including the ZPE scaled by 0.99, are in kcal/mol. [b] The CBS-QB3 and CBS-APNO derived geometries have different bond angles, resulting in an unusually large divergence in $\Delta_fH^0_{298}$ values. [c] The desired geometry could not be found.

Table 3a. Energetic data [a] derived from **CBS-QB3** calculations for minima and connecting transition states of stable ionic isomers of **P1a** (*m/z* 109).

Ionic species	**CBS-QB3 E(total)** [0K]	**QB3 ZPE**	**QB3 $\Delta_fH^0_0$**	**QB3 $\Delta_fH^0_{298}$**
P1a	-357.977039	73.2	300.4	294.5
P1b	-357.974701	72.8	301.9	296.0
P2	-357.949045	71.0	318.0	313.3
P3	-357.994174	68.9	289.7	286.4
P4a	-358.064190	74.0	245.7	239.8
P4b	-357.968261	71.4	305.9	300.9
P5a	-357.985338	68.0	295.2	291.5
P5b	-357.991715	68.1	291.2	287.4
P6	-357.977082	71.4	300.4	295.4
P7	-357.991436	70.1	291.4	286.4
TS **P1a** → **P1b**	-357.952187	71.7	316.0	310.2
TS **P1a** → **P2**	-357.940829	71.3	323.1	317.6
TS **P1a** → **P3**	-357.951316	71.0	316.6	311.0
TS **P1b** → **P4a**	-357.955007	70.1	314.2	308.0
TS **P2** → **P3**	-357.939690	69.4	323.8	319.3
TS **P2** → **P4b**	-357.858465	67.9	374.8	369.4
TS **P3** → **P5b**	-357.908224	66.0	343.6	339.4
TS **P4a** → **P6**	-357.977385	71.3	300.2	294.7
TS **P4a** → **P7**	-357.989944	69.9	292.3	286.9
TS **P5a** → **P5b**	-357.951502	67.8	316.4	312.3
TS **P7** → **A1a** + **HCN**	-357.977247	68.5	300.3	295.6

[a] $E_{(total)}$ in Hartrees, all other components, including the ZPE scaled by 0.99, are in kcal/mol.

Table 3b. Energetic data [a] derived from **CBS-QB3** calculations for minima and connecting transition states of stable ionic and neutral isomers of *N,N*-dimethylethenediimine (**A1a**) (*m/z* 82).

Ionic species	**CBS-QB3 E(total)** [0K]	**QB3 ZPE**	**QB3** $\Delta_fH^0_0$	**QB3** $\Delta_fH^0_{298}$
A1a	-264.691025	58.0	267.6	264.2
A1b	-264.689604	58.0	268.5	265.1
A2a	-264.686095	57.1	270.7	266.8
A2b	-264.679498	57.0	274.9	270.9
A3a	-264.668037	58.4	282.0	278.3
A3b	-264.663817	58.4	284.7	280.9
A4a	-264.708764	57.9	256.5	252.8
A4b	-264.708781	57.9	256.5	252.8
A5	-264.683562	58.7	272.3	268.6
A6	-264.695932	58.1	264.5	260.8
HBA1	-264.676727	54.5	276.6	273.7
TS **A1a** → **2a**	-264.601310	54.9	323.9	319.5
TS **A1a** → **3a**	-264.591450	54.7	330.1	326.4
TS **A1a** → **4a**	-264.605755	54.4	321.1	317.2
TS **A1a** → **5**	-264.596803	55.7	326.7	322.1
TS **A1a** → **6**	-264.609812	55.9	318.6	314.9
TS **A2a** → **HBA1**	-264.657016	55.3	289.0	285.7
TS **A2a** → **4a**	-264.612712	53.9	316.8	312.9
TS **A4a** → **HBA1**	-264.658460	55.0	288.1	284.9
Neutral Species				
A1Na	-264.959955	58.2	98.9	95.0
A2Na	-264.957696	57.7	100.3	96.2
A3Na	-264.923212	58.8	121.9	118.0
A4Na	-264.986925	58.4	81.9	77.7
A5Na	-264.961239	58.7	98.1	94.1
A7Na	-264.927336	58.5	119.3	115.2
TS **A1**Na → **A2**Na	-264.902522	54.8	134.9	130.5
TS **A1**Na → **A3**Na	-264.855742	54.9	164.3	160.2
TS **A1**Na → **A4**Na	-264.861453	54.3	160.7	156.5
TS **A1**Na → **A5**Na	-264.886181	55.0	145.2	140.8
TS **A2**Na → **A7**Na	-264.919293	58.4	124.4	119.5
TS **A2**Na → **A4**Na	-264.901406	55.0	135.6	131.3

[a] $E_{(total)}$ in Hartrees, all other components, including the ZPE scaled by 0.99, are in kcal/mol.

Table 3c. Energetic data for various dissociation products of ionized *N,N*-dimethylethenediimine (**A1a**) derived from **CBS-QB3** calculations [a].

Ionic species	**CBS-QB3 E(total)** [0K]	**QB3 $\Delta_fH^0_0$**	**QB3 $\Delta_fH^0_{298}$**
$CH_3NCCNCH_2^+ + H^\bullet$	-	**326.9**	**324.5**
$CH_3NCCNCH_2^+$	-264.096722	275.3	272.4
$H^\bullet$	-0.499818	51.6	52.1
$CH_3NCCN^+ + CH_3^\bullet$	-	**302.1**	**299.5**
CH_3NCCN^+	-224.891350	265.8	264.0
$CH_3^\bullet$	-39.744795	36.3	35.5
$CH_2NCC(H)N^+ + CH_3^\bullet$	-	**329.0**	**326.1**
$CH_2NCC(H)N^+$	-224.848434	292.7	290.6
$CH_3NCCH_2^{\bullet+} + HCN$	-	**265.6**	**262.8**
$CH_3NCCH_2^{\bullet+}$	-171.406688	233.8	231.1
HCN	-93.287537	31.8	31.7
$CH_3NCH^+ + CH_2NC^\bullet$	-	**298.0**	**295.0**
CH_3NCH^+	-132.804587	211.0	208.5
$CH_2NC^\bullet$	-131.837990	87.0	86.5

[a] $E_{(total)}$ in Hartrees, all other components, including the ZPE scaled by 0.99, are in kcal/mol.

Figure 5.21. Selected optimized geometries (CBSB7 basis set) of stable intermediates and transition states involved in the isomerization and dissociation of ionized and neutral forms of *N*-methylethenediimine (**1**).

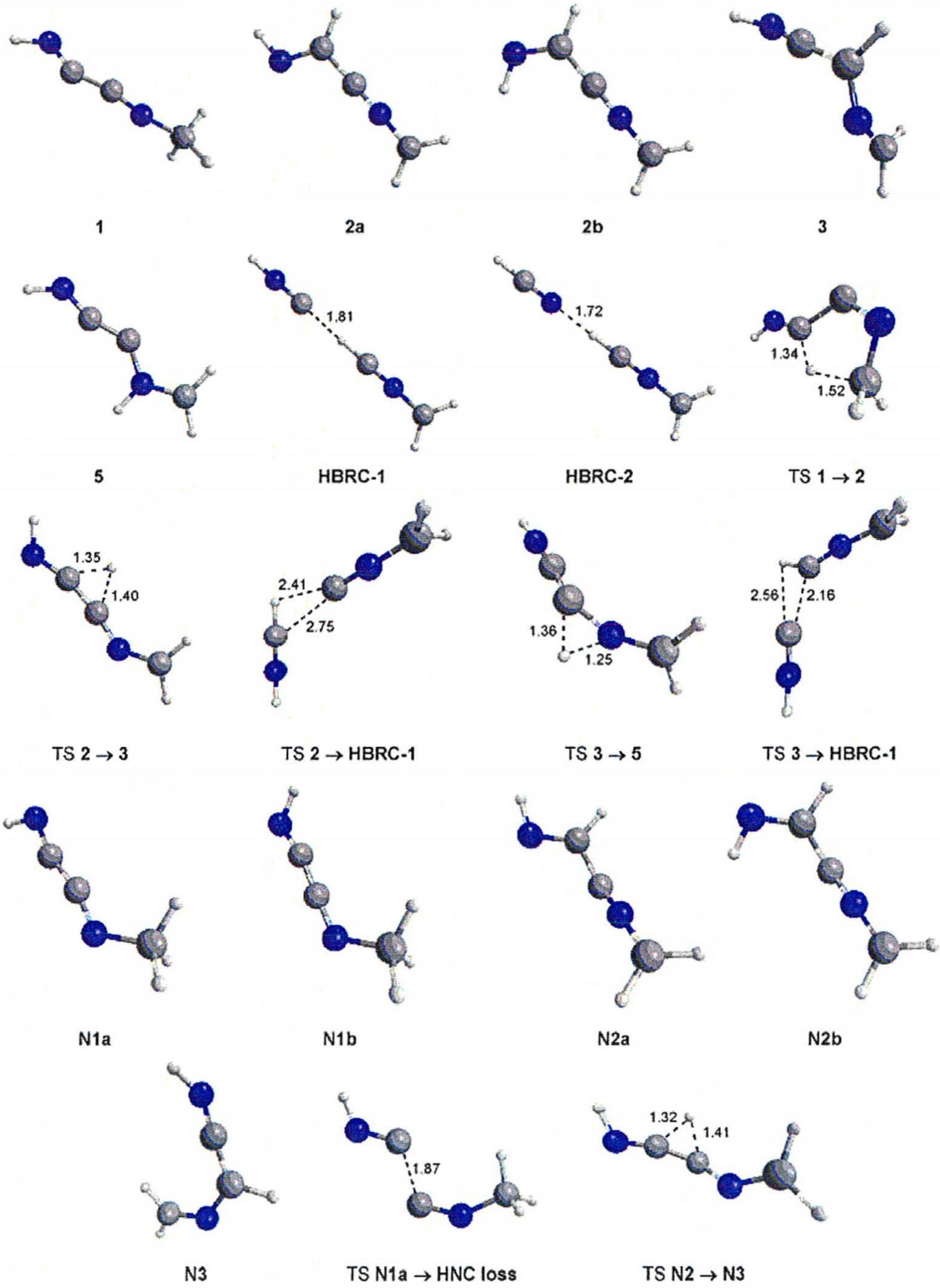

1 **2a** **2b** **3**

5 **HBRC-1** **HBRC-2** **TS 1 → 2**

TS 2 → 3 **TS 2 → HBRC-1** **TS 3 → 5** **TS 3 → HBRC-1**

N1a **N1b** **N2a** **N2b**

N3 **TS N1a → HNC loss** **TS N2 → N3**

Figure 5.22. Selected optimized geometries (CBSB7 basis set) of stable intermediates and transition states involved in the isomerization and dissociation of ionized and neutral **6a**.

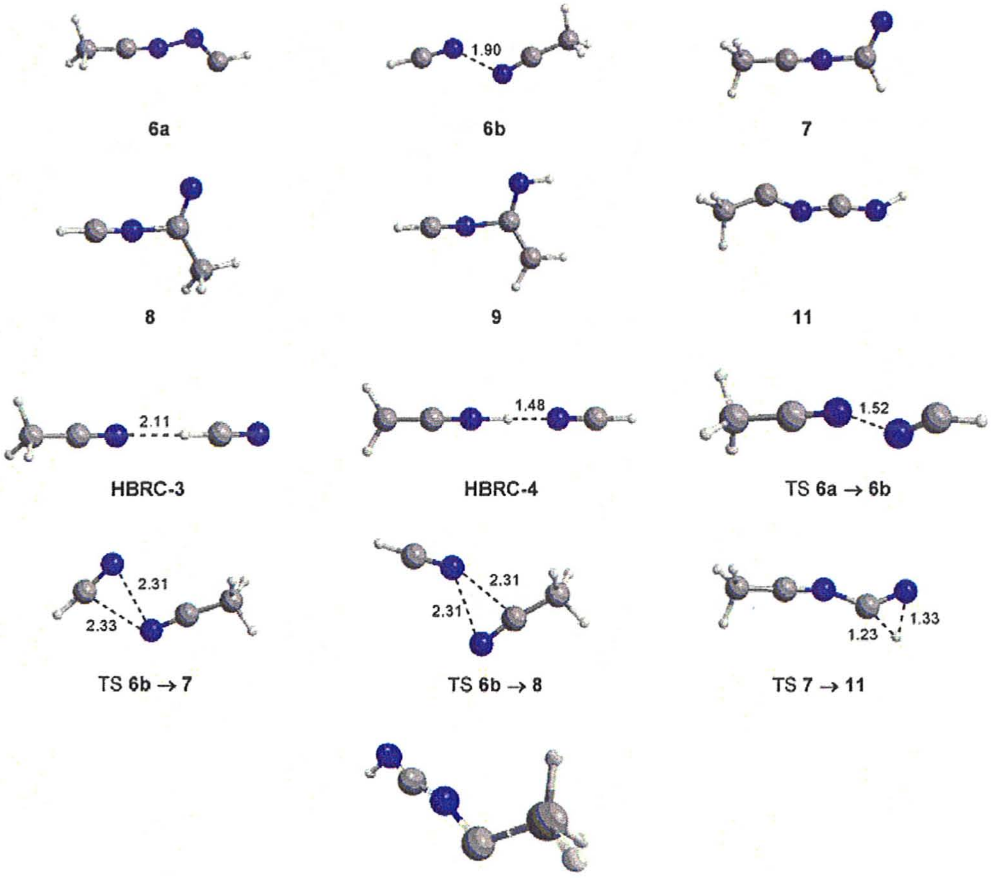

6a **6b** **7**

8 **9** **11**

HBRC-3 **HBRC-4** **TS 6a → 6b**

TS **6b** → **7** TS **6b** → **8** TS **7** → **11**

N11

Figure 5.23. Selected optimized geometries (CBSB7 basis set) of stable intermediates and transition states involved in the isomerization and dissociation of ionized and neutral *N,N*-dimethylethenediimine (**A1a**).

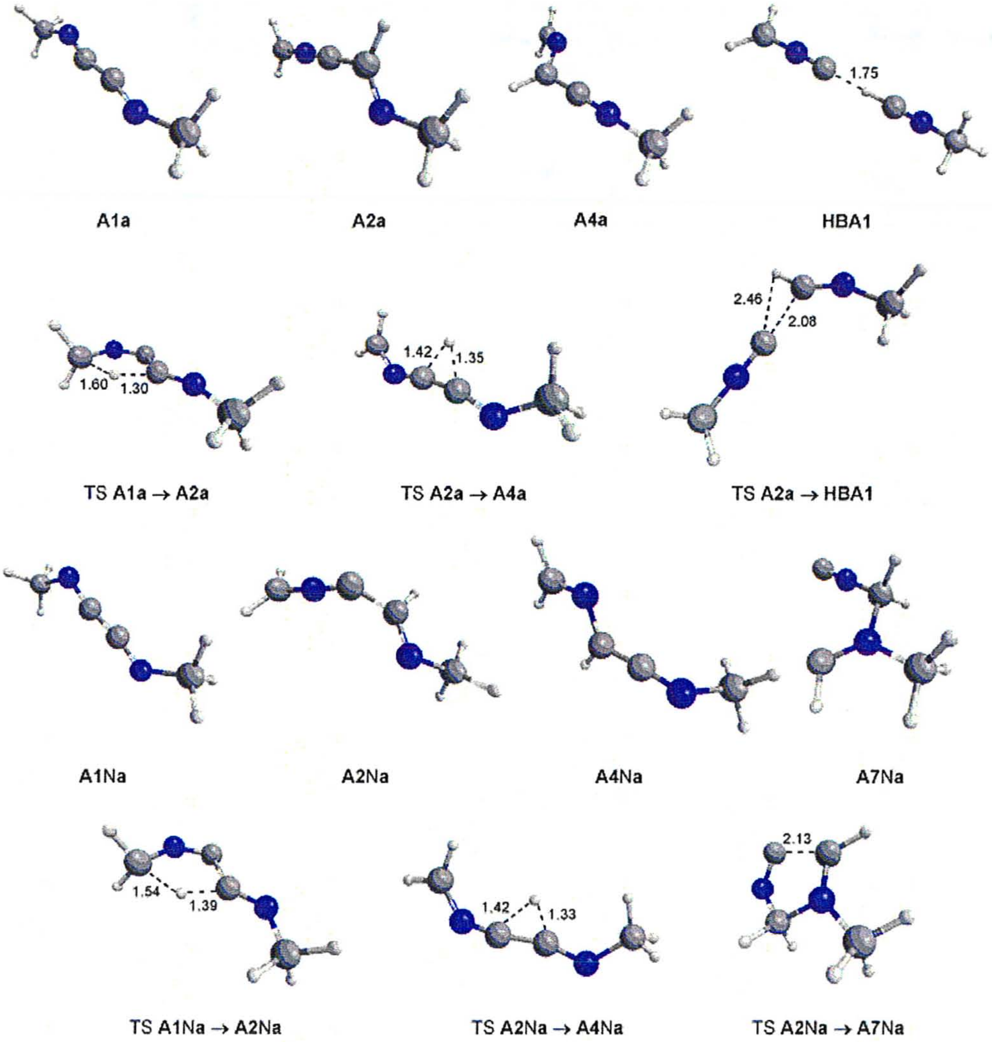

A1a A2a A4a HBA1

TS A1a → A2a TS A2a → A4a TS A2a → HBA1

A1Na A2Na A4Na A7Na

TS A1Na → A2Na TS A2Na → A4Na TS A2Na → A7Na

SUMMARY

The research presented in this thesis is focused on an integrated computational chemistry and mass spectrometric approach to probe complicated isomerization and dissociation chemistries of various gas phase radical cations. In other words, the connectivity, stability and reactivity of all these species were investigated.

In Chapter 2, it is shown that tandem mass spectrometry based experiments and computational chemistry allow for the study of proton transport catalysis by water in the transformation of ionized glycolaldehyde $HOCH_2CHO^{\bullet+}$ into its enol ion $HOCH{=}CHOH^{\bullet+}$. Theoretical findings revealed an energetically more feasible pathway relative to the unassisted isomerization. In spite of this, theory also revealed an alternative pathway involving a hydrogen-bridged radical cation (HBRC) comprised of the ketene ion $CH_2{=}C{=}O^{\bullet+}$ complexed with two H_2O molecules. Model chemistry calculations show that a H_2O molecule in the HBRC catalyzes the otherwise prohibitive transformation of the $HOCH_2CHO^{\bullet+}$ ion into the enol of acetic acid, $CH_2{=}C(OH)_2^{\bullet+}$. Tandem mass spectrometry based experiments reveal that a mixture of $C_2H_4O_2^{\bullet+}$ ions is generated and that the $CH_2{=}C(OH)_2^{\bullet+}$ ion is the major reaction product.

In Chapter 3, various ionic and neutral isomers of $C_2H_2N_2$ were characterized and differentiated by tandem mass spectrometry, particularly the HNC dimer $HN{=}C{=}C{=}NH$ (ethenediimine) and $H_2N\text{-}C\text{-}C{\equiv}N$ (aminocyanocarbene). Both species were separately generated from the stable precursor molecules, xanthine and aminomalononitrile respectively. In addition to the stability of the ionic species seen from metastable and collision induced dissociation (CID) mass spectra, the neutral counterparts are found to be stable as well. The stability of the neutrals in the gas phase was confirmed following the observation of prominent *m/z* 54 'survivor' peaks in their respective NR mass spectra. A different precursor molecule studied, diaminomaleonitrile, is mechanistically shown to generate $HN{=}C{=}C{=}NH^{\bullet+}$ following the loss of HCN from the HBRC, $[HNC{\bullet\bullet\bullet}H_2N\text{-}C\text{-}C{\equiv}N]^{\bullet+}$, via an extraordinary *quid-pro-quo* catalysis.

Analogous to the studies of the previous chapter, Chapter 4 describes the characterization and differentiation of another $C_2H_2N_2^{\bullet+}$ isomer, the HCN dimer, $HC{=}N{-}N{=}CH^{\bullet+}$. Ionized *s*-tetrazine was proposed to generate the ion following the loss of N_2. A mechanistic analysis using the CBS-QB3/APNO model chemistries confirmed the generation of the HCN dimer ion. However, theory further shows that the ion possessed sufficient internal energy to isomerize into the more stable nitrene ion, $HC{=}N{-}C({=}N)H^{\bullet+}$. For purposes of comparison and confirmation, the nitrene isomer was separately generated from *s*-triazine and characterized using CID based techniques. Both ions are found to be stable species in the timeframe of the experiments. However, interpretation of their NR mass spectra revealed that they did not have stable neutral counterparts in the gas phase.

Finally, using model chemistry results and tandem mass spectrometry based experiments, Chapter 5 explains the generation and characterization of several isomers of ionized *N*-methylethenediimine $CH_3N{=}C{=}C{=}NH^{\bullet+}$ and *N,N*-dimethylethenediimine $CH_3N{=}C{=}C{=}NCH_3^{\bullet+}$. The former ion corresponding to *m/z* 68 was generated from two precursor molecules, theophylline and paraxanthine. A CBS-QB3 mechanistic analysis (experimentally confirmed later) of the respective fragmentation pathways revealed that: (i) theophylline generates $CH_3N{=}C{=}C{=}NH^{\bullet+}$ ions in admixture with its 1,4-H shift isomer, $CH_2N{=}C{=}C(H){=}NH^{\bullet+}$, and (ii) paraxanthine generates isomerically pure $CH_3N{=}C{=}C{=}NH^{\bullet+}$ ions. Theoretical calculations on the neutral PES and NR experiments show that $CH_2N{=}C{=}C(H){=}NH^{\bullet+}$ is kinetically more stable than $CH_3N{=}C{=}C{=}NH^{\bullet+}$. Another precursor molecule, *s*-methyltetrazine, was proposed to generate another isomer of *N*-methylethenediimine, $CH_3C{=}N{-}N{=}CH^{\bullet+}$. Model chemistry results in conjunction with experimental observations suggest that these ions are generated with sufficient internal energy to readily isomerize into other isomers yielding a complex mixture of *m/z* 68 ions. Neutral PES calculations revealed that a majority of the ionic geometries studied has no stable neutral counterparts. Ionized caffeine was proposed to generate *N,N*-dimethylethenediimine $CH_3N{=}C{=}C{=}NCH_3^{\bullet+}$ ions. A theoretical mechanistic analysis of the generation of this ion revealed that it is co-generated with its 1,4-H shift isomer, $CH_2N{=}C{=}C(H){=}NCH_3^{\bullet+}$. On the ionic PES, these ions do not readily interconvert prior to dissociation. However, when neutralized, their isomerization barriers are lowered allowing interconversion to yield a mixture of stable neutral isomers. Tandem mass spectrometry based experimental observations agree with all theoretical results.

9109 20